Quantitative analysis of source, reservoir, and cap rocks on the Norwegian Continental Shelf

An integrated study of geology, geophysics, petrophysics and rock physics

Series of dissertations submitted to the
Faculty of Mathematics and Natural Sciences, University of Oslo
No. 2271

ISSN 1501-7710

Cover: Hanne Baadsgaard Utigard.
Print production: Reprosentralen, University of Oslo.

Preface

This dissertation has been submitted to the Department of Geosciences, Faculty of Mathematics and Natural Sciences at the University of Oslo in accordance with the requirements for the degree of Philosophiae Doctor (Ph.D.).

The study was conducted under the project "**ReSource** – Quantitative analysis of Reservoir, Source, and Cap rocks of the Central North Sea". The ReSource project was led by the University of Oslo and funded by Vår Energi AS (formerly Eni Norge). The main supervisor of this work was Prof. Nazmul Haque Mondol (UiO and NGI), and the co-supervisors were Prof. Jens Jahren (UiO) and Prof. Jan Inge Faleide (UiO). Adjunct Prof. Filippos Tsikalas (Vår Energi and UiO) and Prof. Em. Knut Bjørlykke (UiO) were advisors to the project.

The main objective of the study was to characterize source, reservoir and cap rocks as represented by the Jurassic succession on the Norwegian Continental Shelf, centered on rock physics as a tool for integrating seismic, petrophysical, and microscale data.

The thesis consists of two main parts (**Part I. Introduction** and **Part II. Journal Papers**) and an enclosure (**Part III. Appendix**). The scientific contributions that result from the Ph.D. research are documented in three peer-reviewed journal papers of which I am the first author.

Jørgen A. Hansen, Oslo, March 2020

Acknowledgements

Firstly, I would like to express my sincere gratitude to my main supervisor, Professor Nazmul Haque Mondol, for offering me continuous guidance, motivation, and support over the last years. Thank you for always making time for our discussions, whether the topic was work, football or life in general.

I would like to thank my supervisor Professor Jens Jahren for valuable discussions and input to my work, along with the frequent confidence boosts and occasional history lesson. I am also thankful to my supervisor Professor Jan Inge Faleide for sharing his extensive insight and helping me see our research in a broader context. I would also like to express my appreciation to Adjunct Professor Filippos Tsikalas for his guidance and enthusiasm to contribute to all stages of my PhD project. Additionally, I want to thank Professor Emeritus Knut Bjørlykke for contributing with his vast experience in our discussions and meetings.

I am very grateful to Vår Energi AS for funding my PhD project and allowing access to proprietary data. Furthermore, I acknowledge the technical support from Thanusha Naidoo, Salahalldin Akhavan, Michel Heeremans, and Kjetil Bakke at the Department of Geosciences.

I am thankful for the companionship, help and motivation from good friends, fellow students, colleagues, and office-mates over the past years; Henrik, Kristoffer, Hans-Martin, Thea, Honoré, Manzar, Noora, James, Jamil, Hao, Heddi, and Vemund. I also appreciate the continuous encouragement from my other close friends, even when they refuse to believe that I do anything besides play with rocks all day.

Last but not least, I want to thank my parents, Bjørn and Grethe, and my future wife, Veronica, for their never-ending support, and for always being there for me.

List of journal papers

Paper A: Reservoir assessment of Middle Jurassic sandstone-dominated formations in the Egersund Basin and Ling Depression, eastern Central North Sea

J. A. Hansen, N. H. Mondol, J. Jahren and F. Tsikalas

Marine and Petroleum Geology, 2020, **111**, 539-543.

https://doi.org/10.1016/j.marpetgeo.2019.08.044

Paper B: Organic content and maturation effects on elastic properties of source rock shales in the Central North Sea

J. A. Hansen, N. H. Mondol and M. Fawad

Interpretation, 2019, **7**, T477-T497.

https://doi.org/10.1190/INT-2018-0105.1

Paper C: Seal efficiency of Upper Jurassic organic-rich caprock shales on the Norwegian Continental Shelf

J. A. Hansen, N. H. Mondol, F. Tsikalas and J. I. Faleide

Submitted to *Marine and Petroleum Geology*, 31. January 2020.

List of extended abstracts and conference proceedings

Extended abstract A: Estimating exhumation using experimental compaction trends and rock physics relations, with continuation into analysis of source and reservoir rocks: Central North Sea, offshore Norway

J. A. Hansen, H. D. Yenwongfai, M. Fawad and N. H. Mondol

SEG International Exposition and 87th Annual Meeting, 24–29 September 2017, Houston, Texas, USA.

Extended abstract B: Improved Transition Zone Identification Using Relations Between Shear Wave Velocity and Density

J. A. Hansen, N. H. Mondol, F. Tsikalas and S. Doering

Fourth EAGE Workshop on Rock Physics, 11–13 November 2017, Abu Dhabi, UAE.

Extended abstract C: Predicting the Effects of Organic Content and Maturation on the Elastic Properties of Central North Sea Source Rocks

J. A. Hansen and N. H. Mondol

80th EAGE Conference & Exhibition, 11–14 June 2018, Copenhagen, Denmark.

Extended abstract D: Cap rock Evaluation of Central North Sea Shales, Through Log-Derived Poisson's Ratio and Young's Modulus

J. A. Hansen, J. R. Johnson and N. H. Mondol

Sixth EAGE Shale Workshop, 28 April–1 May 2019, Bordeaux, France.

Conference proceeding A: Quantitative characterization of the Central North Sea Jurassic petroleum system

J. A. Hansen, J. R. Johnson, M. Fawad and N. H. Mondol

33rd Nordic Geological Winter Meeting, 7–9 January 2019, Bergen, Norway.

Conference proceeding B: Caprock characteristics of Upper Jurassic organic-rich shales in the Norwegian North Sea and the Barents Sea

J. A. Hansen and N. H. Mondol

34th Nordic Geological Winter Meeting, 8–10 January 2020, Oslo, Norway.

Invited talks and workshops

J. A. Hansen, N. H. Mondol, Jens Jahren, J. I. Faleide and F. Tsikalas. Geological characteristics and elastic properties of organic-rich, Upper Jurassic cap rock shales. *Norwegian Geotechnical Institute (NGI) and University of Oslo Research Workshop*, 10 December 2019, Oslo.

J. A. Hansen, N. H. Mondol, Jens Jahren, Jamilur Rahman. Geological and acoustic characteristics of organic-rich, Upper Jurassic cap rock shales. *Talk delivered at the Prometheus project bi-annual meeting*, 29 November 2019, Oslo.

J. A. Hansen, N. H. Mondol and M. Fawad. QI related to organic-rich shales as source and cap rocks. *OASIS (Overburden Analysis and Seal Integrity Study for CO2 Sequestration in the North Sea) project Annual Meeting*, 1 March 2019, Oslo.

J. A. Hansen, N. H. Mondol, J. Jahren and F. Tsikalas. Quantitative analysis of reservoir, cap and source rocks of the Central North Sea. *Talk delivered at Vår Energi AS office*, 6 February 2019, Oslo.

J. A. Hansen and N. H. Mondol. Variations in velocity-depth relationships for shale and sand. *Talk delivered at UiO-FirstGeo meeting hosted by FirstGeo Oslo*, 5 December 2017, Oslo.

J. A. Hansen and N. H. Mondol. Improved transition zone identification using relations between shear wave velocity and density. *Talk delivered at Oslo Society of Exploration Geophysicists (OSEG) and University of Oslo Geophysical Society (UiOGS) joint annual meeting*, 13 September 2017, Oslo.

J. A. Hansen, M. Fawad and N. H. Mondol. Central North Sea exhumation estimates. *Talk delivered at ReSource project meeting, Eni Norge office*, 17 March 2017, Stavanger.

Contents

Part I
Introduction

Chapter 1
Background

Subsurface exploration is a field of study with a wide range of applications. The primary scope of this particular study is oil and gas exploration, which relies on remote characterization of hydrocarbon storage units (reservoir rocks), the origin of the hydrocarbons (source rocks), and the mechanisms that ensure that generated hydrocarbons accumulate (cap rocks and traps). However, if we consider Carbon Capture and Storage (CCS), the techniques used to evaluate and risk a CCS prospect are largely the same as if evaluating a hydrocarbon prospect. For instance, the original Smeaheia target of the full-scale CCS pilot project Northern Lights rely on the same reservoirs and cap rocks as some of the most important oil and gas fields in the North Sea (Mulrooney et al., 2018). Evaluation of shale composition and brittleness properties is equally applicable to CO_2 storage assessment and hydrocarbon prospect evaluation, both conventional reservoir-cap rock systems and unconventional shale gas reservoirs. Organic content and maturation of organic-rich shales are also vital parameters in unconventional play evaluation, in addition to its application in conventional source rock analysis. Furthermore, incorporating geophysical interpretations of optimal drilling targets (sweet spots) in shale gas or shale oil exploration may reduce the large number of wells typically required for production (Chopra and Marfurt, 2008). Moreover, geophysical methods exploiting petrophysical well log data, seismic, and CSEM data are used to evaluate aquifers in groundwater exploration (e.g., Pedersen et al., 2005; Soupious et al., 2007).

One of the key historical developments affecting modern subsurface exploration is the technique of extracting quantitative properties from seismic data through seismic inversion and AVO analysis, rather than solely relying on

qualitative interpretation of geometries (e.g., anticlines, fault blocks, salt structures) from the seismic reflections. The feasibility of extracting rock properties from seismic data depends on a relationship between the desired property and P-wave velocity (V_P), S-wave velocity (V_S), and/or bulk density (ρ_b). These are the three independent quantities that are obtainable from seismic, excluding attenuation.

Although they are only a "needlepoint" in the scope of subsurface investigation, exploration wells with recorded petrophysical logs are essential to the success of seismic exploration. They serve as calibration points for stratigraphic layers in seismic mapping of horizons, but they also provide continuous in-situ measurements of the acoustic properties that predominantly determine the seismic response. Simultaneously, the well log data along with sampling (cores, sidewall cores, cuttings, pressure tests and fluid tests) provides us with information about the lithology, porosity, and fluid content of different layers in the subsurface. Simply put, these pieces of information can be combined to predict the geological significance of any change in seismic signatures in the proximity of the wellbore. The bridge between the geological properties, understood from field studies or samples and linked with petrophysical measurements, and the seismic signatures, which are determined by elastic/acoustic properties, is called rock physics.

1.1 Outline

The thesis is organized into two main parts and an appendix:

Part I constitutes the introduction, or thesis body, which contains descriptions of the background for the study (Chapter 1), the theoretical basis and important concepts (Chapter 2), the database available to address the objectives (Chapter 3), a summary of the main findings in **Papers A–C** and the context of the scientific contributions (Chapter 4), and finally, some concluding remarks and outlook (Chapter 5).

Part II contains the papers as they are published (**Papers A and B**), or submitted for peer-review (**Paper C**).

Finally, four published extended abstracts are enclosed as appendix A–D in chronological order in **Part III**.

1.2 Motivation and objectives

The overall motivation and aim of the research project were to explore quantitative characterization and evaluation of the three primary constituents of conventional, siliciclastic petroleum systems – source, reservoir and cap rocks – representative of the Norwegian Continental Shelf (NCS). The Central North Sea (schematic cross-section shown in Figure 1) represents different challenges related to exploration, particularly in terms of source rock and reservoir quality, and was the starting point of our investigation. Particularly the eastern part of this area, between the main rift grabens and platforms near mainland Norway, is relatively less explored compared to the northern and southern parts of the North Sea. The primary focus was the Jurassic succession, which varies significantly in thickness and depth within the studied region (Fig. 1). Following the findings in **Papers A** and **B**, the main focus was to investigate the sealing efficiency of potential cap rocks in uplifted basins. This lead to the integration of a dataset from the southwestern Barents Sea with the initial database, representing an area where the primary exploration challenges and burial history differs significantly from the Central North Sea. The Barents Sea data particularly extend the range of net uplift, which is significantly higher. A comparison between the areas is interesting because the cap rock quality and sealing capacity could be equally important, but for very different reasons (**Paper C**). It also serves as important evidence of the generality of observations made in the Central North Sea.

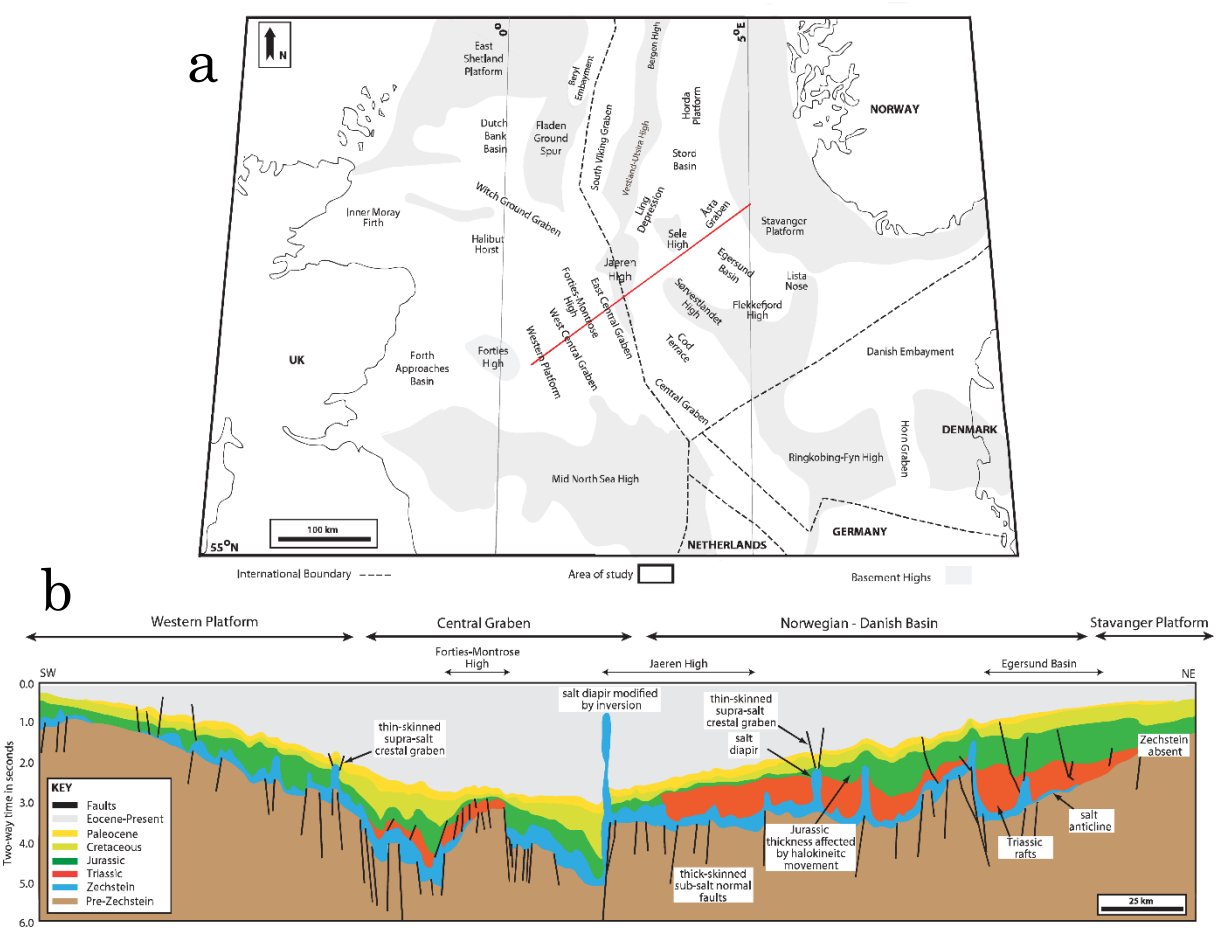

Figure 1: Simplified map of the Central North Sea structural setting (a) where the red line indicates the location of a generalized seismic cross-section (b), modified from Mannie et al. (2014). The Jurassic succession is indicated in green color.

One primary objective of the study was to evaluate the reservoir quality and thickness variations of Middle Jurassic sandstones, which are the main target reservoirs for hydrocarbon exploration in all provinces of the NCS. This includes reservoir characterization and petrophysical analysis to quantify reservoir properties as a function of location, present burial, and maximum burial. Seismic interpretation enables mapping of the thickness and distribution of different formations. Subsequently, established relationships for seismic analysis of reservoir properties could be tested against the sensitivity we observe in well logs, to evaluate the value of seismic exploration for typical parameters of interest such as shale volume (lithology), porosity and water saturation.

The other main objective of the study was to characterize Upper Jurassic shales with respect to composition, burial, organic content, and maturation.

Achieving this goal would lead towards a better understanding of the primary source rocks and cap rocks for the Jurassic play. Maturity is the main concern for source rock formations situated at relatively shallow burial compared to the deeper North Sea rift grabens (e.g., comparing the Central Graben and Egersund Basin in Figure 1). To evolve from established understanding, we should try to not only be able to *identify* source rock units based on their seismic signatures and AVO characteristics, but attempt to *separate* and/or *quantify* variations in organic content, and especially maturation, signs of the expulsion of hydrocarbons and microfracturing. An increasing focus on shale, particularly as unconventional resources (shale oil/gas reservoirs), in recent years has revealed multiple nuances in this type of rock and its seismic properties that were previously ignored (Vernik and Nur, 1992a; Vernik and Landis, 1996; Mondol et al., 2007; Peltonen et al., 2009; Løseth et al., 2011; Sondergeld and Rai, 2011; Vernik and Milovac, 2011; Sayers, 2013a, 2013b). Variations in organic content can significantly alter the seismic expression and AVO signature of a shale layer (Fig. 2; Carcione, 2001; Løseth et al., 2011).

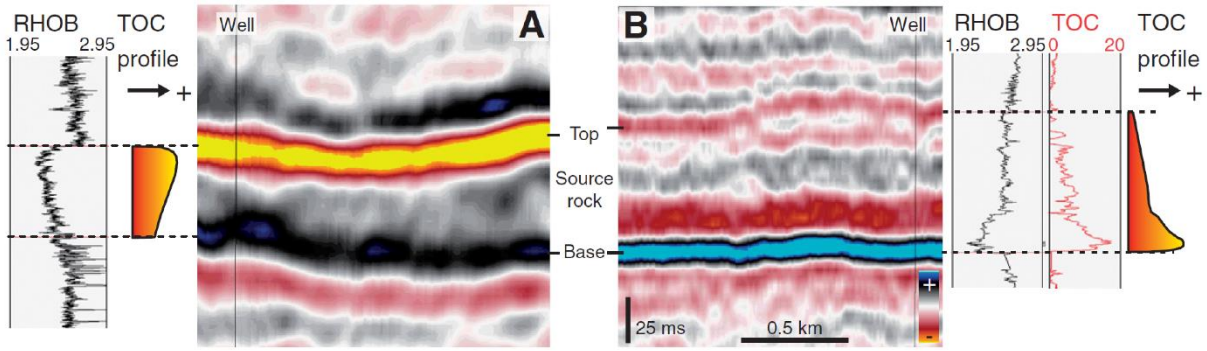

Figure 2: Different vertical distribution of TOC (Total Organic Carbon) in two source rock formations correspond to opposite seismic responses in the respective near stack sections (adapted from Løseth et al., 2011).

Simultaneously, the composition and consolidation of shales will influence its potential as a seal for oil, gas, or CO_2, and thus, remote characterization of these properties is of inherent value. In addition to faulting at different scales, fracturing as a result of overpressure or uplift, and leakage through the cap rock pore volume are mechanisms that may compromise seal integrity (Downey, 1984). When the

cap rock integrity is compromised and hydrocarbons leak from a trap, clear signs may be present in the seismic data. Nevertheless, the exact leakage mechanism (faults, fractures, poor cap rock) may not be as easy to pinpoint, especially when gas distorts and obscures deeper sections of interest (Fig. 3).

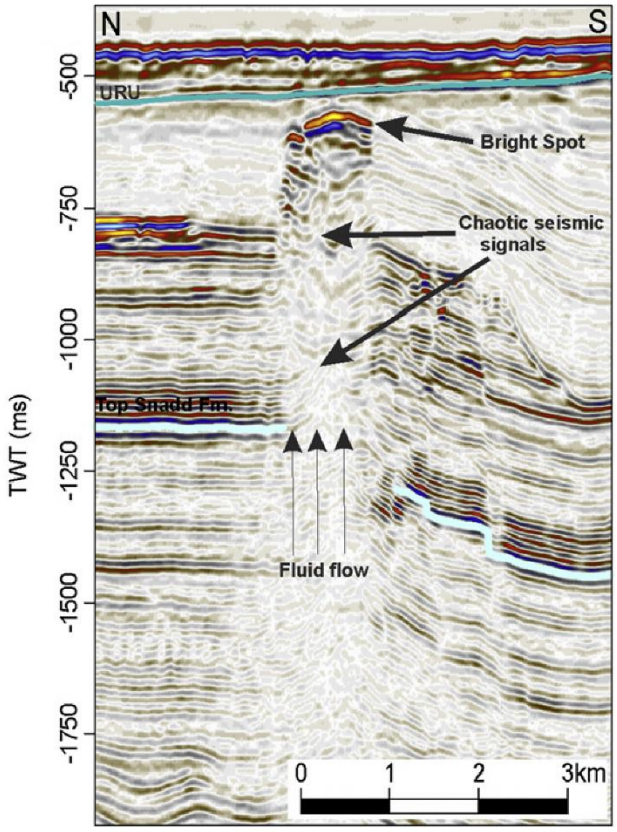

Figure 3: Seismic profile showing a gas chimney in the Barents Sea. Fluid flow is indicated by chaotic seismic reflections above an undefined root zone, with a bright anomaly in the shallow part, suggesting gas accumulation (modified from Vadakkepuliyambatta et al., 2013).

A tangential objective of the study was to investigate compaction behaviour and enable consistent consideration of maximum burial and uplift effects throughout other analyses, through quantification of Neogene uplift and erosion (exhumation). Uplift episodes of different timing and magnitude may have important impact on all parts of the petroleum system: 1) reservoir sandstones may be more or less cemented depending on the time spent in the chemical compaction domain, 2) source rocks may prematurely cease generation of oil and/or gas if uplifted to temperatures that are too low for hydrocarbon generation (oil and

gas windows), and 3) cap rocks may fracture during uplift and stress-release, compromising sealing integrity. Additionally, gas expansion (de-pressurization) and fault reactivation are important risk factors associated with hydrocarbon retention in traps. Being of semi-regional extent, such a study can be valuable in its own right as input for basin modelling and burial history reconstructions.

1.3 Geological setting

The Norwegian Continental Shelf is divided into three provinces, namely the North Sea, the Mid-Norwegian continental margin (Norwegian Sea), and the Norwegian (Western) Barents Sea (Fig. 4). These previously formed a continuous epicontinental sea between Greenland, Svalbard, Norway and the UK, until continental breakup occurred along the North Atlantic rifted margin in the Early Cenozoic and seafloor spreading initiated (Faleide et al., 2015).

1.3.1 Structural framework

The structuring of the NCS sedimentary basins is predominantly a result of rift episodes related to the NE Atlantic continental breakup, where the most prominent phases include the Late Paleozoic, the Late Jurassic–Early Cretaceous, and Late Cretaceous–Palaeocene (Fig. 4; Faleide et al., 2008; 2015).

During Late Triassic–Middle Jurassic times, the break-up of the northern regions of Pangea was still in an early phase. Regional subsidence and high sedimentation rates characterize this period in both the North Sea and Barents Sea basins, following the Late Paleozoic rift phase. The Late Jurassic, on the other hand, was characterized by widespread rifting and fault-block rotation (Torsvik et al., 2002), leading to locally overdeepened basins and high accommodation space (Faleide et al., 2015; Fazlikhani et al., 2017). In the North Sea, sediments near the characteristical rift axis are buried to great depths associated with source rock maturation and hydrocarbon generation. Even deeper are the Bjørnøya and Tromsø basins in the southwestern Barents Sea, where significant rifting also continued later into the Early Cretaceous (Figs. 3 and 6; Faleide et al., 2015). The

final rift phase prior to continental breakup (approximately 55 Ma, Late Paleocene–Early Eocene) initiated in Late Cretaceous and predominantly influenced the westernmost, sheared Barents Sea margin and the Mid-Norwegian margin (Fig. 4).

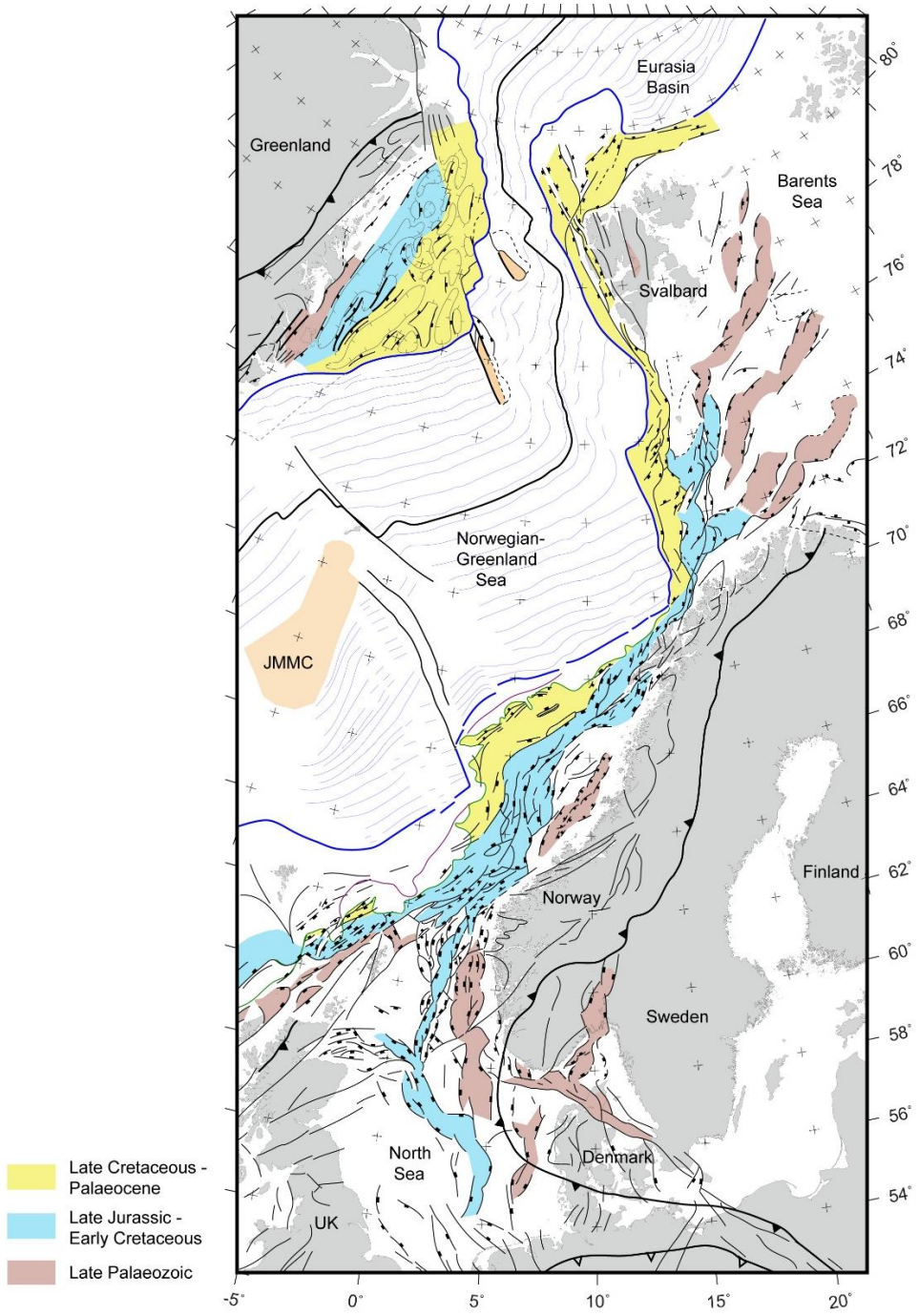

Figure 4: Structural elements, main faults, and related rift phases on the Norwegian Continental Shelf (adapted from Faleide et al., 2015).

Additionally, exhumation occurred in multiple phases that vary in magnitude across the shelf. Most importantly and most recently, significant erosion took place in response to Oligocene and Miocene uplift of southern Norway and laterally variable Plio-Pleistocene glacial erosion, which influenced both the North Sea and Barents Sea (Riis and Fjeldskaar, 1992; Jordt et al., 1995; Baig et al., 2016; 2019).

1.3.2 Lithostratigraphy

The studied formations predominantly range from Upper Triassic to Lowermost Cretaceous in age. As seen in the lithostratigraphic chart (Fig. 5), the Upper Triassic to Middle Jurassic is characterized by continental, fluvial, coastal plain and deltaic deposits, with local influences of marine sedimentation (Fig. 6; Torsvik et al., 2002). The Bryne and Sleipner formations in the central North Sea and the Snadd and Fruholmen formations in the Barents Sea are examples of these predominantly non-marine to paralic sequences. Continental clastics dominate the Upper Triassic mostly in the North Sea. Prominent shallow marine sandstone and shoreface facies are represented in the youngest Middle Jurassic Sandnes, Hugin and Stø formations (Fig. 5).

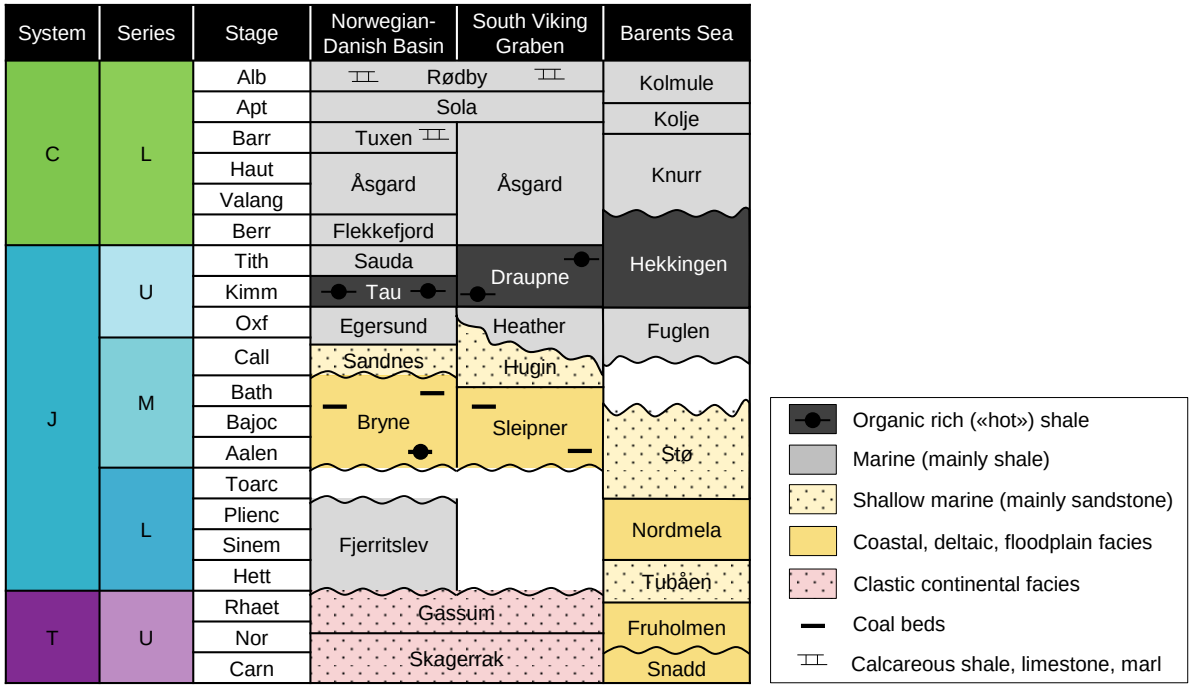

Figure 5: Upper Triassic to Lower Cretaceous lithostratigraphic chart relevant for the studied formations and areas of the NCS (modified from NPD, 2014).

The Upper Jurassic to Lowermost Cretaceous shale dominated formations are clay-dominated and typically contain significant proportions of organic matter (Fig. 5). Notably, the UK Kimmeridge Clay Formation equivalents, i.e., Draupne, Tau, and Hekkingen formations (popularly referred to as hot shales or black [paper] shales) are prolific source rocks for oil and gas and are excellent candidates for studying the effects of changing organic content, composition and maturation (Pedersen et al., 2006). These formations are a result of rising sea level and marine transgression from Bathonian to Kimmeridgian times, coupled with the restricted seafloor environments created by the pronounced Late Jurassic rift topography (Fig. 6; Larsen, 1987; Torsvik et al., 2002; Faleide et al., 2015; Fazlikhani et al., 2017). Low circulation and dysoxic–anoxic conditions coupled with high organic productivity and favourable sedimentation rates were ideal for accumulating and preserving high concentrations of oil-prone organic matter in these fine-grained sequences (Bjørlykke, 2015a; Dembicki, 2017).

The Early Cretaceous was dominated by rapid subsidence and siliciclastic deposition, infill, and draping of the topography generated by the Late Jurassic–Early Cretaceous rifting phase. Sequences from this period mainly consist of fine-grained marine sediments with various calcareous input. Late Cretaceous sediments vary from thick, characteristic Shetland Group carbonate sequences in the North Sea, to siliciclastic (shallow) marine deposits in the Barents Sea that are typically condensed as a result of uplift, erosion, and/or nondeposition (Torsvik et al., 2002; Faleide et al., 2015).

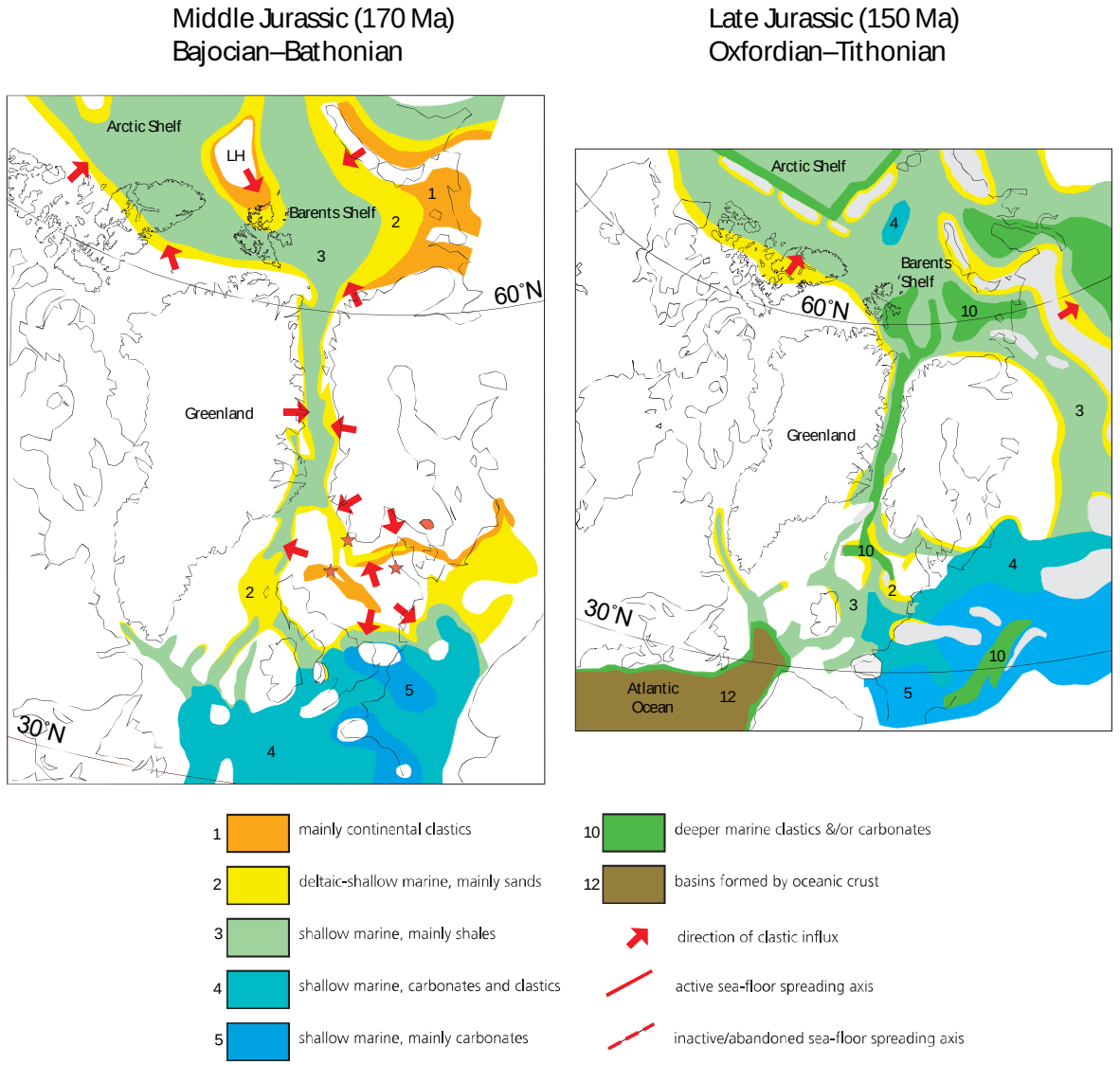

Figure 6: Paleogeographic reconstructions and depositional facies of the Middle and Late Jurassic (modified from Torsvik et al., 2002).

Chapter 2
Theoretical framework

2.1 Composition, compaction, and rock properties

Sandstones are dominantly composed of grains consisting of quartz, feldspar and rock fragments (>62 µm), typically with the addition of some proportion of silt-sized grains (4–62 µm) and clay minerals (<4 µm). Sandstones are usually described in terms of their composition, intergranular volume (IGV, i.e., the sum of pore space, cement, and pore-filling matrix material) and textural parameters such as grain size, sorting, and grain shape (Wentworth, 1922; Folk, 1980; Fawad et al., 2011).

Muds, mudstones, and shales are characterized by a dominant assembly of clay minerals (mainly illite, smectite, kaolinite, and chlorite), as well as variable proportions of silt (quartz, feldspar), pyrite and carbonates (e.g., dolomite, calcite, and siderite). The term "shale" is used relatively liberally in literature to describe fine-grained sediments and does not always implicate consolidated, fissile mudrock with pronounced cleavage as in the original definition of the term (Bjørlykke, 2015b). The initial mud composition depends on the depositional environment (facies) and sediment provenance, but both mineralogy and texture change with diagenesis (i.e., mechanical and chemical compaction). Conversely, clay mineralogy has a dominant influence on the effectiveness of mechanical compaction, and the potential amount of smectite-illite and kaolinite-illite conversions. Organic-rich shales additionally contain a certain amount of organic matter in the form of kerogen (Fig. 7a). The organic content is usually expressed in either volume percent kerogen or as TOC (Total Organic Carbon) in weight

percent (wt. %). Shales with source rock potential can have TOC anywhere from 2-3 to more than 20 wt. % (Gautier, 2005), and the type of organic matter is also an important factor (oil-prone or gas-prone kerogen). Textural features commonly observed are exemplified by the SEM-image shown in Figure 7b, with laminated clay, scattered silt grains of quartz, pyrite, carbonate, and feldspar, and lastly a lenticular distribution of solid organic matter (kerogen), in which significant intraparticle porosity develops when the shale is matured (i.e., kerogen porosity; Fig. 7c). This texture causes intrinsic anisotropy.

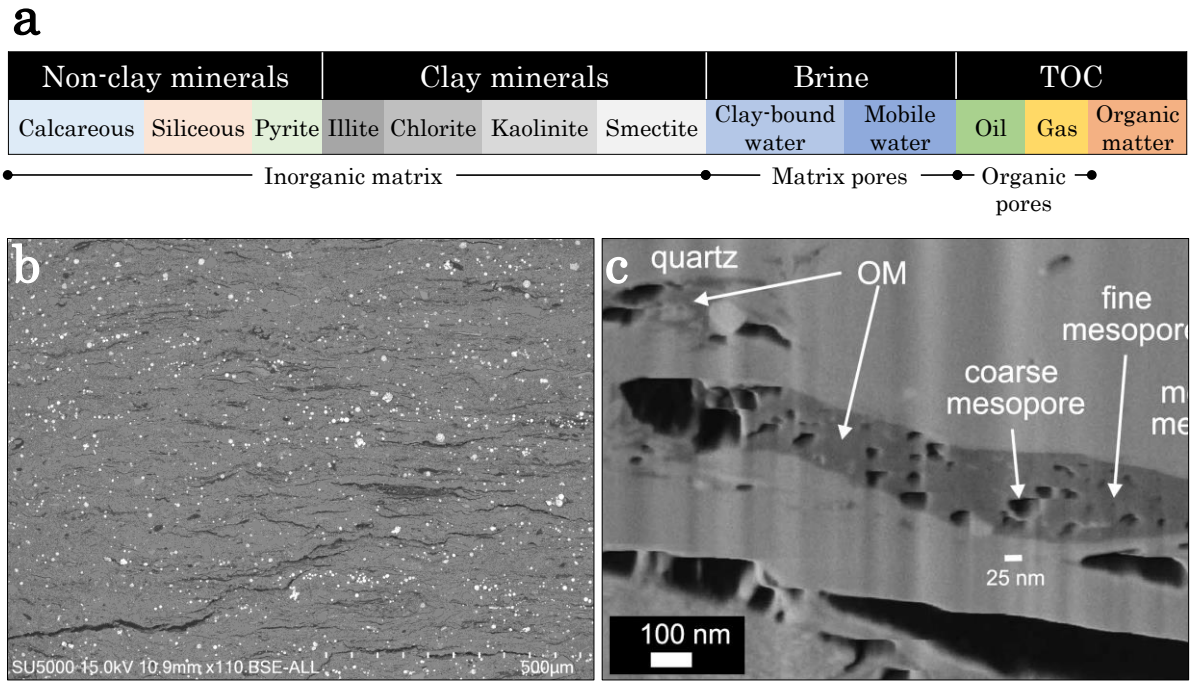

Figure 7: (a) Schematic composition of organic rich shales (redrawn from Zhao et al., 2016), (b) SEM micrograph of a Draupne Formation shale sample, and (c) porosity developed within organic matter as a result of maturation and expulsion of hydrocarbons (Chalmers et al., 2012).

Diagenesis and initial clay composition are highly important for determining the velocity and density of mudrocks and shales (Mondol et al., 2007; Mondol et al., 2008). Generally, the organic-rich shales are often characterized by uniquely high gamma ray signatures and abnormally low density and velocity compared to inorganic shales at similar burial depth (if assuming a similar degree of compaction for mudstones/shales within a narrow depth range), indicating that TOC has a substantial effect on velocity and density. Thermal maturation of the

organic matter, cracking of kerogen, and generation/expulsion of oil and gas will further alter the acoustic properties (e.g., Vernik and Nur, 1992a; Allan et al., 2016).

Shales and sandstones differ significantly with respect to burial, increasing effective stress, and compaction. Sandstone compaction is initially a function of mechanical crushing and reorientation (Fig. 8; Chuhan et al., 2002, 2003; Fawad et al., 2011). After reaching certain temperatures corresponding to chemical compaction (70-80°C), thermodynamically unstable smectite minerals transform to illite in the presence of potassium, a process which releases water and precipitates quartz cement (e.g., Bjørlykke et al., 1989; Bjørlykke and Egeberg, 1993; Bjørkum, 1996; Bjørlykke, 1998; Thyberg and Jahren, 2011). Only a few percent of quartz cement are required to stiffen the rock and inhibit further mechanical compaction, meaning that most of the further porosity-loss is an effect of the amount of quartz precipitated (Lander and Walderhaug, 1999; Bjørkum et al., 2001).

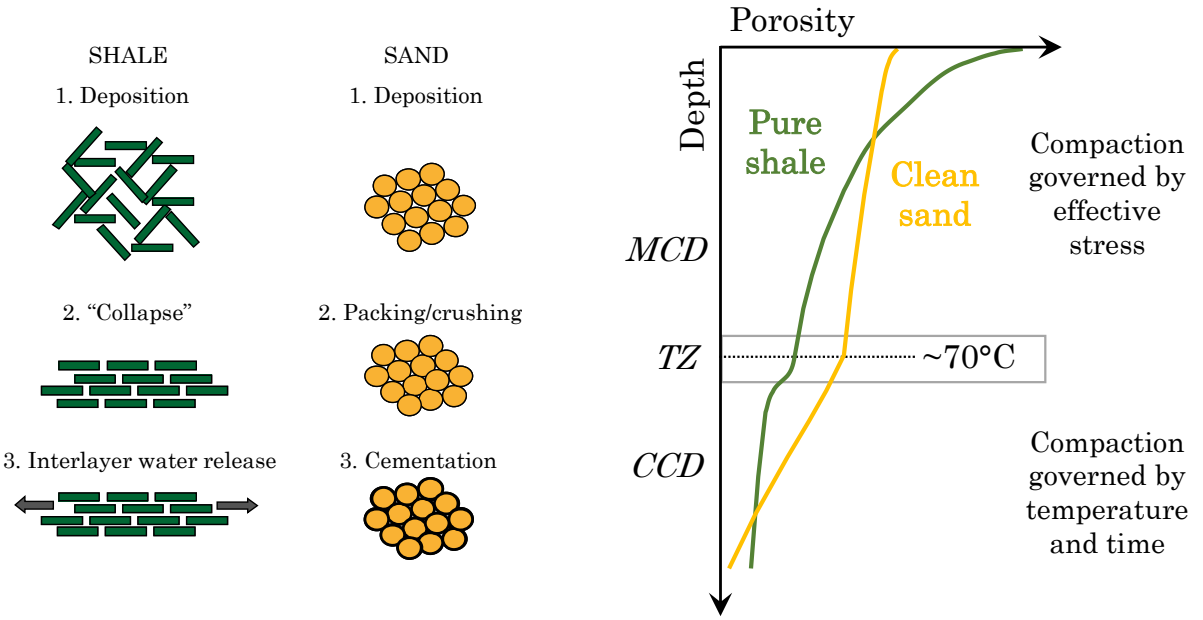

Figure 8: Schematic compaction trends for sand and shale (modified from Avseth et al., 2005; Avseth et al., 2010). MCD = Mechanical Compaction Domain, TZ = Transition Zone, CCD = Chemical Compaction Domain.

Mudstone or shale porosity, while initially very high, is more rapidly reduced in the initial stages of burial (Mondol et al., 2007; 2008), and quartz cement processes, while present (Peltonen et al., 2009; Thyberg and Jahren, 2011), are more influential on shear stiffness than porosity. As shown schematically in Figure 8, this potentially leads to multiple crossovers between reservoir and non-reservoir lithologies in porosity and velocity as a function of depth (Avseth et al., 2005; Bjørlykke, 2015b).

2.2 Fundamental well log analysis of geological properties

Well logs record the in-situ physical, acoustic and electrical properties of the rocks encountered in the subsurface, and also the physical properties in the borehole. Relevant rock properties are calculated and/or interpreted from these measurements, drawing on a range of established equations and assumptions after adequate quality control of the data (Asquith and Krygowski, 2004). Shale volume (V_{sh}) can be calculated from the gamma-ray log via gamma-ray index (I_{GR}) using Equation 1 and some correction, such as Equations 2 or 3 which are applicable to "old" and "young" rocks, respectively (Larionov, 1969):

$$I_{GR} = \frac{GR_{logs} - GR_{max}}{GR_{min} - GR_{max}}\,, \qquad Eq.1$$

$$V_{sh} = 0.33 \times (2^{2\times I_{GR}} - 1)\,, \qquad Eq.2$$

and

$$V_{sh} = 0.083 \times (2^{3.7\times I_{GR}} - 1)\,. \qquad Eq.3$$

Total porosity (ϕ) can be estimated from density (ϕ_ρ) or as a combination of density porosity (ϕ_ρ) and the recorded neutron porosity (ϕ_N), expressed as

$$\phi_\rho = \frac{\rho_{matrix} - \rho_b}{\rho_{matrix} - \rho_{fluid}}\,, \qquad Eq.4$$

and

$$\phi = \sqrt{\frac{\phi_N^2 + \phi_\rho^2}{2}}\,, \qquad Eq.5$$

respectively. Here, ρ_{matrix} is density of the solid phase, ρ_b is bulk density recorded by the log, and ρ_{fluid} is fluid density. Effective porosity (ϕ_{eff}) is sometimes approximated with a shale volume correction as

$$\phi_{\text{eff}} = \phi \times (1 - V_{\text{sh}}). \qquad Eq.6$$

Water saturation (S_w) can be calculated using the Archie (1942) equation

$$S_w = \frac{a \times R_w}{R_d \times \phi^m}^{1/n}, \qquad Eq.7$$

where R_d is deep resistivity, R_w is formation water resistivity, a is tortuosity factor, m denotes the cementation factor, and n is saturation exponent. Subsequently, cutoffs applied to V_{sh}, ϕ, and S_w defines the net-to-gross (N/G) ratios such as N/G reservoir (lithology and porosity) and N/G pay (fluid saturation).

A local relationship between permeability and porosity can be derived from laboratory measurements of core plugs, as they typically display some degree of correlation, but empirical and theoretical alternatives have also been suggested (e.g., Grude et al., 2015). These typically incorporate irreducible water saturation, effective porosity, and potentially require an assumption of certain textural parameters, e.g., the Kozeny-Carman (Kozeny, 1927; Carman, 1937) equation

$$k = \frac{\phi_{\text{eff}}^3 D^2}{72\tau(1 - \phi_{\text{eff}})^2}, \qquad Eq.8$$

where τ is tortuosity and D is grain diameter. Core plug measurements of helium porosity, gas-corrected permeability and water saturation can be used for calibration of the calculated logs.

A commonly used method for petrophysical estimation of organic richness and a qualitative indicator of maturity is called the ΔlogR method, which uses the P-sonic log (Δt) and the deep resistivity log (R_d) as input (Meyer and Nederlof, 1984; Passey et al., 1990). When these logs are overlain and correctly scaled with a baseline in non-organic, fine-grained lithology, the separation between the curves can be interpreted as organic content and/or maturation. The ΔlogR value (separation between the curves) can then be quantified at each depth interval as

$$\Delta\text{logR} = \log_{10}\left(\frac{R_d}{R_{d_{baseline}}}\right) + 0.02 \times (\Delta t - \Delta t_{\text{baseline}}). \qquad Eq.9$$

The total organic carbon (TOC) content in wt% is subsequently predicted as

$$\text{TOC} = (\Delta\text{logR}) \times 10^{(2.297 - 1.1688 * \text{LOM})}, \qquad Eq.10$$

by assuming a Level of Organic Metamorphism (LOM) corresponding to the source rock maturity based on Rock-Eval or vitrinite reflectance data.

An alternative approach is the prediction of TOC from the bulk density log (Vernik and Landis, 1996; Carcione, 2000) through the relationship

$$TOC = a\,\frac{\rho_k(\rho_m - \rho_b)}{\rho_b(\rho_m - \rho_k)}\,, \qquad Eq.11$$

where subscripts to density (ρ) indicate kerogen (k), matrix (m), and recorded bulk (b) densities, and a is a constant related to the fraction of carbon in the organic matter.

2.3 Principles of seismic reflectivity and AVO

The elastic properties of any layer of rock – when considering a simplified earth model assumed to consist of isotropic, elastic, and homogeneous layers – can be described by three parameters. Most commonly and intuitively used are P-wave velocity (V_P), S-wave velocity (V_S), and bulk density (ρ), where the seismic wave velocities are defined by

$$V_P = \sqrt{\frac{K + \frac{4}{3}\mu}{\rho}}, \qquad \text{Eq. 12}$$

and

$$V_S = \sqrt{\frac{\mu}{\rho}}. \qquad \text{Eq. 13}$$

The same can be expressed by combining density with, for example, bulk modulus (K) and shear modulus (μ) or Young's modulus (E) and Poisson's ratio (ν). The P- and S-impedance (denoted I_P and I_S or AI and SI, respectively) of a layer is the product of (P- or S-wave) velocity and density. In turn, the reflection coefficient or reflectivity of the interface between two layers, when considering a seismic P-wave with normal incidence (i.e., zero-offset, incidence angle Θ = 0°), is

$$R_{PP}(0°) = \frac{AI_2 - AI_1}{AI_2 + AI_1}, \qquad \text{Eq. 14}$$

where subscripts 1 and 2 denote the upper and lower layers, respectively.

For seismic waves with an incidence angle to the interface, mode conversion makes the relationship more complicated, because the incoming P-wave creates both reflected and transmitted P- and S-waves (Fig. 9). The angles of the incident, reflected and transmitted waves depend on layer properties and are governed by Snell's law.

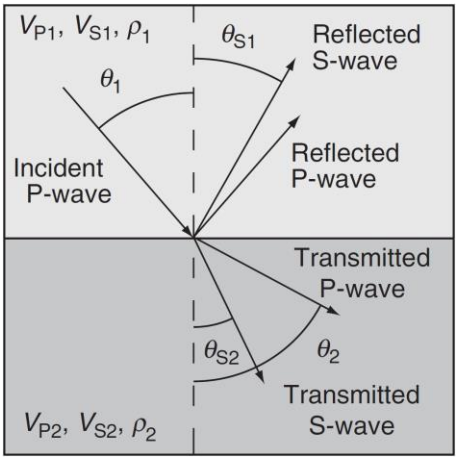

Figure 9: Angles of incident, reflected, and transmitted waves between two media of different velocity and density (adapted from Mavko et al., 2009).

Amplitude Variations with Offset (AVO) theory builds on this phenomenon and our understanding of the physics that govern how much energy is reflected and transmitted as a function of the offset between the seismic source and receivers (i.e., angle of incident P-wave propagation). The equations precisely describing the amplitudes of reflected and transmitted waves are known as the Zoeppritz (1919) equations. Multiple simplifications also exist and are being used in modern seismic applications (e.g., Bortfeld, 1961; Aki and Richards, 1980; Shuey, 1985; Smith and Gidlow, 1987; Castagna, 1993), but these are typically only valid up to ~30-40° and for "small" contrasts between layers (Fig. 10a). P-wave reflection coefficient variations are used for AVO interpretation, and without going into mathematical details, a general form based on Aki and Richards (1980) reads

$$R_{PP}(\theta) = A + B\, sin^2\theta + C(tan^2\theta - sin^2\theta)\,, \qquad \text{Eq. 15}$$

Here, A equals the zero-offset reflectivity $R_{PP}(0°)$, B is called AVO gradient, which describes the amplitude variation at intermediate offsets, and the term C, which is excluded in some approximations and practical applications, denotes the

"curvature" or behaviour at far offsets approaching the critical angle (where refraction occurs). The combination of *A* and *B* forms the basis for AVO classification originally defined for shale-gas sand interfaces (Rutherford and Williams, 1989; Castagna, 1993; Castagna and Swan, 1997; Castagna et al., 1998; Fig. 10b). The change in amplitude at non-zero angles is increasingly related to the V_P/V_S-ratio contrast with increasing angle. AVO classification is applicable to all types of discernible interfaces, even though the most common application is to evaluate changes in the top reservoir reflection amplitude. The AVO signature of a single shale-sand interface changes as a function of compaction, due to the behaviour shown in Figure 8. Similarly, changes in the cap rock stiffness are vital to consider before connecting fluid anomalies to a certain AVO class, as discussed in **Paper A**. Organic-rich shale AVO modelling indicate that such contrasts may, for example, stem from lateral changes in organic content (**Paper B**).

Simply explained, seismic amplitude inversion takes advantage of the relationship between incoming and transmitted seismic waves and the elastic properties of the subsurface, both in the case of poststack and prestack (AVO) seismic data (Barclay et al., 2008). Measured seismic data are mathematically taken back through the physical steps of seismic acquisition (and processing) through different operations (e.g., removing the effect of a wavelet), in order to extract values of acoustic impedance (P- and/or S-impedance, potentially density).

Many variations of inversion at different levels of complexity exist depending on the type of data being inverted. Important considerations and sources of error include the choice and design of wavelet, well-to-seismic ties (time-depth relationships), the low-frequency background model, if applicable, input horizon interpretations, and the quality of the data, including the range of angles can be used with confidence, as per the principles of AVO (Simm and Bacon, 2014).

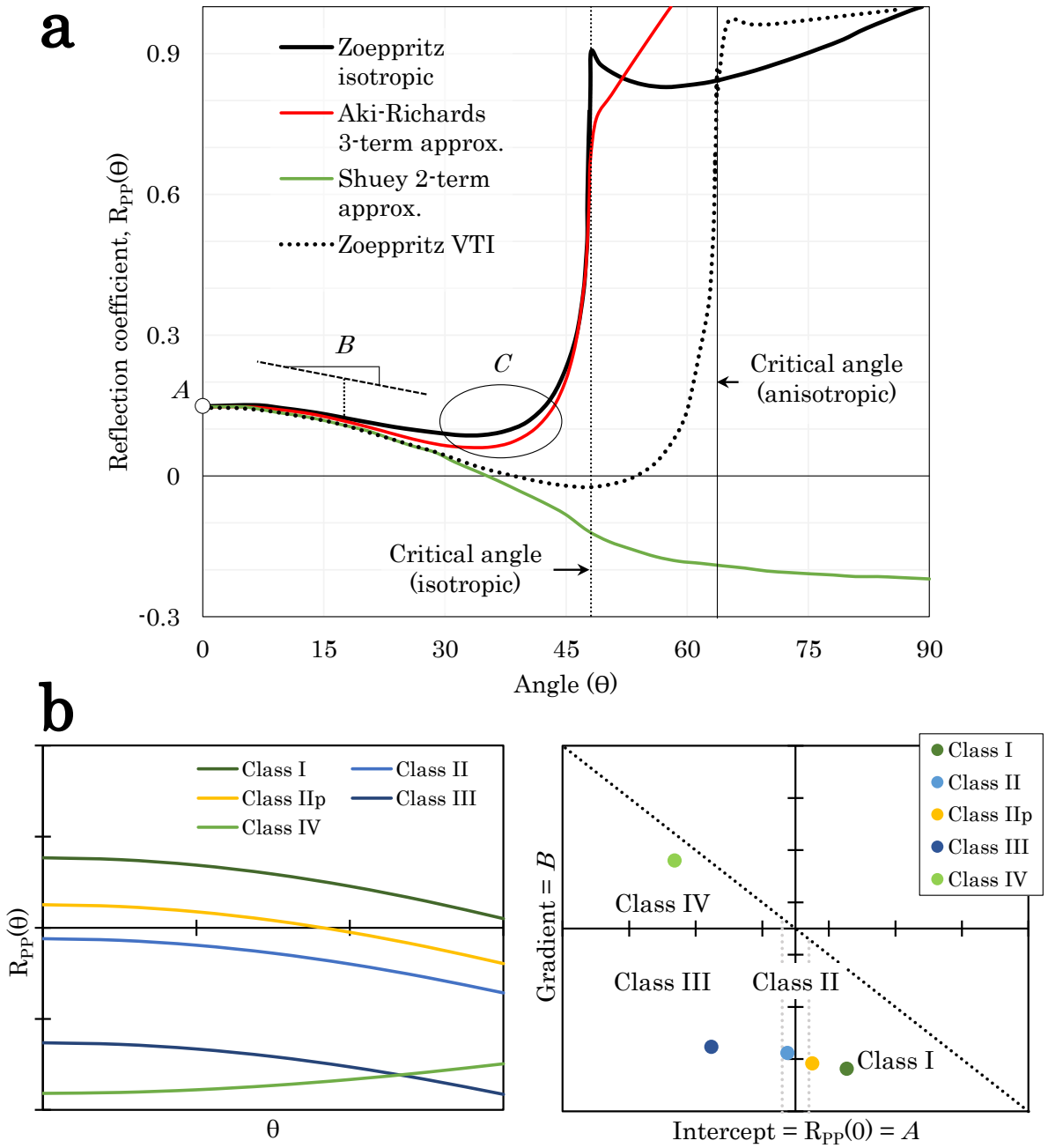

Figure 10: (a) R_{PP}–Θ plot representing a single interface between anisotropic shale (ε and δ values realistic for Kimmeridge shale equivalents; Sondergeld et al., 2000) and brine sandstone. Note that up until ~30°, even the simplest approximation (Shuey, 1985) shows a satisfactory fit with either of the exact solutions (Zoeppritz, 1919). *A*, *B* and *C* represent the three components of the Aki-Richards approximation. (b) Schematic AVO class definitions in the R_{PP}–θ and Intercept (*A*) versus Gradient (*B*) crossplots.

The aforementioned theories and models do not account for anisotropy. Anisotropy means that a seismic wave will propagate with different velocities depending on the orientation of the medium. For example, in a rock layer, there could be a difference between the horizontal (90° to the symmetry axis), bedding-parallel direction and the vertical (0°), bedding-perpendicular direction (Thomsen, 1986; Mavko et al., 2009). Particularly when organic-rich and/or clay-rich shales, or thinly layered sequences are involved, anisotropy can have additional impact on offset-dependent seismic amplitudes (Fig. 10b; e.g., Øygarden et al., 2015). Therefore, there exist more comprehensive, anisotropic versions of the reflectivity equations (e.g., Rüger, 1997) to describe anisotropic AVO. These incorporate the Thomsen (1986) "weak" anisotropy parameters ε, δ, and γ for vertical transversely isotropic (VTI) media. Of these parameters, the most intuitive is P-wave anisotropy, i.e., the fractional difference of the P-wave velocities in the vertical and horizontal direction (Mavko et al., 2009), expressed as

$$\varepsilon \approx \frac{VP(90°) - VP(0°)}{VP(0°)} . \qquad Eq.16$$

Only the first two parameters are needed to model the effect of anisotropy in P-wave AVO when assuming VTI media (Simm and Bacon, 2014; Fig. 10). The main practical challenge with routinely incorporating anisotropy in seismic exploration is to define or obtain realistic values for the Thomsen parameters.

2.4 Rock physics

Rock physics builds on the aspiration of theoretically predicting the elastic moduli of rocks based on the constituent volume fractions, the properties of each constituent phase, and the geometric arrangement of these constituents. Simplified, this means that if the mineralogical and fluid composition of a rock, the K, μ and ρ of each mineral type or fluid, as well as the texture/pore geometry are known, we can (theoretically) know the effective velocities of the full rock composite (Mavko et al., 2009). Rock physics thus provides a link between rock properties (e.g., porosity, shale volume, sorting, fluid content, organic content) and seismic properties (e.g., V_P, V_S, I_P, I_S).

2.4.1 Elastic bounds and granular media (sandstone) modelling

By only assigning values to the two first prerequisites (volume fractions and elastic properties of each phase), and leaving out the geometry, it is possible to predict upper and lower elastic bounds, such as the Voigt (upper), Reuss (lower), or Hashin-Shtrikman (denoted *H-S*$^{+}$ *and H-S*$^{-}$) bounds (Hashin and Shtrikman, 1963; Fig. 11). This assumes isotropic, linear, and elastic constituents and rock.

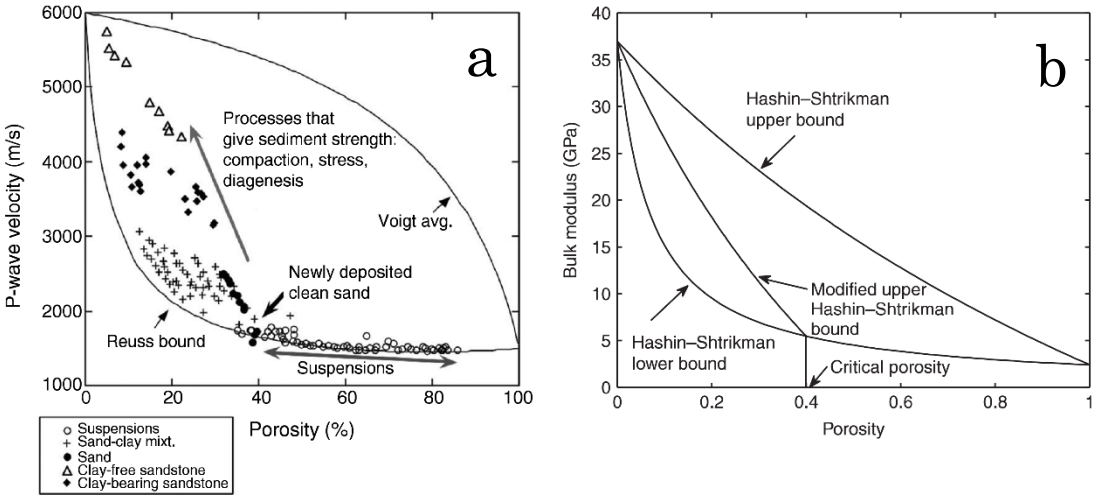

Figure 11: (a) Voigt and Reuss bounds on velocity compared to recorded data (adapted from Mavko et al., 2009) and (b) Hashin-Shtrikman bounds on bulk modulus and their modified versions for critical porosity (Nur et al., 1991; Nur et al., 1998) for a quartz-water system (adapted from Avseth et al., 2010). The modified versions were found to be very useful in practical rock physics applications.

A plethora of different models exist to model sandstone behavior (see Avseth et al., 2005; Mavko et al., 2009; Avseth et al., 2010 for detailed reviews of the subject). Generally speaking, the significant variations in the relationship between velocity and porosity (or P-velocity and S-velocity) of sandstones have been recognized for many years (Fig. 11a; e.g., Raymer et al., 1980; Han, 1986; Vernik and Nur, 1992b; Dvorkin and Nur, 1996; Avseth et al., 2000). Classical empirical relationships between Vp and Vs or Vp and density in different lithologies (also mudrocks and carbonates) include Gardner et al. (1974), Castagna et al. (1985), Krief et al. (1990), and Greenberg and Castagna (1992), and typically take the form of simple linear or power-law functions.

A popular hybrid approach proven useful in multiple settings on the NCS includes a combination of the frequently cited constant cement (Avseth et al., 2000), friable sand, and contact-cement models (Dvorkin et al., 1994; Dvorkin and Nur, 1996), which are shown in Figure 12a (Avseth et al., 2010). These are based on using modified *H-S* bounds to describe the sorting and cementation of sands, by interpolation between high-porosity and low-porosity end-members. The dry elastic properties at the high-porosity starting point (critical porosity where sediments become load-bearing, i.e., 35–45%) is calculated from Hertz-Mindlin (*H-M*) contact theory (Mindlin, 1949). Subsequently, Gassmann (1951) fluid substitution is used to calculate the effective properties of the rock saturated with a given fluid. This model scheme was utilized to test the fluid sensitivity in relatively deeply buried Middle Jurassic sandstones in **Paper A**.

Furthermore, other authors (e.g., Athy, 1930; Ramm and Bjørlykke, 1994) have proposed empirical equations for porosity reduction with depth. These can be combined with *H-M* contact theory and used to approximate the depth-trends of shale, silt, and sand with various fluid saturations (Fig. 12b; Avseth et al., 2001). This approach takes depth-trend modelling of the input parameters to contact theory as a proxy for mechanical compaction based on the porosity at a given depth. Subsequently, chemical compaction at greater burial (as described by input burial curves) that corresponds to higher temperature (above approximately 70°C) can be handled by for instance the Dvorkin-Nur contact cement model as above, but with a more realistic starting point that has accounted for the mechanical compaction. The amount of porosity reduction that should be accounted for with the contact cement model can be calculated as a function of the time spent in the chemical compaction domain using the Walderhaug quartz cement model (Walderhaug, 1996). Lander and Walderhaug (1999) utilize an expression of IGV rather than porosity, but with a similar exponential decline factor, for modelling mechanical compaction. Different approaches produce similar predictions, e.g., Vernik and Kachanov (2010).

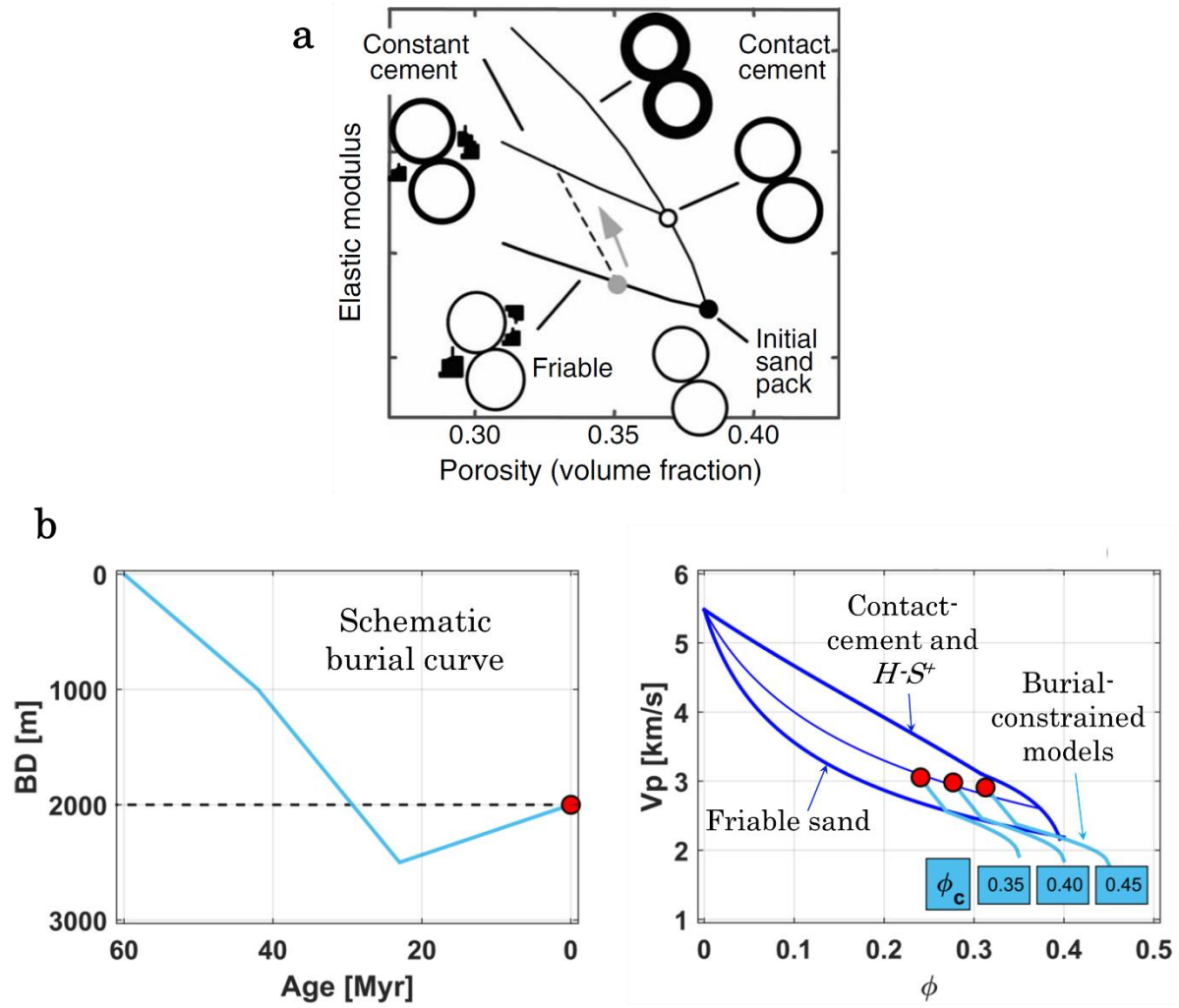

Figure 12: (a) Sandstone models for sorting and cementation (adapted from Avseth et al., 2005). (b) Burial history driven rock physics modelling honouring mechanical and chemical compaction compared to the approach in (a), modified from Avseth and Lehocki (2016).

Regardless of the underlying theory, rock physics models that are constrained by local conditions (depth, temperature, mineralogy, fluid properties, etc.) can be combined in a rock physics template (Fig. 13; Ødegaard and Avseth, 2004) and used for direct interpretation of seismic inversion data. Our approach in **Paper B** further examines the interpretation space shown in Figure 13, by closing in on the behaviour of shale compaction as a function of source rock properties.

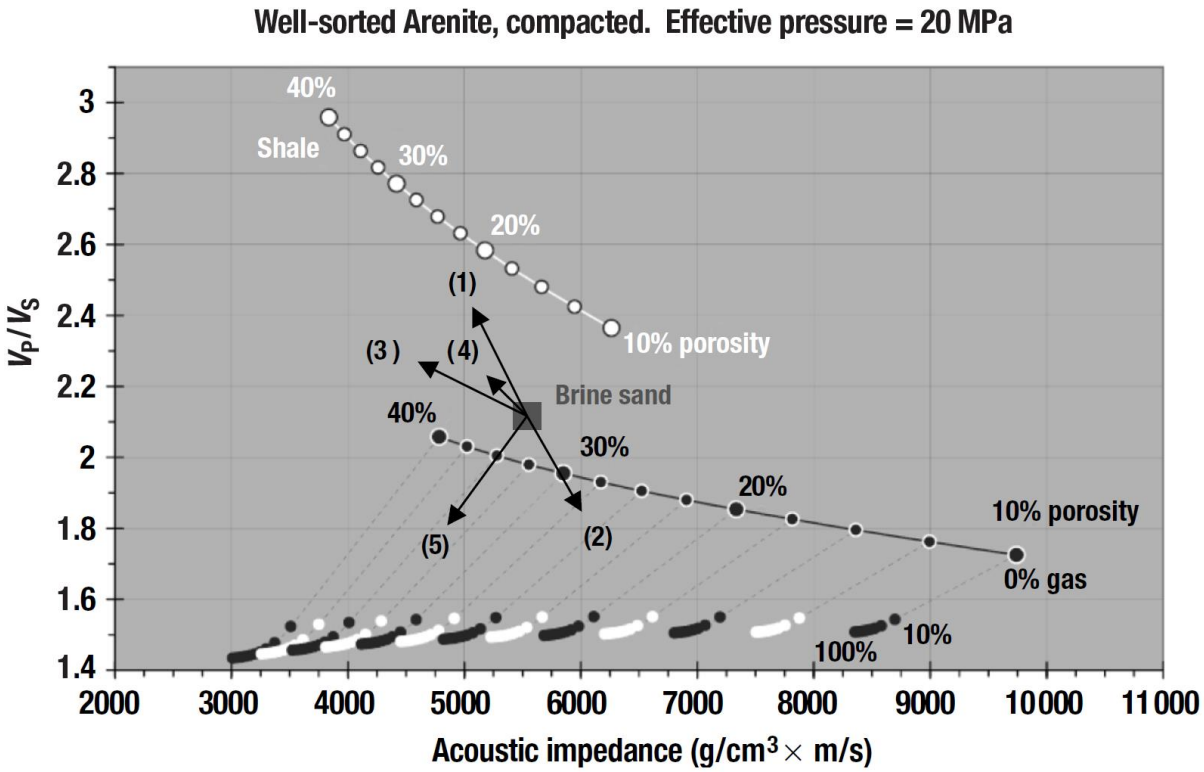

Figure 13: Example rock physics template in the AI–V_P/V_S crossplot for different lithologies (sand and shale) and different gas saturations in sandstone. The arrows indicate conceptual trends on a given brine sandstone point: 1) increasing clay content, 2) increasing cement volume, 3) increasing porosity, 4) decreasing effective pressure and 5) increasing gas saturation (adapted from Avseth et al., 2005).

2.4.2 Shale models

Properties of shales are generally approximated by considering mixtures of clay and silt minerals, as well as kerogen in some cases. A review of multiple shale models is available in Avseth et al. (2005). Semi-empirical models that approximate shale compaction from contact theory, although strictly not very applicable to typical mudstone texture and pore structure, are relatively simple and can to the first order be a good predictor of the depth-dependent relationship between the elastic properties of sands and shales (Avseth et al., 2005). This is the approach we take in **Paper C** to evaluate the continuous spectrum of composition between clean sands and mudrocks. With clay models approximating a "pure" shale, we have the means to vary the proportion of clay and quartz in the theoretical models.

As mentioned in Sections 2.1 and 2.3, mudstones and shales are typically characterized by high intrinsic anisotropy, and are thus approximated as vertical transverse isotropic (VTI) media. Some of the leading causes established to contribute to anisotropy in organic-rich shales are (e.g., Vernik and Landis, 1996):

- Interlayering of different lithologies/laminae (e.g., clay and kerogen) with different elastic properties on a scale much finer than the seismic wavelength
- The preferred orientation of minerals
- Stress-induced fractures and microcracks that show preferential alignment
- Thin layers of carbonate
- Sheet-like quartz cement precipitated parallel to the bedding/laminated clay texture (Thyberg and Jahren, 2011).

The anisotropy can be accounted for in theoretical shale models by defining the rock by five independent elastic constants (Mavko et al., 2009), but this naturally increases the model complexity. For instance, Dræge et al. (2006) provide detailed descriptions of the mechanical and chemical compaction of mudrocks.

Other intricate anisotropic rock physics models aim to predict the effect of organic matter and maturation levels on the elastic properties of source rock shales (Li et al., 2015; Vernik, 2016; Zhao et al., 2016). Vernik (2016) proposed a framework for kerogen substitution modelling (as utilized in **Paper B**), which can be used to model different scenarios similar to Gassmann fluid substitution, but related to the changing organic-rich shale properties rather than the reservoir properties as a function of fluid content (e.g., in AVO studies).

Alternatively, some models target the effects of brittleness and mineralogy, typically in unconventional exploration settings (Guo et al., 2013; Perez and Marfurt, 2014; Li et al., 2015). A common pitfall for the more advanced models is that over-parametrization may remove a lot of the predictive power, and a local, empirically calibrated simple model may better serve the purpose in some cases (Avseth et al., 2005; Mavko et al., 2009). In most cases, relatively accurate assumptions about mineralogical composition must be made for the models to be accurate (e.g., Vernik, 2016).

Chapter 3
Database

This chapter contains a summary of the main database that was available for investigation. Individual analyses described in **Papers A–C** were performed on subsets of data tailored to address each objective, including a selection of wells coupled with other relevant data such as seismic and different types of rock sample analysis data. The details of these subsets are described in each individual paper.

3.1 Exploration wells

A carefully selected primary well dataset consisting of 37 wells constitutes the main basis of our interpretation (Fig. 14). The wells were chosen according to location, interest and data availability, and were subjected to strict quality control considering log spikes, artifacts, carbonate stringers and borehole-related erroneous readings. These wells typically consist of a full well log suite, and often contain either recorded S-wave velocity (vital for rock physics evaluation) and/or laboratory data from cores and cuttings.

The aforementioned exhumation study (described in **Extended Abstract A**), which was part of the groundwork in the eastern Central North Sea, is an exception and utilized an extended well database consisting of 87 exploration wells (with 59 conclusive results), not detailed herein. Normal Compaction Trends (NCT) from literature (Mondol, 2009) were used to quantify net exhumation from velocity data according to present depth.

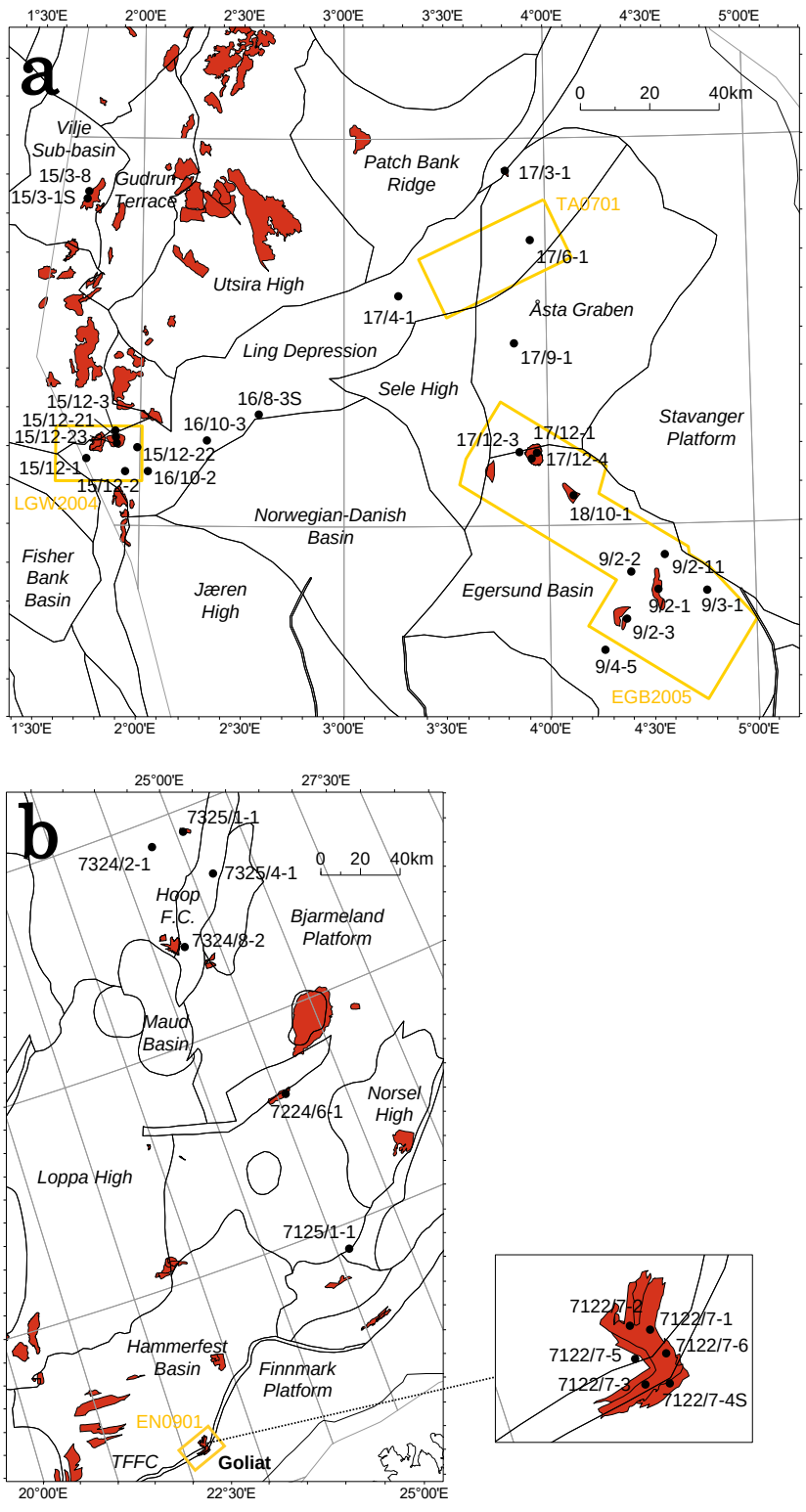

Figure 14: Map outlining structural elements (annotated in italics; adapted from NPD, 2020 FactMaps), hydrocarbon discoveries (red shading), locations of exploration wells (annotated black dots) and 3D seismic cubes (yellow outlines) in the North Sea (a) and Barents Sea (b). 2D seismic data covers the Central North Sea area.

3.1.1 Laboratory analyses of cores and cuttings

Porosity, permeability, water saturation, and grain density measurements from routine core analyses were compiled from the publicly available completion reports provided by the Norwegian Petroleum Directorate (NPD).

Fifteen (15) shale samples (cores and cuttings) were collected from the NPD core store in Stavanger, Norway. XRD and SEM analyses were performed in-house, and geochemical (Rock-Eval) analysis was employed to extract TOC, S1, S2, S3, Tmax, and vitrinite reflectivity (R_o). Additional geochemical data were compiled from public reports (NPD).

3.2 Seismic data

Both 2D and 3D seismic data were available in the study. The North Sea Renaissance (NSR) long offset 2D survey provides regional coverage of good quality, encompassing the Central North Sea and southern Viking Graben (covering the entire extent of Fig. 14a). The 2D lines form a grid of approximately 5.5×5.5 km. Three 3D seismic surveys with a combined area of around 3600 km^2, as shown in Figure 14a, provide detailed coverage of the southwest Ling Depression (MC3D-LGW2004), northeast Ling Depression (TA0701), and the Egersund Basin (MC3D-EGB2005). Finally, a high quality, multi-azimuth prestack 3D seismic dataset (EN0901) covers the Goliat structure in the Barents Sea (Fig. 14b; 209 km^2). These data were acquired in 2009, with three acquisition azimuths of 7°, 67°, and 127° to improve the illumination of the faulted and complex Goliat structure compared to an older survey (Buia et al., 2010). Three angle stacks representing near (17°), mid (32°) and far (45°) angles were available for AVO analysis.

Chapter 4
Scientific contributions

4.1 Summary of papers

4.1.1 Paper A

Reservoir assessment of Middle Jurassic sandstone-dominated formations in the Egersund Basin and Ling Depression, eastern Central North Sea

Objectives and motivation

In well-explored, mature hydrocarbon exploration provinces, even small discoveries may be economically viable, depending on existing infrastructure. The eastern areas of the Central North Sea, situated between the Jurassic–Cretaceous rift system and the platform areas close to mainland Norway (i.e., the older sedimentary basins surrounding the Sele High), are sparsely explored compared to adjacent regions closer to the rift axis. Many wells have been dry, typically attributed to a mostly immature Upper Jurassic source rock, but important discoveries that prove a functioning petroleum system in the area have been made, e.g., 9/2-1 Yme, 17/12-1 Vette and 17/3-1 Bark. The primary objective of this study was to perform a thorough reservoir characterization to look for systematic variations in reservoir quality, thickness and extent. The second objective was to evaluate the feasibility of quantifying such variations based on existing poststack seismic data, and discuss the results in the context of localized matured source rock sites.

Methods

We conducted a detailed petrophysical analysis of the Middle Jurassic reservoir section, where the resulting net-to-gross evaluations were based on calculated shale volume, porosity and fluid saturation calibrated to core plug measurements (where available). The comprehensive 2D seismic dataset coupled with three 3D seismic cubes were utilized to map depth and thickness of key horizons, as well as large-scale structural influences such as faults and salt-structures (coherency attribute and fault interpretations). The sensitivity of seismic properties (e.g., P-impedance, V_P/V_S ratio) to differences in lithology, porosity, and fluids was determined using rock physics relationships and crossplots. AVO half-space modelling was used to theoretically test the sensitivity of prestack seismic data to different reservoir fluid contents.

Key outcomes

- Average reservoir parameters were quantified for all 15 wells, including net and gross thickness, shale volume, porosity, saturation, and N/G, also considering present and maximum burial depths.
- Site-specific findings relating to the first objective involve identification of trends in reservoir properties, which vary from central areas of the Egersund Basin compared to flank areas. For instance, we conclude that the younger, shallow-marine sandstone (Sandnes Formation) is a good reservoir target in the central part and southern flank of the basin near the hydrocarbon source pod, but deteriorates towards the north flank and Ling Depression. The time-equivalent Hugin Formation is excellent in terms of reservoir properties, but also very locally developed in the southwestern Ling Depression. The older, fluvial/coastal plain to deltaic deposits (Bryne Formation) have poorer quality due to porosity deterioration and heterogeneity in the central part, but improves in the shallower buried flank areas. Time-equivalent Sleipner Formation sandstones have intermediate thickness and reservoir properties in the Ling Depression, but thicknesses exceeding that observed in wells is

identified in seismic data near salt structures and faults, somewhat increasing the prospectivity.

- In response to the second objective, a good correlation between porosity and acoustic impedance was found in the area. In the case of oil, only the shallowest reservoir sandstones (2.55–2.65 km BSF) display a clear fluid effect.

4.1.2 Paper B

Organic content and maturation effects on elastic properties of source rock shales in the Central North Sea

Objectives and motivation

Source rock maturity and the corresponding degree of hydrocarbon generation and expulsion that has occurred, which may have been time-restricted, are important risk factors in basins with shallow source rock burial and/or a history of uplift. The principal objective of this paper was to investigate and quantify how organic content, compaction, and maturation influence the seismic properties of source rock shales. The motivation was to see the feasibility of using seismic inversion data to supplement the standard basin modelling procedures used for source rock evaluation.

Methods

Calibration data from the geochemical analysis were tied to measured well logs through theoretical relationships and further explored using suitable rock physics crossplots and templates (Fig. 15). Kerogen- and fluid-substitution modelling were performed to compare theoretical predictions with empirical observations. Established relationships were reviewed and compared to the database, in addition to proposing trends that describe the behaviour of shales as a function of organic content and maturity. Key formations were mapped on 2D seismic reflection data covering the entire study area to see present-day depth variations, and post-stack seismic inversion for P-impedance was performed on a 3D seismic cube covering parts of the Ling Depression.

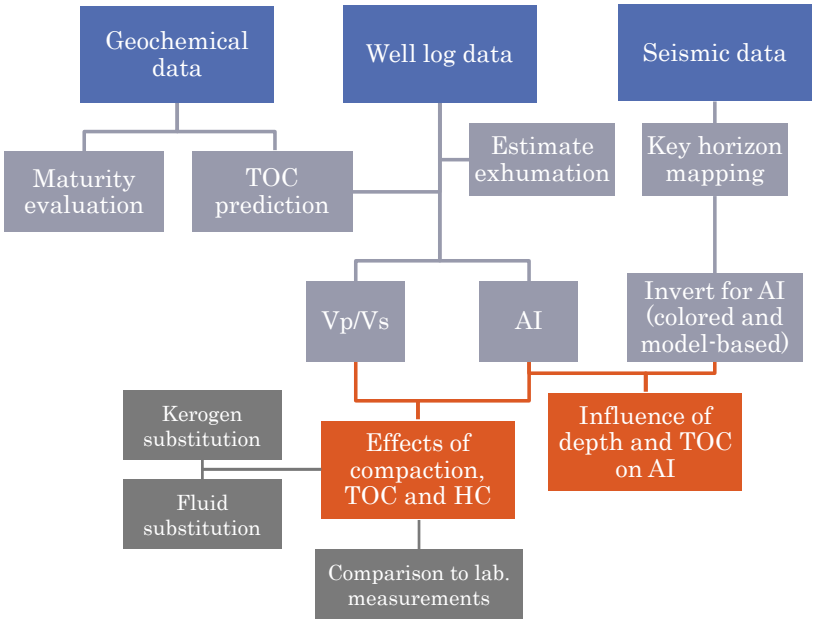

Figure 15: Workflow chart showing the methods applied in **Paper B**.

Key outcomes

- Compaction trends for both organic-lean and organic-rich shales are clearly defined in rock physics crossplots (i.e., increasing AI and decreasing V_P/V_S). The acoustic properties of an immature shale with a given composition at a certain depth is determined by TOC content, contributing to lower velocity and lower density (i.e., AI), and lower V_P/V_S ratio.
- A mature source rock shale, however, distinctly deviates from the compaction trends observed for immature shales with similar TOC. Coupled with a definite increase in resistivity, this indicates an ability to identify a fluid anomaly in mature source rocks (predominantly low values of V_P/V_S) similar to that observed in sandstones.
- Our observations are validated by geochemical data as calibration for organic content and level of maturation, as well as the values reported from ultrasonic laboratory measurements of V_P, V_S and density on Kimmeridge shale core samples (to eliminate upscaling issues). With access to suitable prestack seismic data, we would be able to further verify and test the sensitivity of our observations at the seismic scale, as well as consider issues related to anisotropy.

4.1.3 Paper C

Seal efficiency of Upper Jurassic organic-rich cap rock shales on the Norwegian Continental Shelf

Objectives and motivation

Barents Sea exploration efforts are characterized by many dry wells and technical discoveries, with a minority of commercial discoveries. The NPD states that the presence of a cap rock with sufficient sealing capacity is one of the critical factors for Jurassic plays in this uplifted region. On the other side, as discussed in **Paper B**, only limited amounts of hydrocarbons are assumed to have migrated from the source rock in the Egersund Basin in the Central North Sea. Excellent sealing capacity could in this case be necessary to compensate for small volumes. Similarly, cap rock integrity is a critical parameter in evaluations of prospects for CO_2 sequestration. The main objective of the study was to investigate the sealing efficiency of important cap rock formations on the NCS, using acoustic properties to tie with mineralogical composition, organic content, consolidation, and brittleness.

Methods

Bulk mineralogical composition based on XRD analysis was used to validate a comparison between Upper Jurassic clay-dominated shales in different provinces of the NCS. This includes data compiled from literature as well as seven in-house core/cutting samples. Thin-sections prepared from rock samples were examined to relate trends in the wireline logs to differences in texture and fabric in different stratigraphic levels in well 15/12-21 (Grevling) in the North Sea. Rock physics models were generated for different lithologies as a template for comparing with measured data. A high-quality, multi-azimuth prestack 3D seismic cube covering the Barents Sea Goliat field structure was utilized for understanding the geometry and structure of the Goliat field, identifying amplitude anomalies, and comparing seismic scale inversion data to rock physics models and trends observed in the well logs.

Key outcomes

- We propose a rock physics-based framework for understanding composition and sealing efficiency of shales based on acoustic (seismic) properties. We demonstrate distinct changes in velocity and/or density that differentiate changes in mineralogical or organic content, while considering compaction effects (building on our learnings described in **Paper B**).
- Upper Jurassic shale sealing capacity was found to be excellent, and would generally be discarded as a significant risk factor for hydrocarbon exploration when the sequence is present. Fault-intersections cutting the reservoir interval should, however, be considered a greater risk.
- Uplift is not found to necessarily compromise seal integrity, even when as substantial as in the northern part of the Barents Sea study area. We see indications that this is linked to the degree of consolidation and cementation prior to uplift, and consequently more ductile or brittle behaviour during stress-release.
- Concurring evidence that supports the proposed trends was presented from different scales, in multiple wells, and in two distinct areas of the Norwegian Continental Shelf, indicating that our observations are general for the Upper Jurassic shale succession rather than local features.

4.2 Discussion

Generally, time-equivalent formations in different areas of the North Sea and the southwestern Barents Sea behave very similarly in terms of acoustic properties, which reflects the broadly similar structural settings and depositional evolution through time (Section 1.3). Both the Middle Jurassic sandstones and, particularly, as shown in **Paper C**, the Upper Jurassic shale sequences reflect this observation based on the investigated database. These documented similarities

between different areas demonstrate the universality of our observations and minimize the potential for bias due to localized features.

4.2.1 Sandstone reservoir characterization and fluid sensitivity

Firstly, no existing studies comprehensively addressed quantified variations in reservoir properties within the Central North Sea study area prior to this work. Earlier adjacent works include facies analysis of Jurassic sandstones in the Egersund Basin (Mannie et al., 2014), structural influences on depositional patterns (Jackson et al., 2013; Mannie et al., 2016), petrographic analysis of Hugin Formation core samples in the southern Viking Graben (Maast et al., 2011), and sequence stratigraphic development of the Hugin Formation (Kieft et al., 2010).

More generally, separating oil-saturated and brine-saturated, cemented, dominantly fine-grained sandstones using acoustic properties was found unreliable, due to low fluid sensitivity even at fairly high porosity. For context, fluid separation only appears viable when targeting the shallowest traps in the Egersund Basin, or adjacent basins and highs (more than 22–24% porosity). It is valuable to possess the knowledge of when and where to apply quantitative seismic analysis, as exemplified in **Paper A** where sandstone porosities show good separation due to changes in acoustic impedance, whereas lithology shows a poor correlation. As such, more geologically driven approaches should be considered for further exploration of the area (e.g., basin modelling and seismic mapping of probable migration pathways), but seismic data can plausibly be utilized for mapping porosity. Public site-specific material on the hydrocarbon generation and migration is relatively sparse, but include, e.g., Ritter (1988) and Hermanrud et al. (1990). In turn, the proposed rock physics relationship and reservoir quality trends can be useful in evaluating carrier beds for hydrocarbon migration.

4.2.2 Organic-rich shale characterization

The work presented in **Paper B** builds on observations made by Løseth et al. (2011), who pioneered the use of seismic to quantitatively analyse conventional organic-rich shales as source rocks in terms of P-impedance and TOC. This is a

strong relationship when considering a very restricted depth range, due to the very low velocity and density of organic matter compared to rock-forming minerals. Our findings indicate that similar or improved relationships hold true for the combination of P-impedance and V_P/V_S-ratio, with added confidence due to the inherent expression of compaction (shale trends described in **Paper B**). Consequently, the framework may add to the potential for prestack seismic inversion analysis of source rocks. Our approach is inspired by the concept of locally constrained rock physics templates described in Section 2.4.1 for informed seismic characterization (Avseth et al., 2005). The possibility of going a step further, and simultaneously identify fluid anomalies associated with source rocks that are presently in the oil-window, was relatively sparsely explored using real data prior to our study. Our findings add a potential supplement to the standard basin modelling approach used for petroleum system analysis, which is extra valuable in regions where seismic fluid identification is uncertain. Existing studies were mostly focused on theoretical rock physics models, some of which derived for unconventional shale plays that widely differ in composition and organic content (Carcione and Avseth, 2015; Zhao et al., 2016; Ibrahim and Mukerji, 2017).

Furthermore, **Paper C** supplies a novel, locally consistent framework for characterizing the mineralogical composition and related brittleness of shales guided by rock physics. Methods that were proposed in earlier literature (e.g., Guo et al., 2013; Perez and Marfurt, 2014) are typically derived for quartz- and carbonate-rich shales located in the U.S. and China, and were found lacking to evaluate the clay-rich shales relevant to exploration of the NCS. Multiple leakage mechanisms related directly to the cap rock were considered in the study presented in **Paper C**. Micro-scale SEM analysis of core/cuttings from different shale intervals and calculations of capillary sealing capacity support the observations made in acoustic and petrophysical properties. More indirect (qualitative) means of predicting sealing efficiency have also been suggested in literature, for instance, direct correlations to seal thickness, which may be applicable when the capillary sealing capacity is poor. **Paper C** also addresses the relevance of seal quality in typical, faulted geological setup where leaking traps are well-documented.

Chapter 5
Concluding remarks

The essential output of this thesis revolves around integrating all the information we can acquire about lithology, porosity, organic content, depositional setting, and fluid content from petrophysical well logs, rock samples, and seismic (with rock physics as proxy). Overall, the research has improved our understanding of the effect of compaction, mineralogical composition, organic content, and maturation on the elastic properties of sandstones and shales. Furthermore, the work has culminated in site-specific contributions on reservoir quality, source rock quality, and seal integrity in the Central North Sea and the SW Barents Sea.

The thesis topic is "quantitative analysis", but many of the relationships described are only semi-quantiative in nature, which may lead to confusion. As a result of non-uniqueness due to too few geophysical properties compared to the possible geological scenarios, not everything can be assigned a number or cutoff threshold. A vital contributor to this non-uniqueness from a geological standpoint is the different effect that burial exerts on different lithologies. For instance, a high-TOC, immature source rock shale may display similar elastic properties as a mature, but less organic-rich shale of similar or different mineralogical composition. In turn, this organic-rich shale may be confused for a hydrocarbon-bearing sandstone, which has been the case even in rigorously planned QSI workflows (Avseth et al., 2016). This is nevertheless the relevant stage to incorporate rock physics, to aid a composite interpretation relative to, e.g., temperature, pressure, and depth, and establish the feasibility of quantitative seismic evaluation giving good results.

5.1 Outlook

Several possible directions for further research could be pursued from the findings in this thesis. Fluid sensitivity is a vital issue when discussing deeply buried sandstones, as for example, in the Egersund Basin where quartz cementation may be significant. Also established is the potential positive effect of clay coatings (e.g., Ehrenberg, 1993; Aase et al., 1996; Morad et al., 2010), which may inhibit such cementation, but this is not accounted for explicitly in the conventional sandstone rock physics models utilized in **Paper A** (see Section 2.4.1). The Hugin Formation in our database, for instance, displays a bi-modal porosity distribution that is typically a sign of clay coated intervals (Hansen et al., 2017). A more specialized, burial-consistent rock physics model scheme that incorporates textural parameters and cement predictions as a function of the time-temperature integral (Walderhaug model) could be used to investigate: 1) if the effect of grain size is significant enough on quartz cementation to be important for fluid sensitivity, and 2) if coating can be identified in acoustic and seismic data based on characteristics other than high porosity. The work would ideally be calibrated and validated with both core samples and seismic data to test consistency across the scales. Calibrating to samples from this particular study area could help further explore the overprediction of quartz cement volume in fine-grained sandstones (Lander et al., 2008). This partly also addresses the upscaling issue which can occur between core measurements (ultrasonic velocity, permeability, etc.) to well log resolution and finally going from well log to seismic scale. Existing preliminary petrographic analyses of sandstone samples should be followed up further, as it would be highly valuable to the proposed work.

On a different note, the fact that wells are often drilled on structural highs, rather than deeper in the basin near the typical hydrocarbon kitchen, is a limitation for source rock research. To expand on our findings in **Paper B**, a natural next step would be to broaden the range of organic-rich shale data to better understand mature and over-mature source rocks. Firstly, including wells located closer to the rift axis of the Viking Graben in the North Sea could give insight into a spectrum of oil-, late oil- and gas-mature source rock behaviour. Furthermore,

the Jurassic interval in the far southwestern sedimentary basins in the Barents Sea (Tromsø Basin and Bjørnøya Basin) varies significantly in burial depth over relatively short distances (Henriksen et al., 2011; Clark et al., 2014; Faleide et al., 2015). Given seismic coverage and the presence of Upper Jurassic organic-rich shales, these areas could be used to examine immature (<2.5–3.0 km) to overmature (>5–6 km) source rocks in a restricted study area.

Secondly, our findings would benefit from the availability of prestack seismic data and subsequent inverted acoustic impedance and V_P/V_S ratio to validate the upscaled well log and modelled results (as proposed in **Paper B**). Prestack seismic data covering *mature* source rocks exist for example around the Glitne field in the North Sea, and could be used to evaluate sensitivity to source rock maturation in AVO signature and/or inverted acoustic properties.

In conjunction with other works, **Paper C** established that faults should probably be considered the main risk factor in prospect analysis even when uplift is substantial. New advances in seismic acquisition enable resolution of small-scale faulting that was previously invisible (Faleide et al., 2019). Remote identification of small-scale faults and particularly fracturing is a great challenge for seal assessment. Such high-resolution data could be combined with well logs in presently shallow areas like the Hoop Fault Complex to see if the fracturing/faulting can be related to the petrophysics, using the rock physics relationships for seal characterization established by the current work (**Paper C**).

As discussed in both **Paper A** and **Paper B**, it is well-established that some of the challenges related to seismic fluid characterization arise from the distinctive acoustic and geological properties of organic-rich shales. The aforementioned confusion between hot shales and sandstones can, in some cases, be explained by the common assumption behind many fluid identification methods – that seismic anomalies are defined by a comparison to the signature of the dominantly expected surrounding lithology, i.e., brine-filled, grey, organic-lean shales. As we have shown (**Papers B** and **C**), this is far from the truth when considering shales with high organic content. As such, a case study where many conventional and modern fluid identification techniques were tested on the same dataset in a complex reservoir setting such as observed in the Goliat Field, where the cap rock consists

of organic-rich shales, could help identify the best approaches to evaluate Jurassic reservoirs on the NCS.

Bibliography

Aase, N. E., Bjørkum, P. A. and Nadeau, P. H. (1996). The role of grain-coating microquartz on preservation of reservoir porosity. *AAPG Bulletin*, **80**, 1654-1673.

Aki, K. and Richards, P. G. (1980). Quantitative Seismology. San Francisco, CA, U.S.: W.H. Freeman and Co.

Allan, A. M., Clark, A. C., Vanorio, T., Kanitpanyacharoen, W. and Wenk, H.-R. (2016). On the evolution of the elastic properties of organic-rich shale upon pyrolysis-induced thermal maturation. *GEOPHYSICS*, **81**, D263-D281.

Archie, G. (1942). The Electrical Resistivity Log as an Aid in Determining Some Reservoir Characteristics - SPE-942054-G. *Transactions of the AIME*, **146**, 54-62.

Asquith, G. and Krygowski, D. A. (2004). Basic well log analysis (second edition). *AAPG Methods in Exploration* (Vol. 16). Tulsa, OK, U.S.: The American Association of Petroleum Geologists.

Athy, L. F. (1930). Density, porosity, and compaction of sedimentary rocks. *AAPG Bulletin*, **14**, 1-24.

Avseth, P., Dvorkin, J., Mavko, G. and Rykkje, J. (2000). Rock physics diagnostic of North Sea sands: Link between microstructure and seismic properties. *Geophysical Research Letters*, **27**, 2761-2764.

Avseth, P., Janke, A. and Horn, F. (2016). AVO inversion in exploration — Key learnings from a Norwegian Sea prospect. *The Leading Edge*, **35**, 405-414.

Avseth, P. and Lehocki, I. (2016). Combining burial history and rock-physics modeling to constrain AVO analysis during exploration. *79th EAGE conference & exhibition conference proceedings* (pp. 5). Paris, France: European Association of Geoscientists & Engineers.

Avseth, P., Mavko, G., Dvorkin, J. and Mukerji, T. (2001). Rock Physics and Seismic Properties of Sands and Shales as a Function of Burial Depth. *SEG Technical Program Expanded Abstracts 2001* (pp. 4). Society of Exploration Geophysicists.

Avseth, P., Mukerji, T. and Mavko, G. (2005). Quantitative Seismic Interpretation: Applying Rock Physics Tools to Reduce Interpretation Risk. Cambridge, U.K.: Cambridge University Press.

Avseth, P., Mukerji, T., Mavko, G. and Dvorkin, J. (2010). Rock-physics diagnostics of depositional texture, diagenetic alterations, and reservoir

heterogeneity in high-porosity siliciclastic sediments and rocks — A review of selected models and suggested work flows. *GEOPHYSICS*, **75**, 75A31-75A47.

Baig, I., Faleide, J. I., Jahren, J. and Mondol, N. H. (2016). Cenozoic exhumation on the southwestern Barents Shelf: Estimates and uncertainties constrained from compaction and thermal maturity analyses. *Marine and Petroleum Geology*, **73**, 105-130.

Baig, I., Faleide, J. I., Mondol, N. H. and Jahren, J. (2019). Burial and exhumation history controls on shale compaction and thermal maturity along the Norwegian North Sea basin margin areas. *Marine and Petroleum Geology*, **104**, 61-85.

Barclay, F., Bruun, A., Rasmussen, K. B., Alfaro, J. C., Cooke, A., Cooke, D., et al. (2008). Seismic Inversion: Reading Between the Lines. *Oilfield Review*, **20**, 42-63.

Bjørkum, P. A. (1996). How important is pressure in causing dissolution of quartz in sandstones? *Journal of Sedimentary Research*, **66**, 147-154.

Bjørkum, P. A., Walderhaug, O. and Nadeau, P. H. (2001). Thermally driven porosity reduction: impact on basin subsidence. In P. M. Shannon, P. D. W. Haughton and D. V. Corcoran (Eds.), *The Petroleum Exploration of Ireland's Offshore Basins. Special Publications* (188, pp. 385-392). London, U.K.: The Geological Society of London.

Bjørlykke, K. (1998). Clay mineral diagenesis in sedimentary basins — a key to the prediction of rock properties. Examples from the North Sea Basin. *Clay Minerals*, **33**, 15-34.

Bjørlykke, K. (2015a). Petroleum Geoscience. From Sedimentary Environments to Rock Physics - Second Edition. Springer-Verlag Berlin Heidelberg.

Bjørlykke, K. (2015b). Compaction of Sedimentary Rocks: Shales, Sandstones and Carbonates. In K. Bjørlykke (Ed.), *Petroleum Geoscience. From Sedimentary Environments to Rock Physics - Second Edition* (pp. 351-360). Springer-Verlag Berlin Heidelberg.

Bjørlykke, K. and Egeberg, K. (1993). Quartz cementation in sedimentary basins. *AAPG Bulletin*, **77**, 1538-1548.

Bjørlykke, K., Ramm, M. and Saigal, G. C. (1989). Sandstone diagenesis and porosity modification during basin evolution. *Geologische Rundschau*, **78**, 243-268.

Bortfeld, R. (1961). Approximation to the reflection and transmission coefficients of plane longitudinal and transverse waves. *Geophysical Prospecting*, **9**, 485-503.

Buia, M., Cirone, C., Leutscher, J., Tarran, S. and Webb, B. (2010). Multi-azimuth 3D survey in the Barents Sea. *First Break*, **28**, 65-69.

Carcione, J. M. (2000). A model for seismic velocity and attenuation in petroleum source rocks. *GEOPHYSICS*, **65**, 1080-1092.

Carcione, J. M. (2001). AVO effects of a hydrocarbon source-rock layer. *GEOPHYSICS*, **66**, 419-427.

Carcione, J. M. and Avseth, P. (2015). Rock-physics templates for clay-rich source rocks. *GEOPHYSICS*, **80**, D481-D500.

Carman, P. C. (1937). Fluid flow through granular beds. *Transactions of the Institution of Chemical Engineers*, **15**, 150-156.

Castagna, J. P. (1993). AVO analysis-tutorial and review. In J. P. Castagna and M. Backus (Eds.), *Offset-Dependent Reflectivity – Theory and Practice of AVO Analysis. Investigations in Geophysics* (8, pp. Tulsa, OK, U.S.: Society of Exploration Geophysicists.

Castagna, J. P., Batzle, M. L. and Eastwood, R. L. (1985). Relationships between compressional-wave and shear-wave velocities in clastic silicate rocks. *GEOPHYSICS*, **50**, 571-581.

Castagna, J. P. and Swan, H. W. (1997). Principles of AVO crossplotting. *The Leading Edge*, **16**, 337-342.

Castagna, J. P., Swan, H. W. and Foster, D. J. (1998). Framework for AVO gradient and intercept interpretation. *GEOPHYSICS*, **63**, 948-956.

Chalmers, G. R., Bustin, R. M. and Power, I. M. (2012). Characterization of gas shale pore systems by porosimetry, pycnometry, surface area, and field emission scanning electron microscopy/transmission electron microscopy image analyses: Examples from the Barnett, Woodford, Haynesville, Marcellus, and Doig units. *AAPG Bulletin*, **96**, 1099-1119.

Chopra, S. and Marfurt, K. (2008). Seismic Attributes for Prospect Identification and Reservoir Characterization. *SEG Geophysical Developments Series* (11). Society of Exploration Geophysicists.

Chuhan, F. A., Kjeldstad, A., Bjørlykke, K. and Høeg, K. (2002). Porosity loss in sand by grain crushing. Experimental evidence and relevance to reservoir quality *Marine and Petroleum Geology*, **19**, 39–53.

Chuhan, F. A., Kjeldstad, A., Bjørlykke, K. and Høeg, K. (2003). Experimental compression of loose sands: Relevance to porosity reduction during burial in sedimentary basins. *Canadian Geotechnical Journal*, **40**, 995–1011.

Clark, S. A., Glørstad-Clark, E., Faleide, J. I., Schmid, D., Hartz, E. H. and Fjeldskaar, W. (2014). Southwest BarentsSea rift basin evolution: Comparing results from backstripping and time-forward modelling. *Basin Research*, **26**, 550-566.

Dembicki, H. (2017). Practical petroleum geochemistry for exploration and production. Elsevier.

Downey, M. W. (1984). Evaluating seals for hydrocarbon accumulations. *AAPG Bulletin*, **68**, 1752-1763.

Dræge, A., Jakobsen, M. and Johansen, T. A. (2006). Rock physics modelling of shale diagenesis. *Petroleum Geoscience*, **12**, 49-57.

Dvorkin, J. and Nur, A. (1996). Elasticity of high-porosity sandstones: Theory for two North Sea datasets. *GEOPHYSICS*, **61**, 1363-1370.

Dvorkin, J., Nur, A. and Yin, H. (1994). Effective properties of cemented granular materials. *Mechanics of Materials*, **18**, 351-366.

Ehrenberg, S. N. (1993). Preservation of anomalously high porosity in deeply buried sandstones by grain-coating chlorite: examples from the Norwegian Continental Shelf. *AAPG Bulletin*, **77**, 1260-1286.

Faleide, J. I., Bjørlykke, K. and Gabrielsen, R. H. (2015). Geology of the Norwegian Continental Shelf. In K. Bjørlykke (Ed.), *Petroleum Geoscience. From Sedimentary Environments to Rock Physics - Second Edition* (pp. 603-638). Springer-Verlag Berlin Heidelberg.

Faleide, J. I., Tsikalas, F., Breivik, A. J., Mjelde, R., Ritzmann, O., Engen, Ø., et al. (2008). Structure and evolution of the continental margin off Norway and the Barents Sea. *Episodes*, **31**, 82-91.

Faleide, T. S., Midtkandal, I., Planke, S., Corseri, R., Faleide, J. I., Serck, C. S. and Nystuen, J. P. (2019). Characterisation and development of Early Cretaceous shelf platform deposition and faulting in the Hoop area, southwestern Barents Sea—constrained by high-resolution seismic data. *Norwegian Journal of Geology*, **99**, 1-20.

Fawad, M., Mondol, N. H., Jahren, J. and Bjørlykke, K. (2011). Mechanical compaction and ultrasonic velocity of sands with different texture and mineralogical composition. *Geophysical Prospecting*, **59**, 697–720.

Fazlikhani, H., Fossen, H., Gawthorpe, R. L., Faleide, J. I. and Bell, R. E. (2017). Basement structure and its influence on the structural configuration of the northern North Sea rift. *Tectonics*, **36**, 1151-1177.

Folk, R. L. (1980). Petrology of Sedimentary Rocks. Hemphill Publishing Company.

Gardner, G. H. F., Gardner, L. W. and Gregory, A. R. (1974). Formation velocity and density – the diagnostic basics for stratigraphic traps. *GEOPHYSICS*, **39**, 770-780.

Gassmann, F. (1951). Uber die elastizitat poroser medien. *Vier. der Natur Gesellschaft*, **96**, 1-23.

Gautier, D. L. (2005). Kimmeridgian Shales Total Petroleum System of the North Sea Graben Province. *U.S. Geological Survey Bulletin*, **2204-C**, 1-24.

Greenberg, M. L. and Castagna, J. P. (1992). Shear-wave velocity estimation in porous rocks: theoretical formulation, preliminary verification and applications. *Geophysical Prospecting*, **40**, 195-209.

Grude, S., Dvorkin, J. and Landrø, M. (2015). Permeability variation with porosity, pore space geometry, and cement type: A case history from the Snøhvit field, the Barents Sea. *GEOPHYSICS*, **80**, D43-D49.

Guo, Z., Li, X.-Y., Liu, C., Feng, X. and Shen, Y. (2013). A shale rock physics model for analysis of brittleness index, mineralogy and porosity in the Barnett Shale. *Journal of Geophysics and Engineering*, **10**, 1-10.

Han, D. (1986). *Effects of porosity and clay content on acoustic properties of sandstones and unconsolidated sediments*. Retrieved from Stanford University.

Hansen, H. N., Løvstad, K., Müller, R. and Jahren, J. (2017). Clay coating preserving high porosities in deeply buried intervals of the Stø Formation. *Marine and Petroleum Geology*, **88**, 648-658.

Hashin, Z. and Shtrikman, S. (1963). A variational approach to the elastic behavior of multiphase materials. *Journal of the Mechanics and Physics of Solids*, **11**, 127-140.

Henriksen, E., Ryseth, A. E., Larssen, G. B., Heide, T., Rønning, K., Sollid, K. and Stoupakova, A. (2011). Tectonostratigraphy of the greater Barents Sea: Implications for petroleum systems. In A. M. Spencer, A. F. Embry, D. L. Gautier, A. V. Stoupakova and K. Sørensen (Eds.), *Arctic Petroleum Geology* (35, pp. 163-195). London: Geological Society, Memoirs.

Hermanrud, C., Eggen, S., Jacobsen, T., Carlsen, E. M. and Pallesen, S. (1990). On the accuracy of modelling hydrocarbon generation and migration: The Egersund Basin oil find, Norway. *Organic Geochemistry*, **16**, 389-399.

Ibrahim, M. A. and Mukerji, T. (2017). *Thermal maturation effects on the elastic properties of organic rich mudrocks*. Paper presented at 87th Annual International Meeting, SEG, Houston, Texas, USA.

Jackson, C. A.-L., Chua, S.-T., Bell, R. E. and Magee, C. (2013). Structural style and early stage growth of inversion structures: 3D seismic insights from the Egersund Basin, offshore Norway. *Journal of Structural Geology*, **46**, 167-185.

Jordt, H., Faleide, J. I., Bjørlykke, K. and Ibrahim, M. T. (1995). Cenozoic sequence stratigraphy of the central and northern North Sea Basin: tectonic

development, sediment distribution and provenance areas. *Marine and Petroleum Geology*, **12**, 845-879.

Kieft, R. L., Jackson, C. A.-L., Hampson, G. J. and Larsen, E. (2010). Sedimentology and sequence stratigraphy of the Hugin Formation, Quadrant 15, Norwegian sector, South Viking Graben. In B. A. Vining and S. C. Pickering (Eds.), *Petroleum Geology: From Mature Basins to New Frontiers – Proceedings of the 7th Petroleum Geology Conference* (pp. 157-176). London: Geological Society.

Kozeny, J. (1927). Ueber kapillare Leitung des Wassers im Boden. *Wiener Academie der Wissenschaften*, **136**, 271-306.

Krief, M., Garat, J., Stellingwerff, J. and Ventre, J. (1990). A petrophysical interpretation using the velocities of P and S waves (full-waveform sonic). *Log Analyst*, **31**, 355-369.

Lander, R. H., Larese, R. E. and Bonnell, L. (2008). Toward more accurate quartz cement models: The importance of euhedral versus noneuhedral growth rates. *AAPG Bulletin*, **92**, 1537-1563.

Lander, R. H. and Walderhaug, O. (1999). Predicting Porosity through Simulating Sandstone Compaction and Quartz Cementation. *AAPG Bulletin*, **83**, 433-449.

Larionov, V. (1969). Radiometry of boreholes (in Russian). *Nedra, Moscow*.

Larsen, V. B. (1987). A synthesis of tectonically-related stratigraphy in the North Atlantic-Arctic region from Aalenian to Cenomanian time. *Norwegian Journal of Geology*, **67**, 281-293.

Li, Y., Guo, Z., Liu, C., Li, X.-Y. and Wang, G. (2015). A rock physics model for the characterization of organic-rich shale from elastic properties. *Petroleum Science*, **12**, 264-272.

Løseth, H., Wensaas, L., Gading, M., Duffaut, K. and Springer, M. (2011). Can hydrocarbon source rocks be identified on seismic data? *Geology*, **39**, 1167-1170.

Maast, T. E., Jahren, J. and Bjørlykke, K. (2011). Diagenetic controls on reservoir quality in Middle to Upper Jurassic sandstones in the South Viking Graben, North Sea. *AAPG Bulletin*, **95**, 1937-1958.

Mannie, A. S., Jackson, C. A.-L. and Hampson, G. J. (2014). Structural controls on the stratigraphic architecture of net-transgressive shallow-marine strata in a salt-influenced rift basin: Middle-to-Upper Jurassic Egersund Basin, Norwegian North Sea. *Basin Research*, **26**, 675-700.

Mannie, A. S., Jackson, C. A.-L., Hampson, G. J. and Fraser, A. J. (2016). Tectonic controls on the spatial distribution and stratigraphic architecture of a net-transgressive shallow-marine synrift succession in a salt-influenced rift

basin: Middle to Upper Jurassic, Norwegian Central North Sea. *Journal of the Geological Society*, **173**, 901-915.

Mavko, G., Mukerji, T. and Dvorkin, J. (2009). The rock physics handbook: Tools for seismic analysis of porous media - Second edition. Cambride, U.K.: Cambridge University Press.

Meyer, B. L. and Nederlof, M. H. (1984). Identification of source rocks on wireline logs by density/resistivity and sonic transit time/resistivity crossplots. *AAPG Bulletin*, **68**, 121-129.

Mindlin, R. D. (1949). Compliance of elastic bodies in contact. *Journal of Applied Mechanics*, **16**, 259-268.

Mondol, N. H. (2009). *Porosity and permeability development in mechanically compacted silt-kaolinite mixtures*. Paper presented at SEG Technical Program Expanded Abstracts 2009, Society of Exploration Geophysicists, Houston, TX, U.S.

Mondol, N. H., Bjørlykke, K. and Jahren, J. (2008). Experimental compaction of clays: relationship between permeability and petrophysical properties in mudstones. *Petroleum Geoscience*, **14**, 319-337.

Mondol, N. H., Bjørlykke, K., Jahren, J. and Høeg, K. (2007). Experimental mechanical compaction of clay mineral aggregates—Changes in physical properties of mudstones during burial. *Marine and Petroleum Geology*, **24**, 289-311.

Morad, S., Al-Ramadan, K., Ketzer, J. M. and De Ros, L. F. (2010). The impact of diagenesis on the heterogeneity of sandstone reservoirs: A review of the role of depositional facies and sequence stratigraphy. *AAPG Bulletin*, **94**, 1267-1309.

Mulrooney, M. J., Osmond, J., Skurtveit, E., Wu, L. and Braathen, A. (2018). Smeaheia, A Potential Northern North Sea CO2 Storage Site: Structural Description And De-Risking Strategies. *Fifth CO2 Geological Storage Workshop* (pp. 5). Utrech, Netherlands: European Association of Geoscientists and Engineers.

NPD, 2014. The 2014 Norwegian Petroleum Directorate lithostratigraphic charts, http://www.npd.no/en/Topics/Geology/Lithostratigraphy/. last updated 5. November 2014.

NPD, 2020. Norwegian Petroleum Directorate FactPages, http://factpages.npd.no/factpages/.

Nur, A., Marion, D. and Yin, H. (1991). Wave velocities in sediments. In J. M. Hovem, M. D. Richardson and R. D. Stoll (Eds.), *Shear Waves in Marine Sediments* (pp. 131-140). Dordrecht, Netherlands: Kluwer Academic Publishers.

Nur, A., Mavko, G., Dvorkin, J. and Galmudi, D. (1998). Critical porosity: A key to relating physical properties to porosity in rocks. *The Leading Edge*, **17**.

Passey, Q. R., Creaney, S., Kulla, J. B., Moretti, F. J. and Stroud, J. D. (1990). A practical model for organic richness from porosity and resistivity logs. *AAPG Bulletin*, **74**, 1777-1794.

Pedersen, J. H., Karlsen, D. A., Backer-Owe, K., Lie, J. E. and Brunstad, H. (2006). The geochemistry of two unusual oils from the Norwegian North Sea: implications for new source rock and play scenario. *Petroleum Geoscience*, **12**, 85-96.

Pedersen, L. B., Bastiani, M. and Dynesius, L. (2005). Groundwater exploration using combined controlled-source and radiomagnetotelluric techniques. *GEOPHYSICS*, **70**, G8-G15.

Peltonen, C., Marcussen, Ø., Bjørlykke, K. and Jahren, J. (2009). Clay mineral diagenesis and quartz cementation in mudstones: The effects of smectite to illite reaction on rock properties. *Marine and Petroleum Geology*, **26**, 887-898.

Perez, R. and Marfurt, K. (2014). Mineralogy-based brittleness prediction from surface seismic data: Application to the Barnett Shale. *Interpretation*, **2**, T255-T271.

Ramm, M. and Bjørlykke, K. (1994). Porosity/depth trends in reservoir sandstones: Assessing the quantitative effects of varying pore-pressure, temperature history and mineralogy, Norwegian Shelf data. *Clay Minerals*, **29**, 475-490.

Raymer, L. L., Hunt, E. R. and Gardner, J. S. (1980). An improved sonic transit time-to-porosity transform. *Transactions of the Society of Professional Well Log Analysts*, **21st Annual Logging Symposium, Paper P.**

Riis, F. and Fjeldskaar, W. (1992). On the magnitude of the Late Tertiary and Quaternary erosion and its significance for the uplift of Scandinavia and the Barents Sea. In R. M. Larsen, H. Brekke, B. T. Larsen and E. Talleraas (Eds.), *Structural and Tectonic Modelling and its Application to Petroleum Geology. Norwegian Petroleum Society Special Publication* (Vol. 1, pp. 163-185). Amsterdam, Netherlands: Elsevier.

Ritter, U. (1988). Modelling of hydrocarbon generation patterns in the Egersund Sub-Basin, North Sea. *Advances in Organic Geochemistry*, **13**, 165-174.

Rutherford, S. R. and Williams, R. H. (1989). Amplitude-versus-offset variations in gas sands. *GEOPHYSICS*, **54**, 680-688.

Rüger, A. (1997). P-wave reflection coefficients for transversely isotropic models with vertical and horizontal axis of symmetry. *GEOPHYSICS*, **62**, 713-722.

Sayers, C. (2013a). The effect of kerogen on the elastic anisotropy of organic-rich shales. *GEOPHYSICS*, **78**, D65-D74.

Sayers, C. (2013b). The effect of kerogen on the AVO response of organic-rich shales. *The Leading Edge*, **32**, 1514-1519.

Shuey, R. T. (1985). A simplification of the Zoeppritz equations. *GEOPHYSICS*, **50**, 609-614.

Simm, R. and Bacon, M. (2014). Seismic amplitude - An interpreter's handbook. Cambridge University Press.

Smith, G. C. and Gidlow, P. M. (1987). Weighted stacking for rock property estimation and detection of gas. *Geophysical Prospecting*, **35**, 993-1014.

Sondergeld, C. H. and Rai, C. S. (2011). Elastic anisotropy of shales. *The Leading Edge*, **30**, 324-331.

Sondergeld, C. H., Rai, C. S., Margesson, R. W. and Whidden, K. J. (2000). *Ultrasonic measurement of anisotropy on the Kimmeridge Shale*. Paper presented at 70th Annual International Meeting, SEG.

Soupious, P. M., Kouli, M., Vallianatos, F., Vafidis, A. and Stavroulakis, G. (2007). Estimation of aquifer hydraulic parameters from surficial geophysical methods: A case study of Keritis Basin in Chania (Crete – Greece). *Journal of Hydrogeology*, **388**, 122-131.

Thomsen, L. (1986). Weak elastic anisotropy. *GEOPHYSICS*, **51**, 1954-1966.

Thyberg, B. and Jahren, J. (2011). Quartz cementation in mudstones: sheet-like quartz cement from clay mineral reactions during burial. *Petroleum Geoscience*, **17**, 55-63.

Torsvik, T. H., Carlos, D., Mosar, J., Cocks, R. M. and Malme, T. N. (2002). Global reconstructions and North Atlantic paleogeography 440 Ma to Recent. In E. A. Eide (Ed.), *Mid Norway Plate Reconstructions Atlas with Global and Atlantic Perspectives* (pp. 18-39). Geological Survey of Norway.

Vadakkepuliyambatta, S., Bünz, S., Mienert, J. and Chand, S. (2013). Distribution of subsurface fluid-flow systems in the SW Barents Sea. *Marine and Petroleum Geology*, **43**, 208-221.

Vernik, L. (2016). Seismic petrophysics in Quantitative Interpretation. Society of Exploration Geophysicists.

Vernik, L. and Kachanov, M. (2010). Modeling elastic properties of siliciclastic rocks. *GEOPHYSICS*, **75**, E171-E182.

Vernik, L. and Landis, C. (1996). Elastic anisotropy of source rocks-implications for hydrocarbon generation and primary migration. *AAPG Bulletin*, **80**, 531-544.

Vernik, L. and Milovac, J. (2011). Rock physics of organic shales. *The Leading Edge*, **30**, 318-323.

Vernik, L. and Nur, A. (1992a). Ultrasonic velocity and anisotropy of hydrocarbon source rocks. *GEOPHYSICS*, **57**, 727-735.

Vernik, L. and Nur, A. (1992b). Petrophysical classification of siliciclastics for lithology and porosity prediction from seismic velocities. *AAPG Bulletin*, **76**, 1295-1309.

Walderhaug, O. (1996). Kinetic Modeling of Quartz Cementation and Porosity Loss in Deeply Buried Sandstone Reservoirs. *AAPG Bulletin*, **80**, 731-745.

Wentworth, C. K. (1922). A Scale of Grade and Class Terms for Clastic Sediments. *Journal of Geology*, **30**, 377-392.

Zhao, L., Qin, X., Han, D.-H., Geng, J., Yang, Z. and Cao, H. (2016). Rock-physics modeling for the elastic properties of organic shale at different maturity stages. *GEOPHYSICS*, **81**, D527-D541.

Zoeppritz, K. (1919). Erdbebenwellen VIIIB, On the reflection and propagation of seismic waves. *Göttinger Nachr*, **I**, 66-84.

Ødegaard, E. and Avseth, P. (2004). Well log and seismic data analysis using rock physics templates. *First Break*, **23**, 37-43.

Øygarden, B., Løseth, H. and Njerve, S. (2015). Rock properties of smectite- and ooze-rich claystones. *GEOPHYSICS*, **80**, D89-D98.

Part II
Journal Papers

Paper A

Reservoir assessment of Middle Jurassic sandstone-dominated formations in the Egersund Basin and Ling Depression, eastern Central North Sea

Jørgen André Hansen
Nazmul Haque Mondol
Jens Jahren
Filippos Tsikalas

Marine and Petroleum Geology, 2020

Marine and Petroleum Geology 111 (2020) 529–543

Contents lists available at ScienceDirect

Marine and Petroleum Geology

journal homepage: www.elsevier.com/locate/marpetgeo

Research paper

Reservoir assessment of Middle Jurassic sandstone-dominated formations in the Egersund Basin and Ling Depression, eastern Central North Sea

Jørgen André Hansen[a,*], Nazmul Haque Mondol[a,b], Jens Jahren[a], Filippos Tsikalas[c,a]

[a] Department of Geosciences, University of Oslo, P.O. Box 1047, Blindern, NO-0316, Oslo, Norway
[b] Norwegian Geotechnical Institute (NGI), P.O. Box 3930, Ullevaal Stadion, NO-0806, Oslo, Norway
[c] Vår Energi AS, P.O. Box 101, Forus, NO-4064, Stavanger, Norway

ARTICLE INFO

Keywords:
Norwegian Central North Sea
Reservoir quality
Jurassic sandstone
Depositional trends
Compaction
Cementation
Fluid sensitivity
Seismic

ABSTRACT

Reservoir quality assessment was conducted from petrophysical analysis and rock physics diagnostics on 15 wells penetrating Middle Jurassic sandstone reservoir formations in different regions of the eastern Central North Sea. Seismic interpretation on available 3D and 2D seismic reflection data was utilized to map thickness variations and to draw broad correlations to structural features such as salt structures and faults. In the central Egersund Basin, the Sandnes Formation shows good reservoir properties (gross thickness = 107–147 m, N/G = 33–53%) while the Bryne Formation exhibits poorer reservoir quality (N/G < 20%). Both formations display variable reservoir properties and thicknesses on the northern flank of the Egersund Basin and in the Ling Depression (Sandnes Formation: gross thickness 16–26 m, N/G = 11–81%; Bryne Formation: 30–221 m, N/G = 25–70%). The time-equivalent Hugin and Sleipner formations are more locally developed in the southwest part of Ling Depression, and display good-to-excellent and intermediate reservoir quality, respectively. Furthermore, we use the outcomes of the conducted analyses to correlate observations to further exploration on various reservoir target formations and on seismic prediction of reservoir properties. Thus, the risk on reservoir presence and efficiency for the chased targets is considerably reduced. The main remaining risks within the study area are related to source rocks, their maturity, expulsion and migration of hydrocarbon, and the timing of trap formation.

1. Introduction

The North Sea, offshore Norway (Fig. 1a), is a mature oil and gas province which has been open for exploration since the mid 1960's. Still, the giant Johan Sverdrup field (Fig. 1b) was discovered as late as 2010. Existing fields are predominantly located on the flanks of the Jurassic-Cretaceous rift system, including the Viking, Central and Sogn grabens. These are sourced primarily by Late Jurassic source rock shales (Kimmeridge Clay Formation equivalents) which are mature in the deeper parts of the rift grabens. Large areas between the grabens and the platforms close to mainland Norway are, however, much more sparsely drilled (Fig. 1b). One of the main reasons for lower exploration activity is uncertainty associated with the maturity of the Jurassic source rock shales in this region, namely the time-equivalent Draupne and Tau Formations (Figs. 1c and 2).

The current study area encompasses basin regions around the Sele High, namely the Ling Depression, Egersund Basin, and parts of the Åsta Graben (Fig. 1). The target area is bounded by the Stavanger Platform to the east, Utsira High and Patch Bank Ridge to the north and northwest, and the Jæren and Sørvestlandet highs towards southwest (Fig. 1b). In the study area, the burial depth of the source rock is shallower than within the Viking Graben, and fluctuates around the depths and temperatures associated with the onset of hydrocarbon generation (Hansen et al., 2019). Certain important discoveries (mostly in the Egersund Basin) do however provide evidence of local source rock maturation and expulsion, although it has been described as limited in quantity (Ritter, 1988; Hermanrud et al., 1990). These discoveries include the Yme (9/2-1), Vette (17/12-1), Brisling (17/12-2), Mackerel (18/10-1) in the Egersund Basin, and Bark (17/3-1), Storskrymten (15/12-18S) and Grevling (15/12-21) in the Ling Depression (Fig. 1b). In the case of the SW Ling Depression, e.g., the Grevling discovery (quadrant 15), hydrocarbon migration from deeper Viking Graben regions is potentially more probable than a locally mature source rock due to the graben proximity.

Studies that specifically consider reservoir property variations are rare within and in the vicinity of the study area; however, Mannie et al.

* Corresponding author.
E-mail address: j.a.hansen@geo.uio.no (J.A. Hansen).

https://doi.org/10.1016/j.marpetgeo.2019.08.044
Received 10 April 2019; Received in revised form 22 August 2019; Accepted 23 August 2019
Available online 26 August 2019

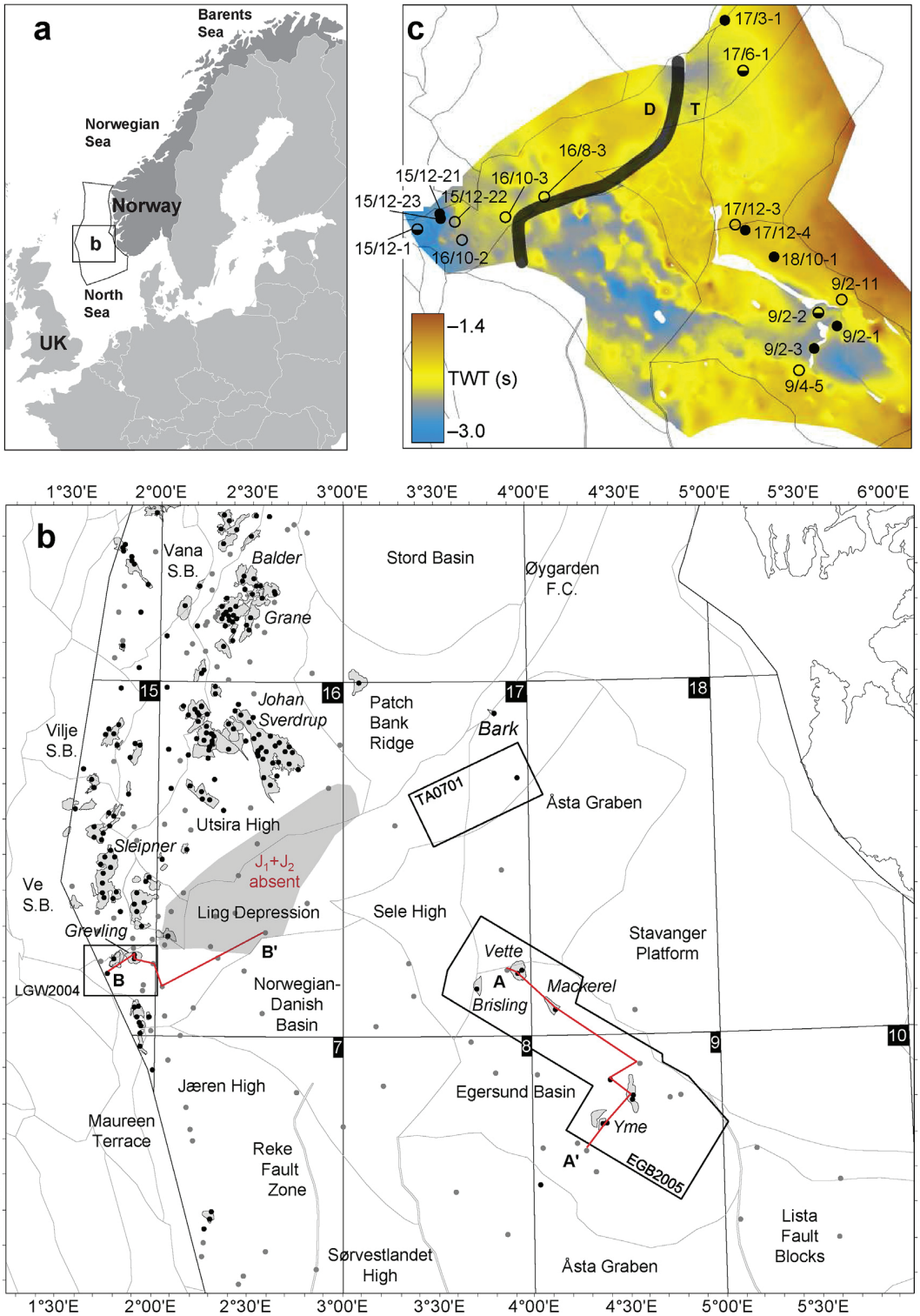

Fig. 1. (a) Location map of the greater study area situated within the Norwegian sector of the North Sea petroleum province (thin black outline). (b) Map outlining the Norwegian Central North Sea and South Viking Graben structural elements (NPD, 2019), with discoveries marked as light grey shading and exploration wells represented by points (grey = dry, black = discovery or hydrocarbon shows). 3D seismic surveys are outlined in black. Dark grey shading indicates absence of the Middle Jurassic reservoir formations within the study area. Red lines represent well correlation panels A–A′ and B–B′ (Fig. 5). (c) Wells selected for detailed investigation in this study, superimposed on the top Tau/Draupne Formation time surface indicating basin geometries. (For interpretation of the references to color in this figure legend, the reader is referred to the Web version of this article.)

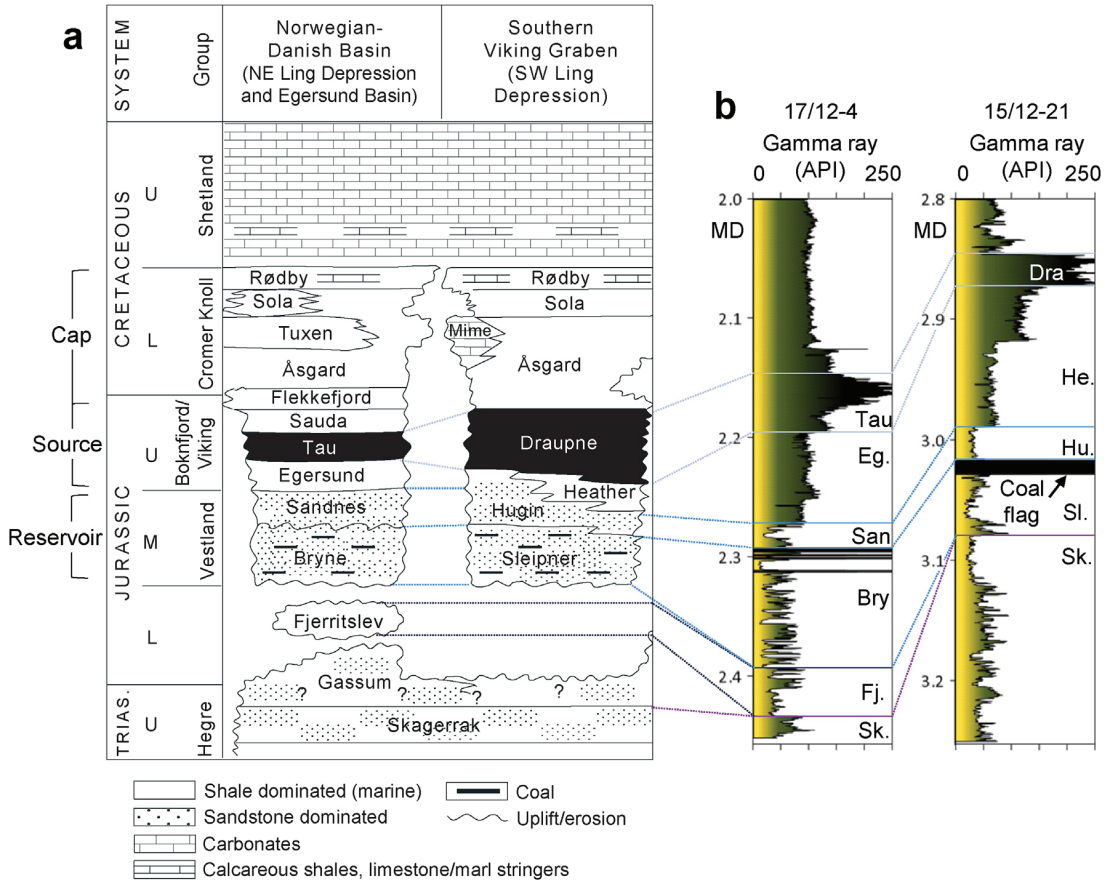

Fig. 2. (a) Upper Triassic–Upper Cretaceous lithostratigraphic chart (modified from Hansen et al., 2019), separated approximately along the black line in Fig. 1c. (b) Correlation of lithostratigraphy in two wells within the study area, 17/12-4 in the Egersund Basin, and 15/12-21 in the SW Ling Depression.

(2014) provide a facies analysis of commonly targeted Middle Jurassic reservoirs formations in the Egersund Basin. Additionally, detailed investigations of structural and halokinetic influences on deposition of relevant sedimentary units are demonstrated by Jackson et al. (2013) and Mannie et al. (2014, 2016). Furthermore, Kieft et al. (2010) studied the sedimentology and sequence stratigraphic development of the Hugin Formation in the South Viking Graben, adjacent to the northwestern border of the study area. Maast et al. (2011) on the other hand performed point-count analysis on 25 core samples from Hugin Formation sandstones in deeper parts of the South Viking Graben.

Reservoir quality is controlled by the burial (and thermal) history of the sediment, which drives porosity loss associated with different compaction mechanisms. The degree of mechanical compaction is a function of the sediment composition, grain size, and textural parameters, and relates closely to the depositional environment. Diagenetic processes, i.e., dissolution and precipitation of minerals (cementation), are chemical reactions driven by temperature and mineral stability (Bjørlykke et al., 1989; Peltonen et al., 2009). These occur over a wide range of depths and temperatures, and can have important implications on reservoir heterogeneity. Some diagenetic processes can also be porosity-preserving, e.g., formation of clay coats and dissolution of early precipitated carbonate cement (Morad et al., 2010).

A thorough reservoir characterization can be valuable to highlight any systematic variations in reservoir quality and extent in connection to areas where hydrocarbon generation and expulsion is suspected to have occurred. Even smaller discoveries in the North Sea can potentially be economically viable, when they are less remote and potentially closer to existing infrastructure. That is indeed the driver and motivation for the current study, with the conducted reservoir quality analysis of sand-prone Middle Jurassic units. We have applied an integrated approach of petrophysical analysis of well log data, rock physics diagnostics, and interpretation and attribute analysis of 3D seismic data to characterize potential reservoirs in the study area.

2. Geological setting and lithostratigraphy

The North Sea basin structure has been largely defined by two major rifting phases; the Late Paleozoic and the Late Jurassic-Early Cretaceous (Faleide et al., 2008). Additionally, the area has been subjected to exhumation in multiple phases; most recently in response to Oligocene and Miocene uplift of southern Norway and laterally variable Plio-Pleistocene glacial erosion (Jordt et al., 1995; Baig et al., 2019). The Norwegian-Danish Basin and second-order structural elements (e.g., Ling Depression and Egersund Basin; Fig. 1b) are mainly Late Paleozoic–Triassic features, less influenced by the characteristic North Sea Jurassic rifting, but have been affected by halokinesis (Fig. 3; Faleide et al., 2015).

The Jurassic sandstone-dominated formations in the Central North Sea area are part of the Vestland Group. In the southern and eastern part of the study area these are referred to as Bryne and Sandnes formations, which are broadly time-equivalent to the Sleipner and Hugin formations (Fig. 2). The latter two formations are present in the southwestern Ling Depression, and extend farther towards the north. For easier separation according to age, the older and younger formations are sometimes herein denoted $\mathbf{J_1}$ (Bryne and Sleipner formations) and $\mathbf{J_2}$ (Sandnes and Hugin formations), respectively. J_1 represents fluvial, deltaic and coastal plain deposits, whereas the J_2 interval can broadly be characterized as a result of shallow marine, nearshore

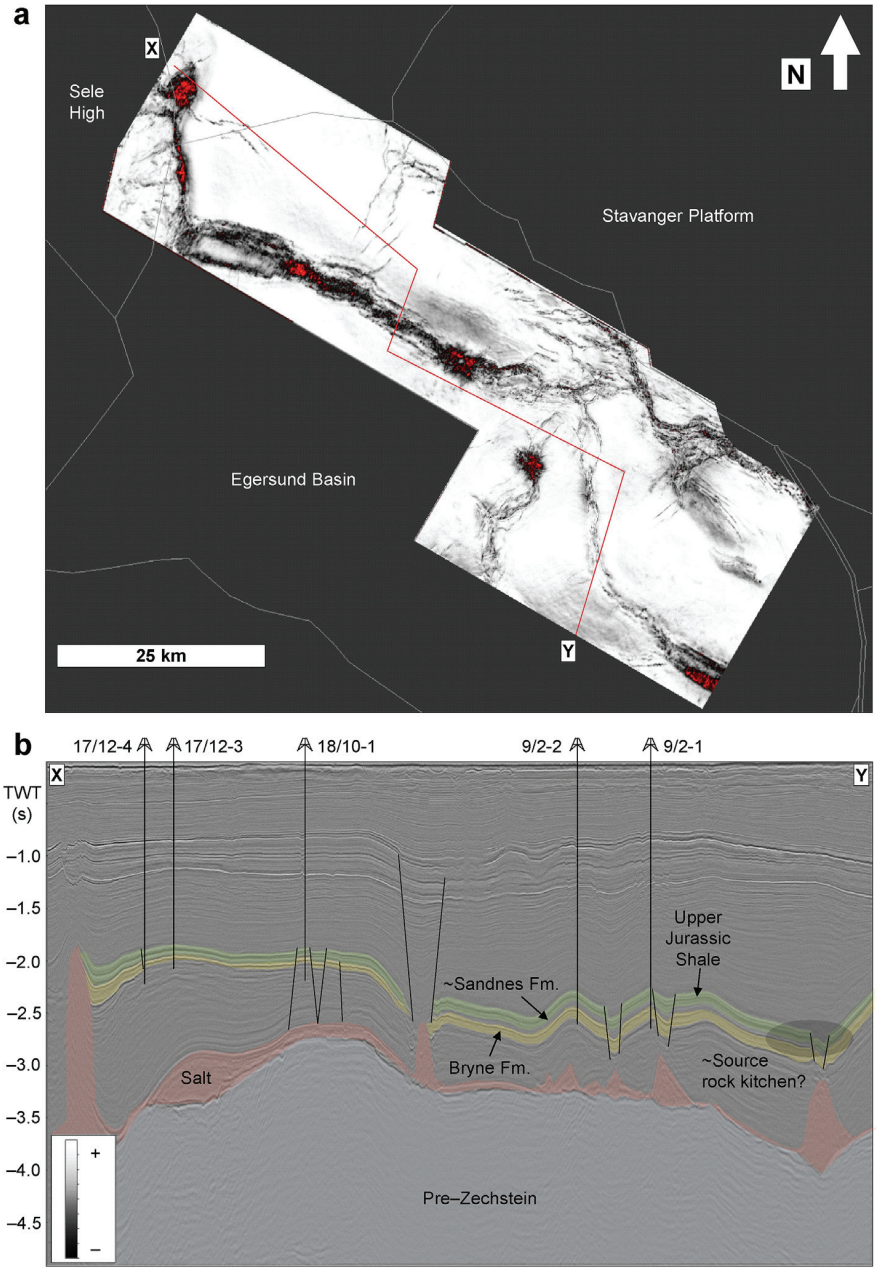

Fig. 3. Example from Egersund Basin seismic survey where the top Bryne Formation variance map (a) broadly indicates large scale structural elements (Sele High and Stavanger Platform), individual faults and fault zones, salt walls and salt diapirs. Cross section X–Y (b) illustrates general basin geometry and interaction between faults and salt structures; see Fig. 1c for lateral depth variation in the Jurassic section.

deposition (Vollset and Doré, 1984; Mannie et al., 2014).

Despite the similarities in depositional facies on time-equivalent formations, there are some differences in provenance. In particular, the Sandnes and Bryne formations are predominantly sourced from elevated areas towards the south and east, e.g., the Stavanger Platform and Norwegian mainland (Mannie et al., 2014), and the early Bryne Formation deposition started in the Egersund Basin prior to Bathonian-Oxfordian flooding of the North Sea Basin (Halland et al., 2011). On the contrary, the Hugin and Sleipner formations are more directly related to the transgression of the South Viking Graben and the accompanying southward retreat of the Brent Delta (e.g., Folkestad and Satur, 2008 and references therein). They are characterized by laterally different ages and controls on depositional patterns, and are potentially affected by Jurassic rifting to a greater degree than the Bryne and Sandnes formations (Folkestad and Satur, 2008; Kieft et al., 2010). Only the southernmost extent of these formations coincide with the study area, where the Hugin Formation consists mainly of deltaic wave-to tidal-influenced shoreline deposits that interfinger with continental facies of the underlying Sleipner Formation and the fine-grained marine deposits of the overlying Heather or Draupne formations (Kieft et al., 2010, Fig. 2).

Lower-Middle Jurassic and Triassic sediments are absent in certain regions of the Central North Sea due to erosion and/or non-deposition on structural highs, or due to uplift of the Mid-North Sea Dome during Early Jurassic (Ziegler, 1992; Mannie et al., 2014). This is evident for instance in the region around well 16/8-3 (Lupin) in the Ling Depression where none of the formations of interest are encountered (Fig. 1b). An elevated north-south trending structure between the Utsira High and

Table 1
Overview of well database selected for the study. Note availability of shear wave velocity (V_S). Prospect names (for discoveries and dry wells alike) are noted to ease further references to individual wells.

Well	Prospect	Area	Content	TD (m)	TVD (m)	Exhumation (m)	Seismic survey	Year drilled	V_S
9/4-5	–	EGB	Dry	5881	5874	250	2D	2006	–
9/2-3	Yme	EGB	Oil	3424	3421	300	EGB2005	1990	–
9/2-2	–	EGB	Oil shows	3577	3548	500	EGB2005	1987	–
9/2-1	Yme	EGB	Oil	3756	3755	500	EGB2005	1987	–
9/2-11	Aubrey	EGB	Dry	2861	2836	620	EGB2005	2010	✓
18/10-1	Mackerel	EGB	Oil	2800	–	450	EGB2005	1980	–
17/12-3	Vette (Bream)	EGB	Dry	2730	–	375	EGB2005	1980	–
17/12-4	Vette (Bream)	EGB	Oil	2470	2470	400	EGB2005	2009	✓
17/6-1	Svaneøgle	NE Ling D.	Oil shows	3065	3064	550	TA0701	2011	✓
17/3-1	Bark	NE Ling D.	Gas	2852	2852	500	2D	1995	–
16/10-2	–	SW Ling D.	Dry	3150	3148	–	2D	1991	–
15/12-21	Grevling	SW Ling D.	Oil	3310	3310	–	LGW2004	2009	✓
15/12-22	Storkollen	SW Ling D.	Dry	3035	3035	–	LGW2004	2010	✓
15/12-23	Grevling	SW Ling D.	Oil	3485	3478	–	LGW2004	2010	✓
15/12-1	–	SW Ling D.	Oil shows	3269	3269	–	2D	1975	–

EGB = Egersund Basin; NE Ling D. = Northeast Ling Depression; SW Ling D. = Southwest Ling Depression.

the Jæren High was prominent in this region during Bathonian and Callovian times (Folkestad and Satur, 2008).

3. Database and methods

The utilized database consists of 15 vertical or near-vertical exploration wells distributed across the study area, as well as many 2D seismic lines and three 3D seismic cubes (Fig. 1b; Table 1). Additionally, core plug measurements of porosity and permeability were compiled from public reports obtained via Diskos (NPD, Norwegian Petroleum Directorate). The database was selected to cover a wide range of reservoir depths, and to cover regions of interest for hydrocarbon exploration either where there are possibilities for external migration or signs of locally mature source rock (Hansen et al., 2019). Firstly, the reservoir formations were classified in terms of lithology, porosity and fluid content from petrophysical well log data, using consistent net-to-gross definitions based on suitable cutoff-values.

Due to different depositional environments and the fact that potential flow barriers such as thin shales and coal layers are commonly observed between the J_1 and J_2 formations (Fig. 2), these are treated as separate reservoir sections in the conducted petrophysical analysis. The Hugin and Sleipner formations are additionally more locally developed and do not always coincide (missing from wells 15/12-23 and 15/12-22, respectively). We also present cumulative or total reservoir thicknesses and properties, i.e., the combination of J_1 and J_2. To predict maximum sandstone burial depth, exhumation magnitude was estimated based on velocity–depth data compared to experimental (normal) compaction trends and published estimates (e.g., Doré and Jensen, 1996; Mondol et al., 2008; Kalani et al., 2015a; Hansen et al., 2017; Baig et al., 2019).

Shale volume (V_{sh}) was calculated using the gamma-ray log and corrected after Larionov (1969) for older rocks, and supplemented with interpretations of properly scaled neutron-density overlays where applicable. Porosity (Φ) was estimated from the average of neutron porosity (Φ_N) and porosity from density (Φ_D), calculated as

$$\Phi = \sqrt{[(\Phi_D^2 + \Phi_N^2)/2]}, \quad (1)$$

and subsequently quality controlled by comparing with core plug porosity where available (Fig. 4). Coal layers, particularly common in the Bryne and Sleipner formations, were excluded based on distinctive density, neutron and sonic signatures. Similarly, carbonate cemented sandstone layers and carbonate stringers display oppositely abnormal values in the same logs (Maast et al., 2011). We employed cutoffs for shale volume and porosity for defining net reservoir (where gross equals total formation thickness), and utilized water saturation (S_w) to define net pay where applicable. Core plug measurements suggest that 11–12% porosity is required to expect permeability around 1 mD (Fig. 4a).

Water saturation (S_w) was calculated from Archie's relation as

$$S_w = [(a \times R_w)/(R_d \times \Phi^m)]^{1/n}. \quad (2)$$

Here, R_d is deep resistivity, and Φ is effective porosity. The constant a represents the tortuosity factor, while m and n denote the cementation factor and saturation exponent, respectively. Commonly utilized values suitable for consolidated sandstone were used as coefficients, $a = 0.81$ and $m = n = 2$ (Asquith and Krygowski, 2004), which provided a satisfactory level of accuracy. Formation water resistivity (R_w) was determined from core reports (NPD, 2019), from brine filled clean sandstones in the same well and stratigraphic level where possible, or approximated as 0.04 Ω-m where no reference was available.

The selected cutoff values applied for net-to-gross estimation were $V_{sh} < 0.3$, $\Phi > 0.12$ and $S_w < 0.6$. Additionally, a minimum reservoir and pay zone thickness of 0.5 m was applied to discriminate the thinnest sands while still allowing for heterogeneous reservoir intervals.

Seismic mapping of target horizons and coherency attributes were employed to understand lateral variations in depth, thickness, and large-scale structural influences. Three poststack 3D seismic surveys (TA0701, EGB2005 and LGW2004) available in the public domain (courtesy of NPD via Diskos) were used for seismic interpretation of reservoir formations (J_1 and J_2) and adjacent key horizons. In total, the surveys cover approximately 3600 km^2, including a large part of the Egersund Basin, the northeast part of the Ling Depression, and the southeast segment of the Ling Depression. Publicly available 2D lines (North Sea Renaissance survey) were used for understanding regional variations outside of the 3D seismic data cubes. Dip illumination and variance attribute maps (Fig. 3a) were used to broadly delineate the main structural elements, faults and salt structures (Fig. 1b). The top Bryne horizon is picked with high confidence on wide-spread coal layers in the upper part of the formation. The Sandnes Formation can be mapped individually in the central part of the Egersund Basin due to greater thickness, but this is not the case in the NE Ling Depression survey (TA0701). In the SW Ling Depression seismic (LGW2004), the resolution and reflector continuity below the Upper Jurassic shale is relatively poor, and consequently the Hugin and Sleipner formations are more difficult to pick with confidence. Due to its rapidly varying thickness (resolution limits visibility) and lack of confidence in horizon tracking, drawing any conclusions from the Hugin isochore was inadvisable.

Based on petrophysical analysis, where we obtained important reservoir parameters related to depositional diversity and degree of compaction, we take advantage of rock physics to link geological

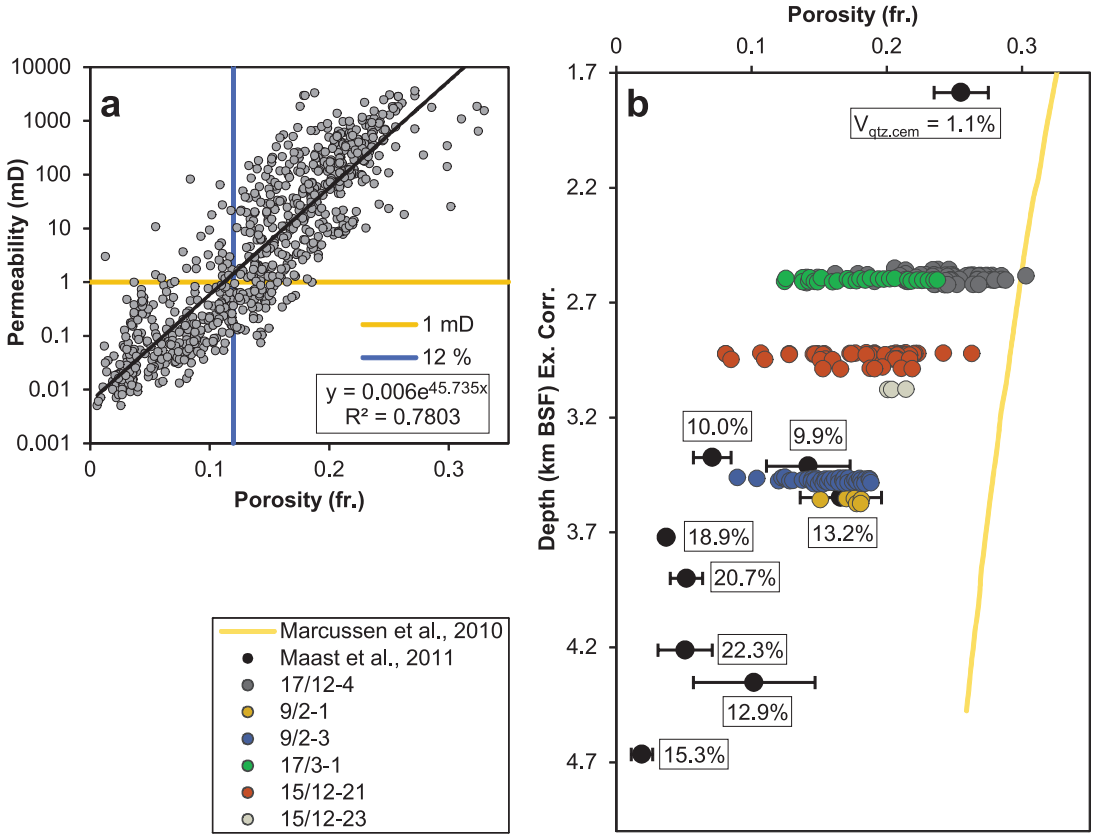

Fig. 4. (a) Core porosity versus permeability showing all available measurements, i.e., not filtered for coal or clay content. (b) Core plug porosity versus depth for clean Middle Jurassic sandstones compared to an experimental compaction curve representing mechanical compaction of loose Etive sandstone (Marcussen et al., 2010). Porosity ranges from thin section point-count analysis of Hugin Formation arenite sandstones (non-carbonate-cemented) are shown as black points and marked with values representing average quartz cement volume (Maast et al., 2011).

variations with elastic parameters that relate to seismic reflection data. Theoretical rock physics models or templates (Ødegaard and Avseth, 2004) can be used to compare different wells, such as in V_P/V_S versus acoustic impedance (AI) crossplots that enable simultaneous interpretation of lithology, porosity (cementation) and fluid sensitivity (i.e., separating brine- and hydrocarbon-saturated sandstones). Furthermore, AVO half-space modeling using the Shuey approximation (Shuey, 1985) was used in selected wells to evaluate the sensitivity of AVO signatures to fluid content in the case of oil versus brine (for angle-stacks up to 30°).

4. Results

In the following, we present the integrated results from the conducted well log characterization, seismic interpretation and rock physics diagnostics of Middle Jurassic reservoir sandstones.

4.1. Petrophysical reservoir quality evaluation

Fig. 5 displays correlations of the Middle Jurassic sandstone–dominated formations in key wells from the Egersund Basin and southwest Ling Depression. Coal layers are marked with dark grey shading. An increasing total gross thickness is evident in wells located towards the center of the Egersund Basin (9/2 block, Yme area). J_2 is thinner than J_1 in all but two wells (15/12-22 and 9/4-5). Wells 9/2-11 (Aubrey) and 9/2-3 do not penetrate the base Bryne horizon, but the Bryne Formation is still inferred from seismic to be thicker than the Sandnes Formation. The latter gradually increases in thickness from the NE Ling Depression (not shown in Fig. 5) and the Vette/Bream area (17/12-3 and 17/12-4), towards a maximum of 147 m in well 9/2-1 (Yme; Fig. 5). Well 9/2-3 is not included in Fig. 5, but has almost identical thickness and log signatures as well 9/2-1 in the Sandnes Formation.

The Hugin Formation on the other hand displays large local thickness variations, from 154 m in the Storkollen well (15/12-22) to being absent in well 15/12-23 (on the Grevling discovery) 6.3 km farther west (Fig. 5). It is also drastically thinner or absent towards the north-east in the Ling Depression (wells 16/10-3 and 16/8-3S included for context in Fig. 5). The J_1 interval is consistently thinner in the Ling Depression than in the Egersund Basin, with the exception of the southernmost studied well 9/4-5 (53 m). The Sleipner Formation is only present in the three westernmost wells (Fig. 5).

Output values from the petrophysical analysis are presented as averages in Table 2. The corresponding Fig. 6 visualizes relationships between various reservoir parameters to better compare and contrast different formations. Highlighted clusters and trends indicate differences in reservoir potential corresponding to basin location for the Bryne and Sandnes formations.

The total Middle Jurassic net reservoir thickness is generally greater in the Egersund Basin (60–116 m) compared to the Ling Depression (12–52 m). A notable exception is found in well 15/12-22 (Storkollen), with 153 m of high-porosity Hugin Formation sandstone. The net-to-gross (N/G) reservoir parameter serves as a more general indicator of reservoir quality irrespective of formation thickness. J_2 displays a wide range of N/G values from 11 to 99% with an average of 60% across all wells (Table 2; Fig. 6a). The reservoir maximum burial depth does not correlate with N/G value (Fig. 6c). On the other hand, J_1 varies from 7 to 70% N/G, with an average value of 36% (Fig. 6b). In this case, we

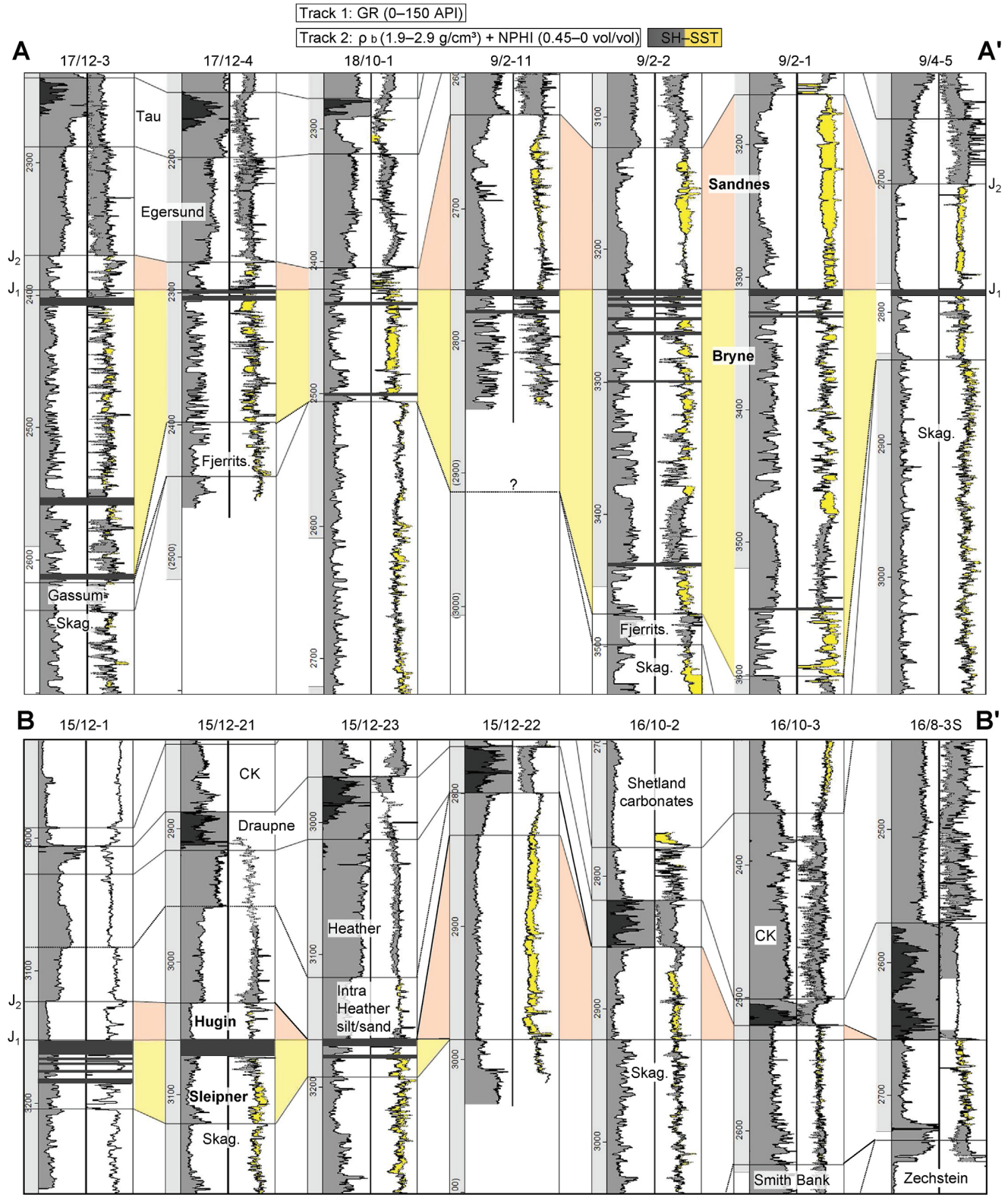

Fig. 5. Well correlation panels for Middle Jurassic reservoir formations, flattened on the J_1–J_2 transition. A–A′ is located in the Egersund Basin, and is oriented from the northwest flank through the central part to the south flank. B–B′ is oriented west–east in the SW Ling Depression. Well correlation panel locations are shown in Fig. 1b. J_1 (Bryne and Sleipner formations) and J_2 (Sandnes and Hugin formations) are indicated by yellow and light red shading, respectively. (For interpretation of the references to color in this figure legend, the reader is referred to the Web version of this article.)

Table 2
Results of the petrophysical analysis, with values reported as averages per zone. Depths are stated in meters below sea floor, corrected for estimated exhumation.

Location	Well (prospect)	Top depth (m)	Ex.corr.	Gross (m)		Net reservoir (m)			N/G reservoir[c] (%)			V_{sh} reservoir zone (%)			Φ reservoir zone (%)			Net pay (m) = S_w < 0.6		
				J_1[a]	J_2[b]	J_1	J_2	Tot.	J_1	J_2	Tot.	J_1	J_2	Tot.	J_1	J_2	Tot.	J_1	J_2	Tot.
EGB S. Flank	9/4-5	2832		53	80	133	35	75	110	66	93	83	10	6	8	21	22	21			
Egersund Basin Central	9/2-3	3448		[d]33	121	154	4	64	68	13	53	44	10	9	9	17	15	15		5	5
	9/2-2	3551		245	107	352	36	35	71	15	33	20	8	16	12	16	16	16			
	9/2-1 (Yme)	3534		292	147	439	21	67	88	7	46	20	6	12	10	13	13	13	2	44	46
	9/2-11 (Aubrey)	3122		[d]90	132	222	18	63	80	20	48	36	14	16	16	17	18	18			
EGB N. Flank	18/10-1 (Mackerel)	2734		85	16	101	59	2	61	70	11	61	10	14	10	22	22	22	9	1	10
	17/12-3	2608		221	26	247	102	15	116	46	57	47	11	13	11	22	20	22			
	17/12-4 (Vette)	2549		100	21	121	50	10	60	50	49	50	10	15	11	23	20	23	20	1	21
NE Ling Depression	17/6-1 (Svaneøgle)	2890		79	17	96	20	3	23	25	19	24	5	20	7	19	14	18			
	17/3-1 (Bark)	2589		30	23	53	16	18	35	54	81	66	11	8	10	21	23	22	1		1
SW Ling Depression	16/10-2	2749			70	70		52	52		75	75		10	10		23	23			
	15/12-21 (Greviling)	2902		63	28	91	20	24	44	31	88	49	14	14	14	16	21	19	20	24	44
	15/12-22 (Storkollen)	2723			154	154		153	153		99	99		11	11		24	24			
	15/12-23	3051		28		28	12		12	43		43	10		10	17		17	8		8
	15/12-1	3003		52	29	81	24	14	38	27	82	47	15	6	9	19	20	20			
Average				113	69	156	32	43	70	36	60	51	10	12	10	19	19	19			

[a] Bryne/Sleipner.
[b] Sandnes/Hugin.
[c] $V_{sh} < 0.3$, $\Phi > 0.12$.
[d] Base Bryne not penetrated.

observe a clear decrease in the N/G parameter from Bryne reservoirs between ~2.6 km and 3.7 km (Fig. 6d). The Sleipner Formation reservoirs at intermediate depths fall along the same trend.

After filtering out shaly and low-porosity intervals, the net reservoir porosity is observed to vary fairly consistently with the reservoir maximum burial depth, between 13 and 24% (Fig. 6e). Where both J_1 and J_2 successions have representative net reservoir thicknesses, only minor variations are observed in average porosity. As seen in Table 2, there is a maximum difference of 5% between the older and younger reservoir sandstones in any given well location.

4.2. Thickness variations

Fig. 7 displays time-thickness (isochore) maps of different reservoir intervals. 2D seismic lines are used to cover the southwest part of the Egersund Basin, the Åsta Graben between the EGB2005 and TA0701 3D surveys, and part of the NE Ling Depression. Drawbacks include poorer lateral resolution and some inconsistencies when compared to the 3D surveys, but the 2D seismic reflection dataset provides better semi-regional context for the extent of the Bryne Formation. Fairly uniform Bryne Formation thickness can be observed in the Åsta Graben and the NE Ling Depression. We take note of likely structural influences, e.g., increased thickness east of a NW-SE trending fault located east of well 17/6-1, as well as towards the Øygarden Fault Complex in the north (Fig. 7a). In the Egersund Basin, the Bryne Formation varies quite substantially, displaying greater thickness overall in the southern part, and particularly along salt walls (c.f. Fig. 3a). Where mapped, the Sandnes Formation exhibits very similar behavior (Fig. 7b).

The Sleipner time–thickness (isochore) map (Fig. 7c) reflects the overall thinning out towards the eastern part, as observed in well correlation (Fig. 5). Additionally, we can identify similar local thickening towards larger faults. Salt related structures were observed, as was the case in the Egersund Basin, which causes problems with reflector discontinuities and consequent interpretation above salt (gaps in thickness maps). Some of the marked faults correlate with deeper salt structures, whereas other could stem from Jurassic extension and creation of the adjacent Viking Graben. Thickness variations in the areas that are not heavily influenced by faulting could indicate depositional features. For instance, channel-like geometries are sporadically identified within the Sleipner Formation in the seismic (Fig. 7c).

4.3. Rock physics relationships and sensitivity

Typically for poststack seismic, the output data that can be analyzed consist of acoustic impedance volumes derived from seismic inversion. Well-log derived acoustic impedance from primary cap rock and reservoir formations (without filters) at different depths is shown in Fig. 8a, revealing rough depth trends for sand and shale that are shifted slightly in relation to each other. No coherency is however observed in AI (acoustic impedance) as a function of smaller shale volume variations within reservoir formations, either when examining individual wells or as exemplified compositely for all wells in Fig. 8b. AI varies predominantly between 7 and 11 g/cm^3 × km/s for reservoir sections encountered above 3.2 km maximum burial, and from approximately 9–13 g/cm^3 × km/s in formations with greater burial (Fig. 8b). Particularly when considering the cleaner sand proportion ($V_{sh} < 0.3$), AI instead correlates highly with porosity (Fig. 8c). A decrease in porosity from 30% to 5% yields an increase in AI of approximately 5 g/cm^3 × km/s.

When shear velocity information is incorporated, using V_P/V_S–AI crossplots, we can get combined information about shale content, porosity, and fluids, and we are able to compare to theoretical compaction trends for clean quartz sand (Ødegaard and Avseth, 2004). Fig. 9 indicates differences in elastic properties as a function of clay content, porosity and associated cementation, as well as fluid content. An empirical shale trend based on organic-lean shale data (Hansen

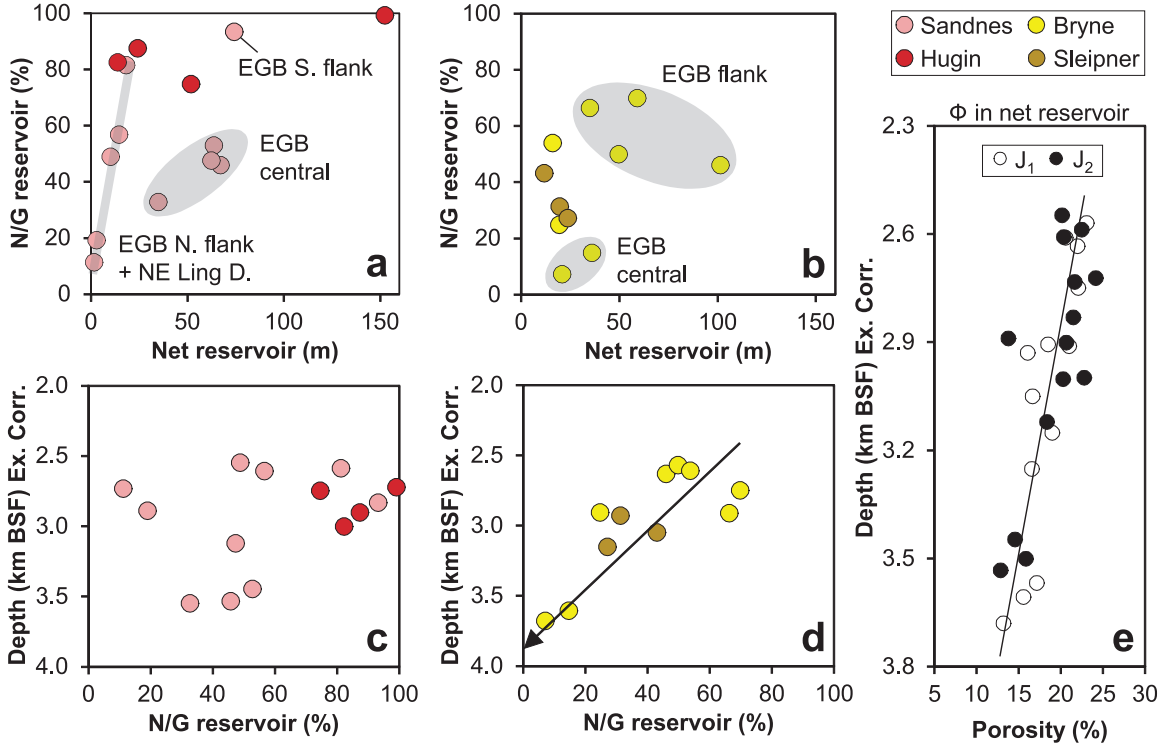

Fig. 6. Relationships between reservoir parameters separated according to formation and age; net reservoir thickness versus net–to–gross (N/G) reservoir (a, b), net–to–gross compared to top reservoir depth (c, d), and average net reservoir porosity as a function of maximum burial depth (e; BSF = below seafloor, Ex. Corr. = corrected for estimated exhumation). Wells that do not penetrate the base Bryne horizon have been excluded from plots (b) and (d).

et al., 2019) and a generalized brine–oil sandstone template assuming 30 MPa effective pressure are superimposed for reference. We observe improved discrimination of shaly intervals in reservoir formations, which plot towards slightly higher V_P/V_S values than clean sands (Fig. 9a). Porosity deterioration as a function of burial and cementation relates to AI as shown in Fig. 8. Additionally, we observe a corresponding decrease in V_P/V_S from around 2.1 to 1.65 for sandstone porosities between 30% and 5%, albeit with substantial scatter in the y–axis direction (Fig. 9b).

In well 17/12-4, we observe that data from brine-saturated sandstones plot predominantly above the brine sandstone model (Fig. 9c). Oil sandstone data fall mainly between the 100% brine and 100% oil line, although some overlap scatter is evident. The brine and oil clusters are consequently separated by approximately 1.6 g/cm^3 × km/s in AI and 0.1 in V_P/V_S when considering averages. In Fig. 9d, we take note of two features; firstly, the separation between two brine-sandstone populations in the Storkollen well as a result of porosity is clearly pronounced ($\Delta AI = 1.1$, $\Delta V_P/V_S = -0.13$). The lower-porosity population has an average $\Phi = 23\%$. Secondly, the overlap between the lower part of the brine-sand cluster and the oil-sand data is substantial, both of which plot primarily above the brine sandstone model (Fig. 9d). Only a handful of data points from the oil leg plot closer to the oil-sand model.

4.4. Synthetic AVO modeling

The intercept (R_0) versus gradient (G) crossplot in Fig. 10 displays the forward-modeled AVO signatures of top reservoir interfaces, in-situ and fluid substituted, corresponding to the wells in Fig. 9c and d. A simplified background shale trend assuming $V_P/V_S = 2$ is superimposed. The Bryne Formation contains both oil- and brine-saturated sandstones in-situ, where the oil saturation in the former was interpreted to be high from petrophysical data. For comparison, these two chosen oil- and brine intervals have been substituted to 100% brine and 90% oil, respectively (Fig. 10a). The properties of a shaly layer between the Sandnes (brine in-situ) and Bryne Formation (oil in-situ) were used for the cap rock in the modeling. The fluid effect from substitution is predicted to be smaller (circle–circle and triangle–triangle) than what is apparent when comparing the in-situ brine and oil sandstones (Fig. 10a; triangle–circle). In both cases, AVO class II is predicted for brine sandstone, whereas class III is predicted for oil. The Sandnes Formation, which is brine-filled in-situ, is predicted to move from AVO class I to IIp in the case of oil (Fig. 10a; squares). In this case the cap rock was assigned properties corresponding to the lowermost Egersund Formation shale.

For all cases in Fig. 10b, representing the Storkollen and Grevling prospects, the predicted fluid separation is fairly small. Properties of Heather Formation shale were used to represent the cap rock in both wells. We can see that AVO class III is predicted in the Grevling well, whereas higher-porosity Hugin Formation sandstones in the Storkollen well plot as class IV.

5. Discussion

Firstly, we review the implications of the conducted reservoir analysis for hydrocarbon exploration and how different formations compare and vary. Secondly, the feasibility of using seismic properties to predict reservoir parameters on seismic reflection data is discussed based on observed rock physics trends. Finally, we put the reservoir analysis into context with plausible areas of hydrocarbon generation and discuss potential challenges.

5.1. Reservoir quality assessment

Based on the range of burial depths of Middle Jurassic Formations (> 2.5 km), the expectation is that all encountered sandstones are at least somewhat cemented. The observed porosity range (Table 2) and

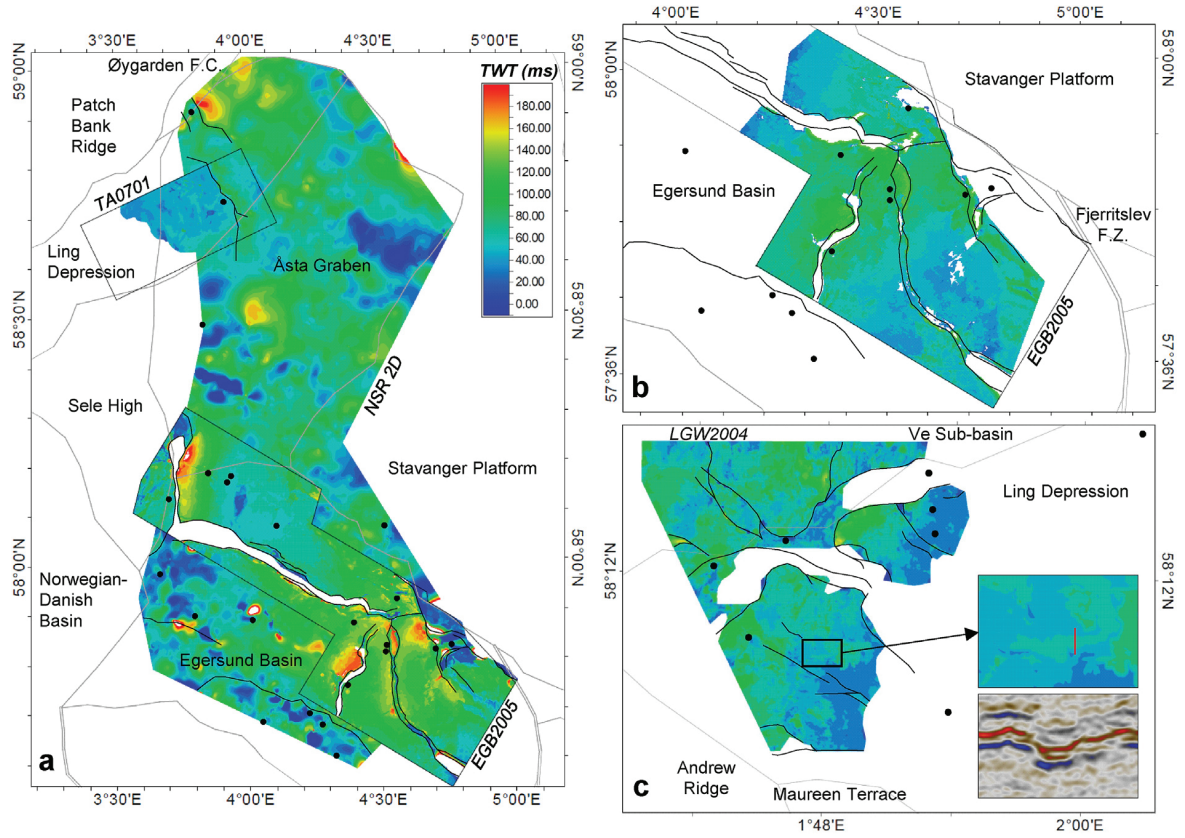

Fig. 7. Time-thickness (isochore) maps representing (a) the Bryne Formation in the Egersund Basin and NE Ling Depression based on two 3D surveys and the available 2D seismic dataset, (b) the Sandnes Formation based on the EGB2005 3D survey, and (c) the Sleipner Formation in the SW Ling Depression based on the LGW2004 3D survey (see Fig. 1b for relation to structural elements). Note possible resolution of channel-like geometries, appearing as very subtle features in the thickness map.

deviations in core plug porosity compared to a suitable mechanical compaction trend (Fig. 4b) also indicate that chemical compaction and quartz cement is influential at all relevant reservoir depths in the study area. Petrographic information from Middle Jurassic sandstones within the study area and nearby vicinity is unfortunately scarce. Only limited information restricted to the Hugin Formation is available from nearby wells (Maast et al., 2011). The latter information contributes to an understanding of the spread in core plug porosity seen in Fig. 4b. The Hugin Formation data show high inter-granular volume (IGV) post mechanical compaction (ranging between 28% and 38% with an average close to 33%) and also rather high detrital clay content (range of 1–11% with an average of 7%). The content of cements other than quartz is low, less than 2%. Therefore, the variability seen in the core plug porosity data in Fig. 4b must be related to variations in IGV and detrital clay content. A variable detrital clay effect on the rate of quartz cementation, which is probably related to the distribution between pore-filling and pore-lining clay may also contribute to the observed porosity variability and associated permeability ranges.

The Sandnes Formation has clearly the most favorable and consistent reservoir potential where it is well-developed in terms of thickness, i.e., mainly around the central Egersund Basin. On the flanks of the basin, as well as in the NE Ling Depression, more variable N/G is observed, and an additional limiting factor is the drastic decrease in thickness (Fig. 6a). The reason for lower N/G is likely related to the depositional environment and varying amounts of sand (e.g., Svaneøgle well 17/6-1), as it shows little correlation with formation depth (Fig. 6c). These observations fit well with core descriptions and facies associations (Mannie et al., 2014), where shoreface facies is found to dominate the Sandnes Formation except for certain wells on the north flank of the Egersund Basin where offshore facies are prevalent. In well 9/4-5 on the south flank of the Egersund Basin, the Sandnes Formation properties and thickness are better developed and/or preserved than on the north side.

Conversely, the Bryne Formation has poorer reservoir quality in the central Egersund Basin, predominantly as a result of deeper burial and consequent porosity deterioration (Fig. 6b and d). Most likely, the porosity relates to pore-filling quartz cement (Fig. 4b). On the flanks of the basin however, the Bryne Formation shows intermediate to high cumulative reservoir sandstone thickness, and increased N/G and sandstone porosity. Heterogeneity and possible fluid barriers (fine-grained coastal deposits) could be an issue; however, well 17/12-4 encounters multiple levels of oil-bearing sandstones interbedded with shale.

Thickness variations of Sandnes and Bryne formations in the Egersund Basin are largely coherent with the location of salt structures. As discussed in Mannie et al. (2014), the movement of salt created accommodation space, explaining the increased thicknesses observed on the flank or to the sides of salt structures. The Norwegian-Danish Basin similarly has a high density of salt structures which, depending on the extent of reservoir formations, could have had the same positive impact on the development of sand-dominated formations. The influence of salt in the Ling Depression is less prominent, particularly in the northeast which is consistent with the more uniform thickness of the Bryne Formation observed in the northeast Ling Depression (Fig. 7a).

Considering areas farther southwest in the Ling Depression, the Hugin Formation displays consistently good reservoir quality within the examined wells, with excellent properties and thickness in the Storkollen well 15/12-22 (Table 2; Fig. 6a). Rapid thickness variations

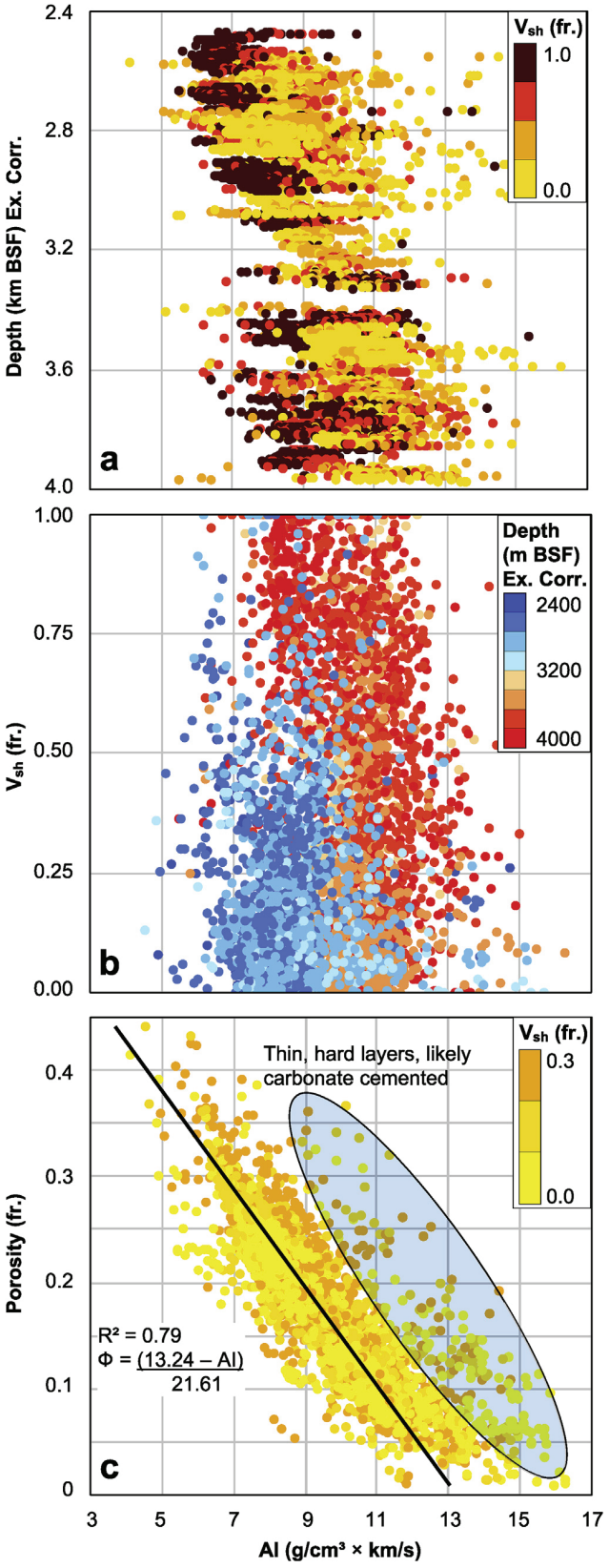

Fig. 8. (a) Crossplot of AI versus depth providing an overview of the Middle Jurassic reservoir formations and immediate cap rocks (Egersund and Heather formations) in all 15 wells, color coded with V_{sh}. (b) AI versus V_{sh}, reservoir formations only, color coded with depth. (c) AI versus porosity for clean sand data only, displaying a best fit $R^2 = 0.79$. (For interpretation of the references to color in this figure legend, the reader is referred to the Web version of this article.)

based on wells and poorly constrained seismic expression result in uncertain lateral extent of this formation. The Sleipner Formation, while easier to constrain on seismic, is similarly not regionally continuous. Our limited sample pool indicates no better than intermediate, albeit consistent, reservoir quality compared to the time-equivalent Bryne Formation (Fig. 6d). If the channel structures observed in the seismic data (Fig. 7c) correspond to fluvial deposits, these would be of substantial thickness when considering the seismic resolution. Consequently, the indication is a depositional environment that could accommodate larger, concentrated channels.

5.2. Predicting reservoir properties from seismic reflection data

Initially, we assessed the complete dataset, looking for trends both in Middle Jurassic reservoir formations and immediate relevant cap rock formations. As the stratigraphy in the region is well understood and some well control exists in most areas, seismic mapping provides the main framework for separating sand- and shale-dominated units. Subsequently, more focus was given to relating elastic properties to porosity variations and fluid anomalies. Overall, we find that seismic properties display fair separation between different lithologies, as well as good sensitivity to porosity. When discussing cementation in the context of reservoir quality in the study area, the primary concern is the precipitation of quartz cement driven by the transformation of thermally unstable smectite to illite, starting at around 70 °C (Bjørlykke, 1998), which is the main process for porosity-reduction when considering burial depths greater than ~2–2.5 km (Bjørlykke et al., 1989; Marcussen et al., 2010). Grain-coating clay or microquartz can prevent or retard cementation, thereby serving as porosity-preserving mechanisms (Morad et al., 2010; Maast et al., 2011). We do not explicitly consider carbonate cement, which relates to processes that occur at much shallower depths, and unless dissolved during burial, is often found to severely compromise the primary porosity of the sand (e.g., Bjørlykke et al., 1989). Additionally, the carbonate stringers and carbonate cemented sandstone layers identified in the studied wells (see "Database and methods") are very thin compared to the gross sand thickness (Fig. 5). Bulk density and AI in these layers typically surpass 2.5–2.6 g/cm^3 and 12–14 g/cm^3 × km/s, respectively.

AI alone is found to be a poor attribute for distinguishing detailed intra-reservoir shale variations, regardless of examination depth (Fig. 8b). Conversely, it serves as a very good predictor of porosity in clean sandstone (Figs. 8c and 9b). In certain areas and/or formations inferred to be less prone to heterogeneity and clay contamination, AI can be used more confidently to predict and map porosity variations. Depending on the resolution of seismic data and interpretations, candidates for this approach would be the Hugin Formation, the Sandnes Formation in the central Egersund Basin, and possibly the Bryne Formation on the Egersund Basin flanks. When doing a combined evaluation of shale content, depth and porosity in the V_P/V_S–AI domain, superimposed on theoretical models for ease of reference, we attain slightly better discrimination of shaly intervals, as well as an accurate porosity resolution. Thus, geophysical data could be suitable for simultaneously discriminating good sands and accurately predicting porosity variations when evaluating prospects, particularly in locations not too far from existing wells. This approach assumes the existence and availability of prestack seismic data.

Ultimately, the main goal of seismic reservoir characterization is to

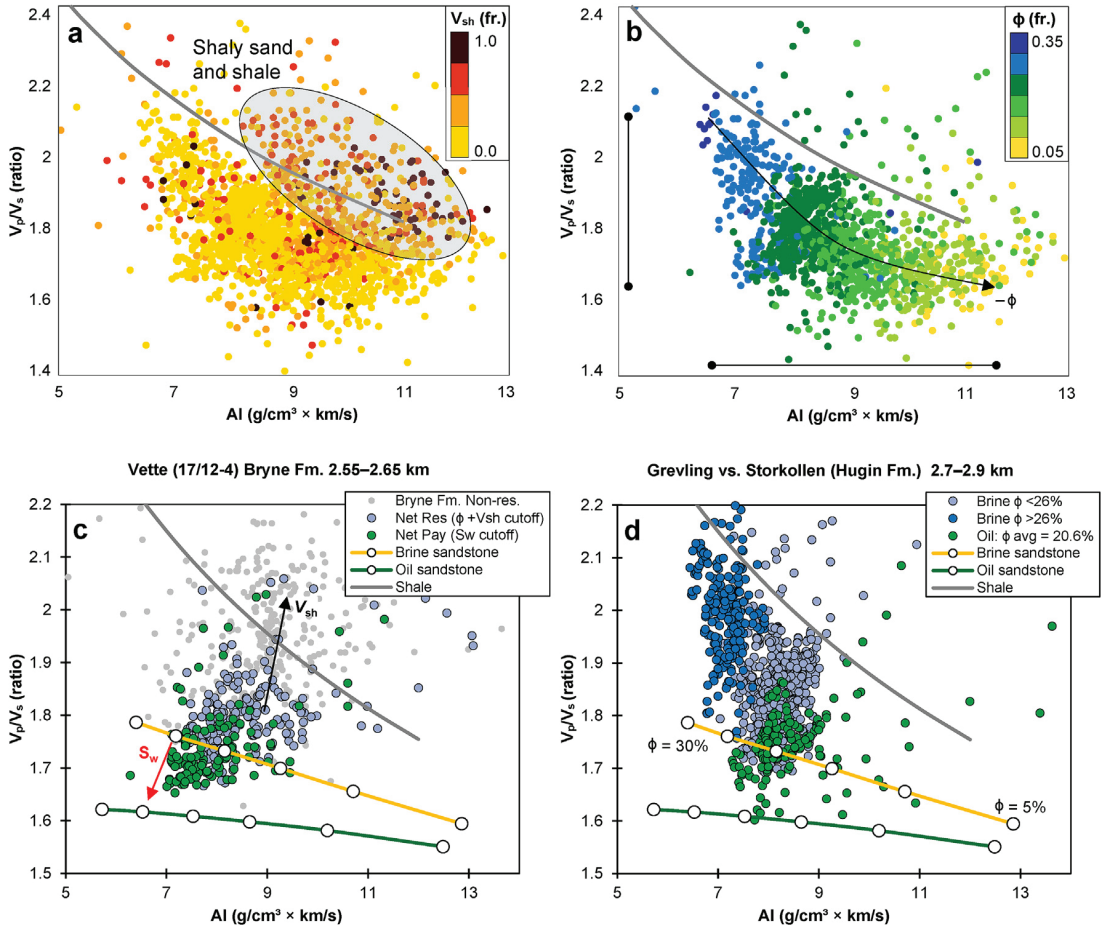

Fig. 9. V_P/V_S–AI crossplots highlighting the feasibility of analyzing reservoirs through seismic properties. Data from six wells (see Table 1) with shear velocity data is color coded with shale volume (a), and clean sand data only (V_{sh} < 0.3) is color coded with porosity (b). Reservoir sandstones at different depths indicate variable fluid discrimination, represented by the Vette discovery (c) and by comparing the Grevling discovery to the dry Storkollen prospect (d). (For interpretation of the references to color in this figure legend, the reader is referred to the Web version of this article.)

predict fluid content. Based on kerogen types and maximum potential burial of source rocks in the Egersund Basin and Ling Depression (Hansen et al., 2019), the expected hydrocarbon phase is oil, which has properties close to brine. Based on rock physics diagnostics, only the shallowest Jurassic reservoir data at 2.55–2.65 km BSF maximum burial indicate plausible ability to separate brine sand from hydrocarbon sand based on seismic properties (Fig. 9c). At this depth, we already expect the initial stages of quartz cement, which stiffens the grain framework and reduces fluid sensitivity. Data from oil- and brine-saturated Hugin Formation sandstones at 2.7–2.9 km burial depth largely overlap, indicating minor to negligible fluid separation in the V_P/V_S–AI attributes (Fig. 9d). There is a small decrease in average porosity from the brine sand compared to the slightly deeper oil-sand, yet we can infer that accounting for this difference would only further increase the degree of overlap based on the observed porosity trend (Fig. 9b). In combination, this suggests a required porosity of at least ~22–24% for enabling any meaningful separation based on the regional porosity–depth trend (Fig. 6e). For context, completely overlapping oil- and brine sand properties are found in Triassic sandstones at 3–3.2 km burial depth in the Grevling well, meaning that no fluid sensitivity is expected in elastic properties. A maximum burial depth of ~2.5–2.6 km mostly applies to the very shallowest structures in the studied region, meaning that exploration targeting Middle Jurassic reservoirs will face challenges related to fluid prediction.

AVO analysis can as an alternative, when carefully considering encasing shale properties and depth trends, aid fluid interpretation from seismic data (Avseth et al., 2008). Such analysis naturally complements the use of inverted elastic properties from seismic, but no prestack data were available for this study to further evaluate either of these approaches for our specific targets. From the conducted synthetic testing, changes in AVO attributes as a function of saturation are small compared to the inherent angle-dependent behavior of modeled sand-shale interfaces (Fig. 10). AVO class-changes corresponding to fluid substitution are observed in well 17/12-4, but this relationship will change rapidly with depth. Fig. 10b gives a good impression of the effect of reservoir porosity, represented by two sandstones in well 15/12-22 (Storkollen) with different porosities, and the lower-porosity Hugin Formation in the Grevling well. However, even when porosity is high, the fluid change has limited influence due to the small differences in petrophysical and elastic properties (i.e., density and bulk modulus) between oil and brine (Fig. 10b). The AVO class IV prediction is attributed to the large difference between cap rock and reservoir properties in the high-porosity Hugin sandstones in the Storkollen well. In this location, the Heather Formation is fairly hard (AI = 8–9 g/cm³ × km/s), sandy to silty in the lower part and is fining upwards. On the other hand, the Egersund Formation in the Vette well is quite soft (AI = 6–7 g/cm³ × km/s), resulting in the appearance of a hard, AVO class I Sandnes Formation sandstone underneath it. In both cases, our observations highlight that differences in cap rock properties have a far greater influence on the AVO behavior than the difference in fluid content for the studied wells. We inferred certain trends for the two different areas in terms of fluids and AVO classification, but the

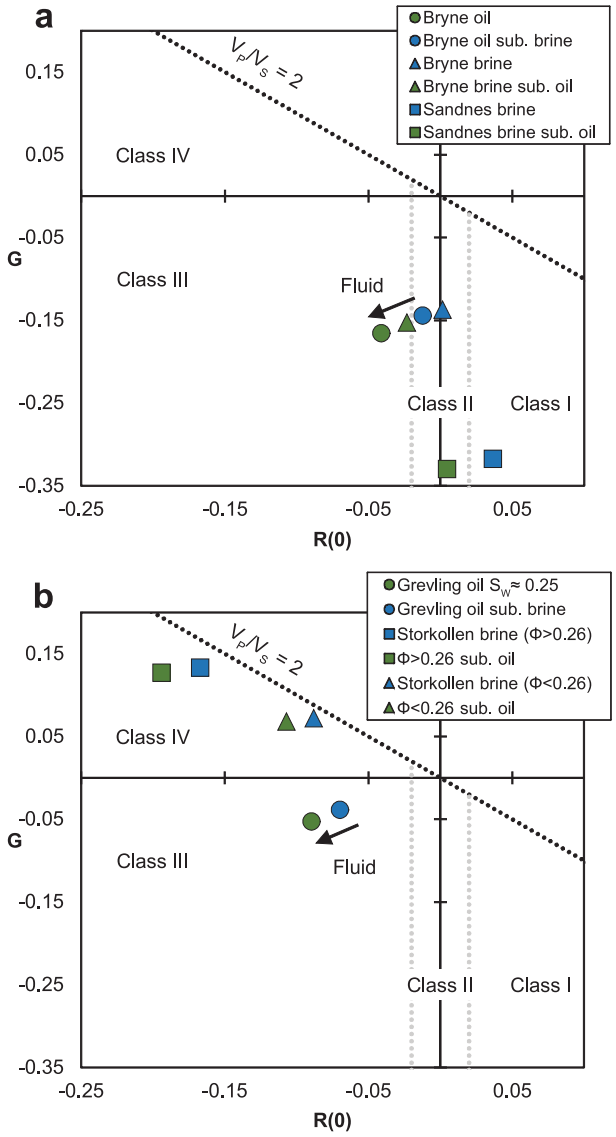

Fig. 10. Sensitivity test to fluid substitution on synthetic AVO signatures in the intercept–gradient crossplot. (a) Sandnes and Bryne formations in well 17/12-4 (Vette). (b) Hugin Formation in wells 15/12-21 (Grevling) and 15/12-22 (Storkollen).

maximum observed changes in R(0) and G between in-situ brine and in-situ oil in well 17/12-4 are −0.04 and −0.03, respectively, which are relatively discrete differences.

5.3. Relating reservoirs to source rocks and hydrocarbon kitchen

Considering previous discoveries, the thickness variations observed in seismic data, and local source rock burial (deep versus shallow), the Egersund Basin should have potential for hosting new discoveries. Particularly the great thicknesses observed in the Sandnes Formation, which is typically more consistent and clean in sandstone content compared to other formations, is favorable (Figs. 5 and 7). Depending on either fault juxtaposition of source and reservoir intervals (e.g., around well 9/2-1, Fig. 11) or pressure-induced expulsion stratigraphically downwards, the Sandnes Formation is also the most likely carrier bed for hydrocarbons. Conversely, the quality of the Bryne Formation is poorer close to the source rock, as evident in wells 9/2-1, 9/2-2 and 9/2-3. On the other hand, reservoir quality in the immediate proximity to the source rock is increasingly irrelevant the greater the volume of hydrocarbons that has been generated and expelled, which relates to possible migration distance. Older estimates based on basin modeling exist (e.g., Ritter, 1988; Hermanrud et al., 1990), but accurate quantification of actual generated hydrocarbon volumes and interpretation of possible migration pathways are sparse in public material. Importantly, these do not account for Cenozoic exhumation (Kalani et al., 2015a; Hansen et al., 2017; Baig et al., 2019), which would influence maximum burial depth and temperature in the models. Furthermore, microfracturing suggested to relate with the onset of kerogen cracking has been observed by Kalani et al. (2015b), indicating that minor maturation has occurred in some well locations.

Discoveries on the north flank of the basin (e.g., Vette and Mackerel) hint towards longer distance migration from the Egersund Basin kitchen, as no other source area is immediately apparent. Conversely, wells drilled on the south flank (e.g., well 9/4-5 which targeted Rotliegend Group sandstone) where good Sandnes Formation reservoirs are present close to the kitchen area, have so far been dry (Fig. 11). Lack of hydrocarbons in these wells could relate to migration issues across the large fault separating the kitchen and reservoir areas (Fig. 11). If the deeper parts of the Tau or Egersund formations in the Ling Depression (on the opposite side of Sele High) at some point generated significant amounts of hydrocarbons, there would likely have been more evidence of this in well 17/6-1 (Svaneøgle, minor oil shows) or 17/3-1 (Bark, small gas accumulation). In sum, oil in the Vette discovery is more likely to stem from the central Egersund Basin.

Lacking the ability to independently interpret fluid content from seismic amplitudes or inverted elastic properties instigate a greater focus on alternative and complementary methods of investigation. Such approaches could for instance involve more detailed modeling of the basin development, thermal history of source rocks (considering maximum burial and uplift episodes), and understanding of the most probable migration pathways (Iyer et al., 2018). Complementary, Hansen et al. (2019) investigated how relationships between elastic and geological properties in organic-rich shales could be incorporated in seismic source rock characterization. In any case, potential hydrocarbon accumulations can thus be predicted from a more geological perspective, and combined with information about changes and trends in reservoir quality and thickness. Altogether, this will help us better understand the nuances of the Jurassic petroleum system in the eastern Central North Sea region.

6. Conclusions

For further exploration of the eastern Central North Sea, a region with many dry wells, it is important to consider and understand all parts of the petroleum system. There are clearly issues related to overall source rock maturation, but successful wells in certain areas prove local oil generation. In that context, we focus on reservoir quality variations, thickness differences and potential target formations in areas where hydrocarbon generation and migration can plausibly occur. The main outcomes of this analysis are as follows:

- The Sandnes Formation is a good reservoir target in the central Egersund Basin and on the south flank (gross thickness 80–147 m, N/G = 33–93%), but generally poorer thickness (16–26 m) and variable quality (N/G = 11–81%) are found farther northwest (i.e., Egersund Basin north flank and Ling Depression).
- The Bryne Formation has poorer reservoir quality due to porosity deterioration and heterogeneity in the central Egersund Basin (N/G < 20%), but good sandstones are found at shallower depths on the flanks and partially in the Ling Depression (N/G = 25–70%).
- The Hugin Formation generally exhibits excellent quality, but rapid thickness differences (28–154 m) and local development are observed in the study area.
- Intermediate thickness (28–63 m) and reservoir quality (N/

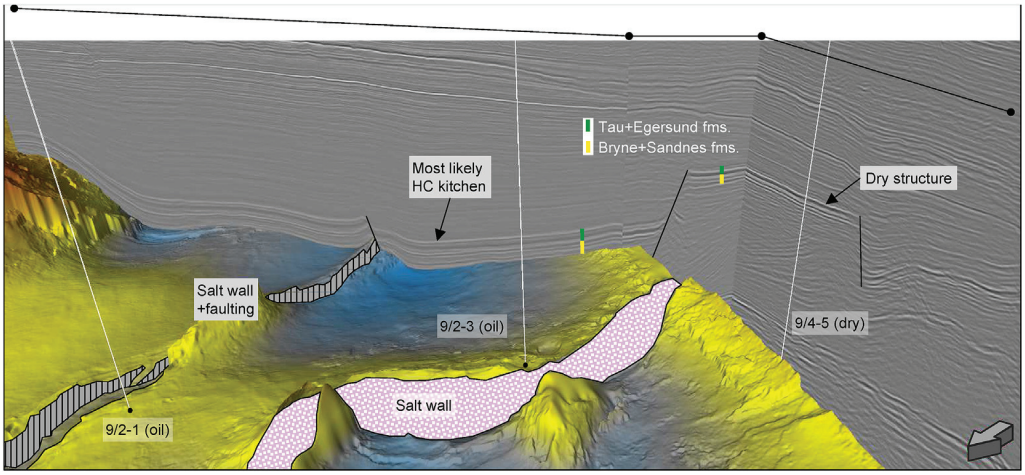

Fig. 11. The 4-way closure structure across the large fault near the deepest source rock burial in the Egersund Basin was found dry (well 9/4-5, close to 2D line). The draped base Bryne horizon time-structure grid illustrates the general basin configuration. The 3D arbitrary line on the left side of the image has opposite polarity in comparison to the two 2D composite sections covering the structure.

G = 27–43%) are recognized in the Sleipner Formation based on our limited sample pool. Thicknesses surpassing that observed in wells, apparently related to salt structures and faults, are clear on seismic reflection data. Subtle depositional features on the seismic scale have also been identified, which could be an indicator of thicker fluvial channel sandstones to target compared with the Bryne Formation.

Rock physics diagnostics of well-log data demonstrate the feasibility of predicting lithology, porosity and fluids from different types of seismic data. In this context, we further discuss connections and challenges with source rock intervals and potential migration. The observed fluid sensitivity in the case of oil at relevant reservoir depths indicates that more geologically driven approaches could be advantageous to explore for predicting potential hydrocarbon accumulations in the study area.

Acknowledgements

The authors are grateful to Vår Energi AS (previously Eni Norge) for funding and supporting the “ReSource – Quantitative analysis of reservoir, cap, and source rocks of the Central North Sea” R&D project. This work was carried out at the University of Oslo with academic licenses for Petrel (Schlumberger), Interactive Petrophysics (Lloyd's Register) and Hampson-Russell (CGG) commercial software packages. All data are courtesy of the Norwegian Petroleum Directorate (NPD) through the DISKOS national data repository.

Appendix A. Supplementary data

Supplementary data to this article can be found online at https://doi.org/10.1016/j.marpetgeo.2019.08.044.

References

Asquith, G., Krygowski, D.A., 2004. Basic Well Log Analysis, second ed. AAPG, Tulsa.
Avseth, P., Dræge, A., van Wijngaarden, A.-J., Johansen, T.A., Jørstad, A., 2008. Shale rock physics and implications for AVO analysis: a North Sea demonstration. Lead. Edge 27, 788–797. https://doi.org/10.1190/1.2944164.
Baig, I., Faleide, J.I., Mondol, N.H., Jahren, J., 2019. Burial and exhumation history controls on shale compaction and thermal maturity along the Norwegian North Sea basin margin areas. Mar. Pet. Geol. 104, 61–85. https://doi.org/10.1016/j.marpetgeo.2019.03.010.
Bjørlykke, K., 1998. Clay mineral diagenesis in sedimentary basins — a key to the prediction of rock properties. Examples from the North Sea Basin. Clay Miner. 33, 15–34.
Bjørlykke, K., Ramm, M., Saigal, G.C., 1989. Sandstone diagenesis and porosity modification during basin evolution. Geol. Rundsch. 78, 243–268.
Doré, A.G., Jensen, L.N., 1996. The impact of late Cenozoic uplift and erosion on hydrocarbon exploration: offshore Norway and some other uplifted basins. Glob. Planet. Chang. 12, 415–436. https://doi.org/10.1016/0921-8181(95)00031-3.
Faleide, J.I., Tsikalas, F., Breivik, A.J., Mjelde, R., Ritzmann, O., Engen, Ø., Wilson, J., Eldholm, O., 2008. Structure and evolution of the continental margin off Norway and the Barents Sea. Episodes 31, 82–91.
Faleide, J.I., Bjørlykke, K., Gabrielsen, R.H., 2015. Geology of the Norwegian continental shelf. In: Bjørlykke, K. (Ed.), Petroleum Geoscience. From Sedimentary Environments to Rock Physics, second ed. Springer-Verlag Berlin Heidelberg, pp. 603–638. https://doi.org/10.1007/978-3-642-34132-8.
Folkestad, A., Satur, N., 2008. Regressive and transgressive cycles in a rift-basin: depositional model and sedimentary partitioning of the Middle Jurassic Hugin formation, southern Viking graben, North Sea. Sediment. Geol. 207, 1–21. https://doi.org/10.1016/j.sedgeo.2008.03.006.
Halland, E.K., Gjeldvik, I.T., Johansen, W.T., Magnus, C., Meling, I.M., Pedersen, S., Riis, F., Solbakk, T., Tappel, I., 2011. CO2 Storage Atlas - Norwegian North Sea. Norwegian Petroleum Directorate, Stavanger, Norway.
Hansen, J.A., Yenwongfai, H.D., Fawad, M., Mondol, N.H., 2017. Estimating exhumation using experimental compaction trends and rock physics relations, with continuation into analysis of source and reservoir rocks: central North Sea, offshore Norway. In: 88th Annual International Meeting, Expanded Abstracts, pp. 3971–3975. https://doi.org/10.1190/segam2017-17783053.1.
Hansen, J.A., Mondol, N.H., Fawad, M., 2019. Organic content and maturation effects on elastic properties of source rock shales in the Central North Sea. Interpretation 7, T477–T497. https://doi.org/10.1190/INT-2018-0105.1.
Hermanrud, C., Eggen, S., Jacobsen, T., Carlsen, E.M., Pallesen, S., 1990. On the accuracy of modelling hydrocarbon generation and migration: the Egersund Basin oil find, Norway. Org. Geochem. 16, 389–399. https://doi.org/10.1016/0146-6380(90)90056-6.
Iyer, K., Schmid, D.W., Rüpke, L.H., Skeie, J.E., 2018. Importance of evolving fault seals on petroleum systems: southern Halten terrace, Norwegian Sea. AAPG (Am. Assoc. Pet. Geol.) Bull. 102, 671–689. https://doi.org/10.1306/0208171616417017.
Jackson, C.A.-L., Chua, S.-T., Bell, R.E., Magee, C., 2013. Structural style and early stage growth of inversion structures: 3D seismic insights from the Egersund Basin, offshore Norway. J. Struct. Geol. 46, 167–185. https://doi.org/10.1016/j.jsg.2012.09.005.
Jordt, H., Faleide, J.I., Bjørlykke, K., Ibrahim, M.T., 1995. Cenozoic sequence stratigraphy of the central and northern North Sea Basin: tectonic development, sediment distribution and provenance areas. Mar. Pet. Geol. 12, 845–879. https://doi.org/10.1016/0264-8172(95)98852-V.
Kalani, M., Jahren, J., Mondol, N.H., Faleide, J.I., 2015a. Compaction processes and rock properties in uplifted clay dominated units - the Egersund Basin, Norwegian North Sea. Mar. Pet. Geol. 68, 596–613. https://doi.org/10.1016/j.marpetgeo.2014.08.015.
Kalani, M., Jahren, J., Mondol, N.H., Faleide, J.I., 2015b. Petrophysical implications of source rock microfracturing. Int. J. Coal Geol. 143, 43–67. https://doi.org/10.1016/j.coal.2015.03.009.
Kieft, R.L., Jackson, C.A.-L., Hampson, G.J., Larsen, E., 2010. Sedimentology and sequence stratigraphy of the Hugin formation, quadrant 15, Norwegian sector, South Viking graben. In: Vining, B.A., Pickering, S.C. (Eds.), Petroleum Geology: from Mature Basins to New Frontiers – Proceedings of the 7th Petroleum Geology Conference. Geological Society, London, pp. 157–176. https://doi.org/10.1144/0070157.
Larionov, V., 1969. Radiometry of Boreholes (In Russian). Nedra, Moscow.
Maast, T.E., Jahren, J., Bjørlykke, K., 2011. Diagenetic controls on reservoir quality in Middle to upper Jurassic sandstones in the south Viking graben, North Sea. AAPG (Am. Assoc. Pet. Geol.) Bull. 95, 1937–1958. https://doi.org/10.1306/03071110122.

Mannie, A.S., Jackson, C.A.-L., Hampson, G.J., 2014. Structural controls on the stratigraphic architecture of net-transgressive shallow-marine strata in a salt-influenced rift basin: Middle-to-Upper Jurassic Egersund Basin, Norwegian North Sea. Basin Res. 26, 675–700. https://doi.org/10.1111/bre.12058.

Mannie, A.S., Jackson, C.A.-L., Hampson, G.J., Fraser, A.J., 2016. Tectonic controls on the spatial distribution and stratigraphic architecture of a net-transgressive shallow-marine synrift succession in a salt-influenced rift basin: Middle to Upper Jurassic, Norwegian Central North Sea. J. Geol. Soc. 173, 901–915. https://doi.org/10.1144/jgs2016-033.

Marcussen, Ø., Maast, T.E., Mondol, N.H., Jahren, J., Bjørlykke, K., 2010. Changes in physical properties of a reservoir sandstone as a function of burial depth – the Etive Formation, northern North Sea. Mar. Pet. Geol. 27, 1725–1735. https://doi.org/10.1306/08220808044.

Mondol, N.H., Bjørlykke, K., Jahren, J., 2008. Experimental compaction of clays: relationship between permeability and petrophysical properties in mudstones. Pet. Geosci. 14, 319–337. https://doi.org/10.1144/1354-079308-773.

Morad, S., Al-Ramadan, K., Ketzer, J.M., De Ros, L.F., 2010. The impact of diagenesis on the heterogeneity of sandstone reservoirs: a review of the role of depositional facies and sequence stratigraphy. AAPG (Am. Assoc. Pet. Geol.) Bull. 94, 1267–1309.

NPD, 2019. Norwegian Petroleum Directorate Fact Pages. http://factpages.npd.no/factpages/.

Ødegaard, E., Avseth, P., 2004. Well log and seismic data analysis using rock physics templates. First Break 23, 37–43. https://doi.org/10.3997/1365-2397.2004017.

Peltonen, C., Marcussen, Ø., Bjørlykke, K., Jahren, J., 2009. Clay mineral diagenesis and quartz cementation in mudstones: the effects of smectite to illite reaction on rock properties. Mar. Pet. Geol. 26, 887–898.

Ritter, U., 1988. Modelling of hydrocarbon generation patterns in the Egersund sub-basin, North Sea. Adv. Org. Geochem. 13, 165–174. https://doi.org/10.1016/0146-6380(88)90036-8.

Shuey, R.T., 1985. A simplification of the Zoeppritz equations. Geophysics 50, 609–614. https://doi.org/10.1190/1.1441936.

Vollset, J., Doré, A.G., 1984. A Revised Triassic and Jurassic Lithostratigraphic Nomenclature for the Norwegian North Sea. NPD-Bulletin, 3. Norwegian Petroleum Directorate, pp. 53.

Ziegler, P.A., 1992. North Sea rift system. Tectonophysics 208, 55–75. https://doi.org/10.1016/0040-1951(92)90336-5.

Part III
Appendix

Extended abstract B

Improved Transition Zone Identification Using Relations Between Shear Wave Velocity and Density

Jørgen André Hansen
Nazmul Haque Mondol
Filippos Tsikalas
Sascha Doering

Fourth EAGE Workshop on Rock Physics
11–13 November 2017, Abu Dhabi, UAE

EAGE

RP18

Improved Transition Zone Identification Using Relations Between Shear Wave Velocity and Density

J.A. Hansen* (University of Oslo), N.H. Mondol (University of Oslo and Norwegian Geotechnical Institute), F. Tsikalas (Eni Norge), S. Doering (Eni)

Summary

In this study, we present a method for identification of the transition zone between mechanical and chemical compaction in data from shaly lithologies. By utilizing crossplots of wireline log-measured shear wave velocity (Vs) and bulk density (ρb), we observe an increased sensitivity compared to compressional wave velocity (Vp) to the onset of chemical compaction/cementation, while eliminating uncertainties related to porosity estimations. A clear change in the velocity (Vs) gradient with increasing density is shown to occur in data from eight exploration wells. Data above and below a certain velocity value (Vs = 1350 m/s) show substantially different behavior which is expected to be a result of cementation. A linear relation in the Vs –density domain is derived from the data and suggested as a representative trend for mechanical compaction in the study area. Our suggestion is that whenever recorded with sufficient vertical coverage, direct measurements of Vs and density are trust-worthy parameters for identifying the transition zone between mechanical and chemical compaction.

Introduction

Compaction and porosity loss in sedimentary rocks is expected as a result of increasing burial depth, effective stress and temperature in a normally subsiding basin. The transition from mechanical to chemical compaction has an effect on the elastic properties of the rocks, which subsequently will manifest in their seismic signatures. In this study, we present a method for identification of the transition zone between mechanical and chemical compaction in data from shaly lithologies. By utilizing wireline log-measured shear wave velocity (V_s) and bulk density (ρ_b), we observe an increased sensitivity compared to compressional wave velocity (V_p) to the onset of chemical compaction/cementation at 70-80°C. The V_s-density crossplot eliminates uncertainties associated with porosity estimation (porosity from neutron, density or sonic logs) – an important parameter for the commonly used V_p-porosity crossplot to identify transition zone. Our suggestion is that whenever recorded with sufficient vertical coverage, direct measurements of V_s and density are the most trust-worthy parameters in identifying the transition zone between mechanical and chemical compactions.

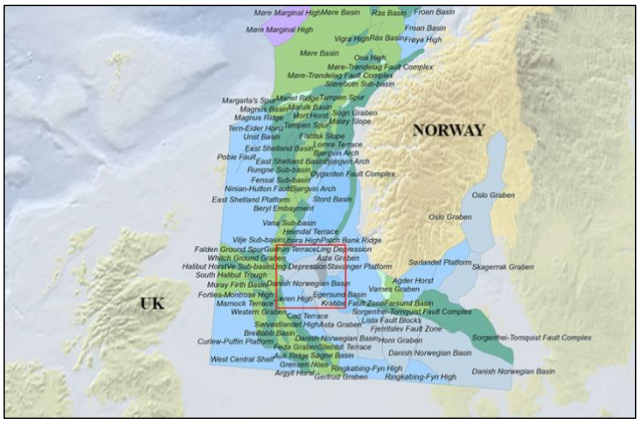

Figure 1 *Location of the study area, with structural elements of the Norwegian Continental Shelf indicated (source: NPD FactMaps - http://gis.npd.no/factmaps/html_20/).*

Methods and theory

A transition from mechanical compaction (i.e. overburden stress causing crushing, reorientation and packing of grains) to chemical compaction (temperature driven chemical reactions) during subsidence is expected at a certain temperature level (60-80°C), yet the transition is somewhat different between shale and sand. Quartz cement in sand is a result of mineral dissolution and precipitation which occurs at temperatures more than 60-70°C (Bjørlykke, 2015). In mudrocks, smectite minerals are expected to become thermally unstable and dissolve at approximately 70-100°C, which leads to precipitation of illite and quartz cement (Bjørlykke, 2015). Biogenic silica (Opal A), if present, can react to form Opal CT at lower temperatures (~45° C) which similarly will have a stiffening effect on mudstones (i.e. increased shear resistance). Additionally, kaolinite becomes unstable at burial depths corresponding to temperature above 120-130°C if there is K-feldspar present, which leads to further release of silica resulting in quartz precipitation. The initial few percent of cement is however assumed to result in the most apparent change in physical properties such as V_p, V_s, bulk and shear moduli.

Quantification of cement volume in clean sands is discussed by Avseth et al. (2010), who discuss the use of V_p or V_s versus density crossplots in detail for sand. Marcussen et al. (2010) derived a linear relation between V_p and quartz cement volume (%) for sandstone from well log data which shows good correlation for the Etive Sandstone Formation in the northern North Sea (Eq.1).

$$\text{Cement volume (\%)} = (V_p - 2775) / 84.825 \qquad \text{Eq. 1}$$

An important quality control for both these models involves analysis of thin sections to quantify cement, porosity, sorting, and so forth, which is not as easily replicable for shales.

This study consequently presents a data-driven investigation of the transition between the mechanical and chemical compaction domain in shales. Shale volume was estimated by calculating the gamma ray index (Eq.2) based on the interpretation of gamma ray values representing clean sand (V_{sh} < 0.25) and pure shale (V_{sh} > 0.75), and correcting after Equation 3 (Clavier et al. 1971). Uncertainties in shale volume estimation from gamma ray are largely due to interpreter's bias in identifying a gamma ray value to represent pure shale (Mondol, 2015). To minimize the error, neutron-density relations were used as a second shale indicator for quality control. Due to small amount of data with V_{sh} > 0.75, data representing V_{sh} > 0.5 were considered shaly lithologies and utilized in further analysis.

$$I_{GR} = (GR_{max}-GR_{log})/(GR_{max}-GR_{min}) \quad \text{Eq. 2}$$

$$V_{sh} = 1.7 - [(3.38 - (I_{GR} + 0.7)^2]^{1/2} \quad \text{Eq. 3}$$

The analysis is conducted in crossplots using direct measurements of elastic properties, mainly S-wave velocity (V_s) versus density (ρ_b). By using density directly, we avoid the uncertainties related to porosity estimation to obtain a more robust trend, and maintain the direct relation to seismic properties. Uncertainties in calculating porosity from density are mainly related to the assumption of matrix density which varies with lithology, and fluid density which varies with fluid type and salinity. Neutron porosity is highly influenced by lithology, shaliness and gas (Mondol, 2015). V_s measurements have the added benefit over V_p of being independent of pore fluid (Avseth et al. 2010), and thus assumed to be more sensitive to cementation (rock stiffness). We utilize data from eight exploration wells from the study area (Fig. 1), and data representing the Zechstein Salt, Shetland Group Carbonates and known organic-rich source rock intervals are excluded as they all generally display a different behaviour of elastic properties than the mudrocks being studied.

Results and discussion

By examining all data in the V_s-ρ crossplot color coded by shale volume in Figure 2a, we can observe differences of compaction behavior of sand and shale. Data representing shaly lithologies display a more continuous trend, as the sedimentary succession in the study area is largely clay dominated. Particularly in the shallower section (i.e. towards lower values of V_s and ρ), shaly lithologies are more abundant. Figure 2b shows only data from the shale dominated fraction (V_{sh} > 0.5), and is color coded by shear modulus. If examining how velocity change with increasing density (i.e. an indication of decreasing porosity), we can see a difference between the lower and upper part of the plot (Fig 2b). Between density values of ~2.15 to 2.45 g/cm^3, the increase in V_s is approximately 550 m/s (800 to 1350 m/s). Slightly higher scatter is observed in data above ~1350 m/s, but the approximate mean velocity increases with around 1150 m/s (1350 to 2500 m/s) between density values of 2.45 g/cm^3 and 2.65 g/cm^3. The change in velocity gradient correlates with a shear modulus value of around 4-5 GPa (color coded in Figure 2b), and is assumed to indicate initial cementation (transition zone) which causes increased rock stiffness (V_s) without dramatically reducing porosity or increasing density (ρ).

Purely for comparison of our transition zone indicator with the relation between velocity and cement valid for sand (Eq. 1) suggested by Marcussen et al. (2010), the same data (V_{sh} > 0.5) is color coded with calculated cement volume in Figure 3. Even though the relation is derived from a substantially different lithology, the initial few percent of cement is predicted in the proximity of what was inferred to be the transition zone from observing the knee-point in the data marked in Figure 2b. A linear regression best fit line for all data is included in Figure 3a (solid line), which shows a correlation of 0.619 (R^2) but does provide a good fit for the overall trend. If instead applying a separate linear regression to data above and below the knee-point (approximately V_s = 1350 m/s), we can see a clear representation of different trends (Fig 3b). For low-density and -velocity rocks, the correlation with our data is now close to 70% (R^2 =

0.682). The relation between density and velocity (Eq. 3) can consequently be argued to be an acceptable representation of the mechanical compaction trend for shales in the study area.

$$\rho = 1.656 + 0.000593V_s \qquad \text{Eq. 3}$$

For data assumed to represent the chemical compaction domain, the spread is shown to be too large to obtain an acceptable correlation. A second observation is related to the scatter of the data from the chemical compaction domain, which seems to diminish at higher values of velocity and estimated cement volume (dashed lines in Fig. 3a).

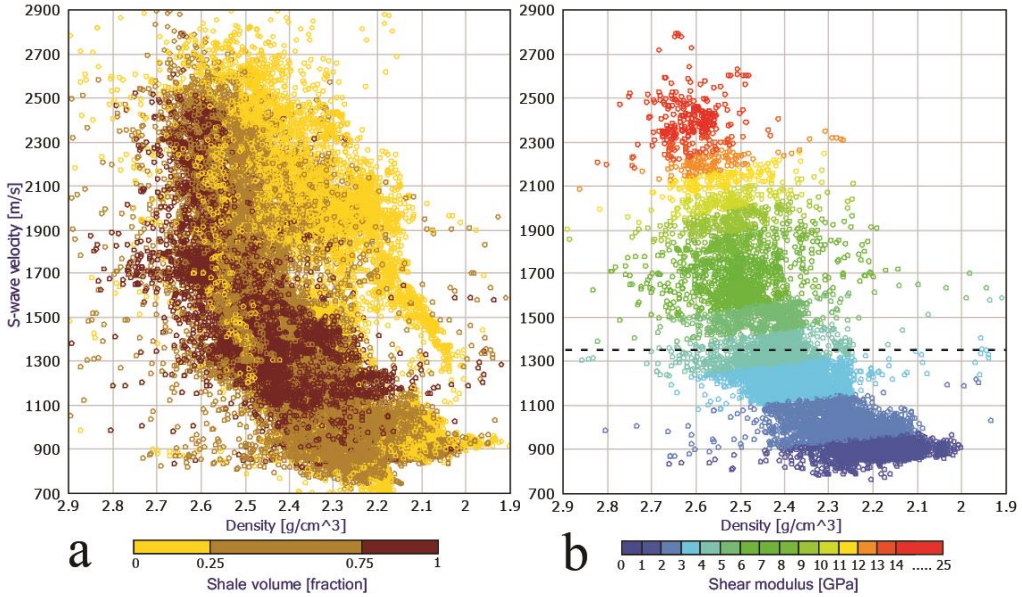

Figure 2 *Crossplots of V_s versus density. a) All data from the eight studied wells, color coded with shale volume. b) Data with V_{sh}>0.5, color coded with shear modulus. Stippled line indicates approximate transition zone.*

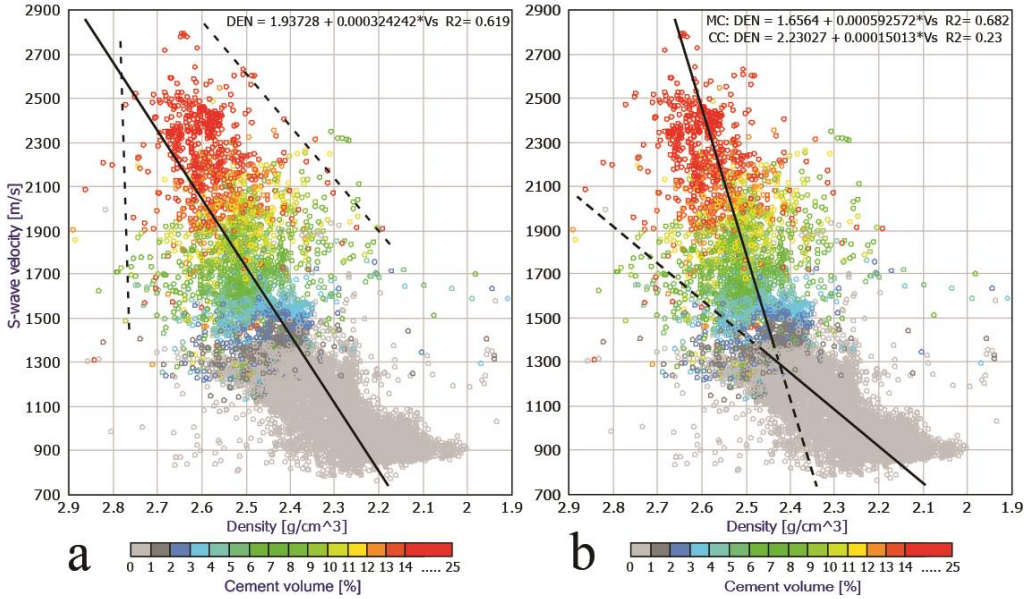

Figure 3 *Crossplots of V_s versus density, color coded with cement volume. a) Linear regression line based on all data (solid), and approximate maximum and minimum density in the chemical compaction area (dashed lines). b) Linear regression lines and equations based on data above and below V_s =1350 m/s.*

As more cement is precipitated in the pore space of the rock, the rocks are homogenized and the elastic properties become increasingly similar. In the plot of same data points of V_p versus density (Fig. 4), the scatter is less, which can possibly be attributed to the lower sensitivity of V_p to cement volume compared to V_s (Fig. 2b). Additionally, we can observe that the data falls along a somewhat more linear, slightly curved trend and a knee point is harder to confidently suggest. The contrast between mechanical and chemical compaction consequently appear to be less clear than was the case when utilizing V_s.

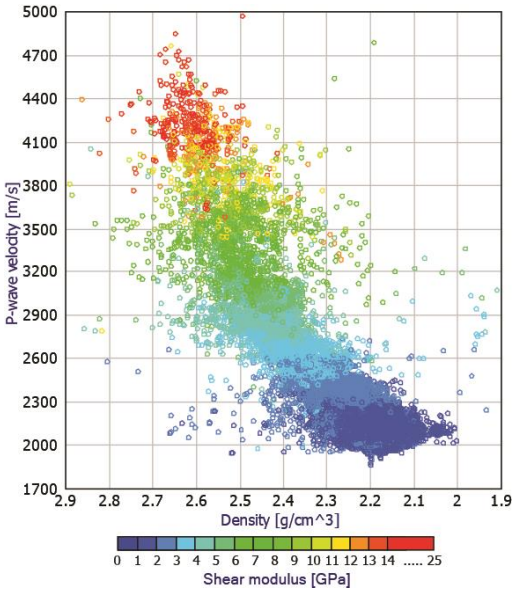

Figure 4 *Compressional velocity (V_p) versus density crossplot, color coded with shear modulus.*

Conclusions

This study has demonstrated a method for identifying the transition zone between mechanical and chemical compaction, using direct measurements of V_s and density. The sensitivity to rock stiffening and insensitivity to fluids in shear velocity makes it a superior cement indicator compared to compressional velocity. The use of density eliminates uncertainties related to porosity estimations. A clear change in the velocity (V_s) gradient with increasing density is shown to occur in data from eight exploration wells. Data above and below a certain velocity value (V_s = 1350 m/s) show substantially different behavior which is expected to be a result of cementation, and separate linear trends can be derived for mechanical and chemical compaction. The relation representing mechanical compaction can be suggested with a higher degree of confidence, as the higher velocity data display large density variations.

Acknowledgements

This study was carried out under the ReSource project, an R&D collaboration between the University of Oslo and Eni Norge. We extend our sincere thanks to Eni Norge for funding the project. Data used in this study was provided by DISKOS.

References

Avseth, P., Mukerji, T., Mavko, G. and Dvorkin, J. [2010] Rock-physics diagnostics of depositional texture, diagenetic alterations, and reservoir heterogeneity in high-porosity siliciclastic sediments and rocks — A review of selected models and suggested work flows. *Geophysics*, **75**, 75A31-75A47.

Bjørlykke, K. [2015] Compaction of sedimentary rocks: Shales, sandstones and carbonates, In Bjørlykke, K. (Ed.) *Petroleum Geoscience. From Sedimentary Environments to Rock Physics - Second Edition.* Springer-Verlag Berlin Heidelberg, 351-360.

Clavier, C., Hoyle, W. and Meunier, D. [1971] Quantitative interpretation of thermal neutron decay time logs: Part I. Fundamentals and techniques. J*ournal of Petroleum Technology*, **23**, 743-755.

Marcussen, Ø., Maast, T. E., Mondol, N. H., Jahren, J. and Bjørlykke, K. [2010] Changes in physical properties of a reservoir sandstone as a function of burial depth – The Etive Formation, northern North Sea. *Marine and Petroleum Geology*, **27**, 1725-1735.

Mondol, N. H. [2015] Well logging: Principles, Applications and Uncertainties, In Bjørlykke, K. (Ed.) *Petroleum Geoscience. From Sedimentary Environments to Rock Physics -Second Edition*. Springer-Verlag Berlin Heidelberg, 385-425.

Extended abstract C

Predicting the Effects of Organic Content and Maturation on the Elastic Properties of Central North Sea Source Rocks

Jørgen André Hansen
Nazmul Haque Mondol

80th EAGE Conference & Exhibition
11–14 June 2018, Copenhagen, Denmark

2018 EAGE ANNUAL
80TH CONFERENCE + EXHIBITION
COPENHAGEN | DENMARK

Tu P2 03

Predicting the Effects of Organic Content and Maturation on the Elastic Properties of Central North Sea Source Rocks

J.A. Hansen* (University of Oslo), N.H. Mondol (University of Oslo and Norwegian Geotechnical Institute)

Summary

The maturity of source rocks due to their shallow burial is a critical factor in the Central North Sea. In order to examine lateral variations of maturity of the source rocks, quantitative analysis of seismic data is required. The motivation for this study is to investigate the effects and relative impact of organic content, thermal maturity and hydrocarbon generation on elastic properties of organic rich shales. Using some established models, realistic approximations and reference trends that are calibrated to our area and applicable to our well log data, we can begin to predict how our data will behave as conditions change. We observe consistent compaction trends for immature to early mature shales at similar levels of TOC, and can from there infer the effect of hydrocarbon generation in data from a deeply buried, mature source rock. These trends can potentially help us evaluate seismic inversion results and data from other wells where TOC content and source rock maturity are in question.

Introduction

In recent years, research on characterization of organic-rich shales has become more visible due to the popularity of exploiting unconventional shale reservoirs. However, the understanding and theories that have been developed are in principle equally applicable for characterization of organic rich shales as conventional source rocks. In areas where only localized generation of hydrocarbons may have occurred due to their relatively shallow maximum burial of source rocks compared to the expected peak oil window, a good understanding of lateral variations in these source rocks can be valuable. The maturity of source rocks due to their shallow burial is a critical factor in the Central North Sea. In order to examine lateral variations of maturity of the source rocks, quantitative analysis of seismic data is required. A proper understanding of how organic content and subsequent thermal maturity affects the elastic properties of the rock is also important. The motivation for this study is to investigate the effects and relative impact of organic content, thermal maturity and hydrocarbon generation on elastic properties of organic rich shales. The goal is to understand the feasibility of characterizing clay rich source rocks in terms of TOC and thermal maturity from seismic data, based on realistic approximations and trends from well log data using examples from potential source rock formations in the Central North Sea. The Tau and Draupne formations (Kimmeridge shale time equivalents) are the main potential source rocks in the area. Seven exploration wells with shear velocity measurements in the organic-rich shale interval of interest have been used for investigation, although only three are shown in the examples presented here. One of which (well 15/3-8) is used as a representative of deeply buried source rock from a proven mature area for comparison (Isaksen and Ledje, 2001).

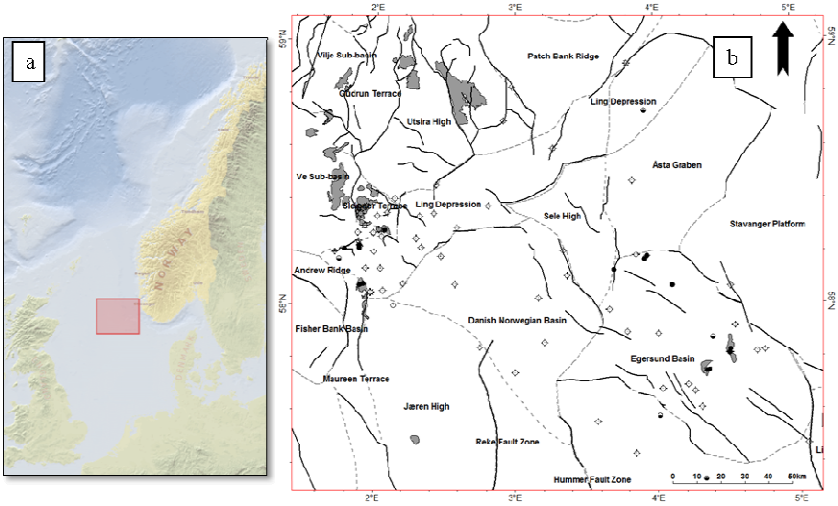

Figure 1 *(a) Map showing the Central North Sea study area. (b) Prolific areas shown in grey shading in the NW part of the study area.*

Theory and methods

A relation between TOC in weight percent and bulk density (Eq. 1) appeared to provide consistent predictions in the investigated wells when compared to TOC from core/cuttings in the same or nearby calibration wells (Vernik and Landis, 1996; Carcione and Avseth, 2015).

$$TOC\ (wt.\%) = a * [\rho k\ (\rho s - \rho b)] / [\rho b(\rho s - \rho k)] \qquad \text{Eq.1}$$

where ρ_k is kerogen density which is assumed to vary between 1.1-1.4 g/cm^3 from initial maturation to late oil generation (Vernik and Landis, 1996), ρ_s is matrix density (which in reality varies according to mineralogy and compaction; Carcione and Avseth, 2015), and ρ_b is the bulk density log measurement. *a* is a constant related to the fraction of carbon in organic matter and can vary slightly (*a* = 67 assumed here). We utilize a popular rock physics crossplot, velocity ratio (Vp/Vs) versus acoustic impedance (AI), in order to establish a link between seismic properties and geological variations in our observations. Previously presented templates based on rock physics models exist for characterization of organic-rich shales (e.g. Guo et al., 2013; Carcione and Avseth, 2015; Zhao et al.,

2016; Vernik, 2016). Vernik (2016) provides a framework for deriving Vp, Vs and ρ on a kerogen free basis (kerogen substitution), which can be helpful in understanding quantitatively how the organic-rich shales differ from inorganic equivalents. Additionally, effects of organic content, maturation, microfracturing and more on velocity and anisotropy have been discussed in detail with focus on unconventional reservoirs (Vernik and Landis, 1996; Alfred and Vernik, 2012). Guo et al. (2013) describe effects of changing porosity and clay content on elastic properties of organic-rich shales. Zhao et al. (2016) present a model that considers different maturity stages, but only simple comparison to either of their templates does not seem to explain data from our more shallow, assumedly immature to early mature source rocks, which may be explained by an overall low carbonate content compared to the models (<5%). Carcione and Avseth (2015) suggests an RPT for clay-rich mature source rock, which seem to capture data from well 15/3-8 by predicting some level of hydrocarbon content regardless if considering the Backus averaging or Gassmann fluid substitution models (Fig 2a, b). It is however assumed that gas has not been generated at this maturity stage, which is indicated by the latter model. In order to fully take advantage of modelling schemes such as mentioned that carefully consider many aspects of the organic-rich shales, a detailed calibration to data from our study area would be required.

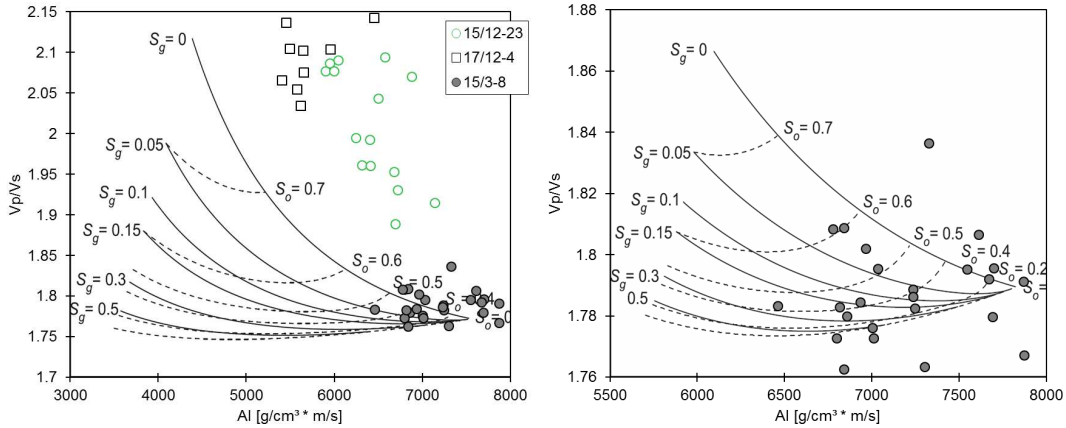

Figure 2 *Upscaled data from our wells superimposed on rock physics templates from Carcione and Avseth (2015).Backus averaging model (left) and Gassmann equation model (right).*

Alternatively, we can attempt to derive some locally calibrated trends that might be useful to explain our data in detail, without replicating or amending complex models, which may be useful for e.g. interpretation of seismic inversion results. A rock physics template (Ødegaard and Avseth, 2004) is created to serve as reference trends for our area, and has been calibrated to well log observations (Fig. 3). The behaviour of organic rich shales in the area can subsequently be compared to these trends. Firstly, a background trend from shale dominated formations with low organic content is established in the Vp/Vs-AI crossplot from well log data distributed across the study area (Fig. 3a). The utilized data are from formations proximal in depth to the source rock formations, and are assumed to represent a local reference for increasing depth and compaction. Secondly, a brine saturated sandstone trend can be calculated (Hashin-Shtrikman upper bound interpolation) and calibrated to well log data in predominantly clean sandstones. Though available in sparse amounts, mineralogical data indicate that lateral variations in source rock formations being investigated are not negligible, but assumed acceptable for comparison. It is however inevitable that even relatively minor changes in quartz and feldspar content can have implications for stiffness and elastic properties and thereby cause uncertainty in subsequent interpretations.

Examples

Based on some approximations and assumptions about the properties of the kerogen and non-kerogen fractions for the organic-rich shale at a well location, a kerogen substitution method (Vernik, 2016) can be employed to predict elastic properties at different TOC levels. Both the Flekkefjord and Fjerritslev formations are generally characterized as dark grey shales, meaning that on a kerogen-free

basis they are assumed to be overall similar to the Tau Formation in the example from well 17/12-4 (Fig 3a). Supported by the relation between these over- and underlying formations, the shift observed in the source rock formation data after kerogen substitution provides an expected trend for changing TOC in the Vp/Vs-AI space (Fig. 3a). Within a narrow depth window, potential source rock formations are expected to have significantly lower acoustic impedance (Løseth et al., 2011), and slightly lower velocity ratio. Figure 3b shows data with TOC in the range 4-6 wt. % for three wells at different maximum burial depth. We can see that by shifting the compaction line in the direction of increased TOC, data from intervals of similar TOC range is captured for the shallow wells. Corresponding shifted clusters as a function of kerogen substitution also shows somewhat altered TOC trends with increasing depth/effective pressure.

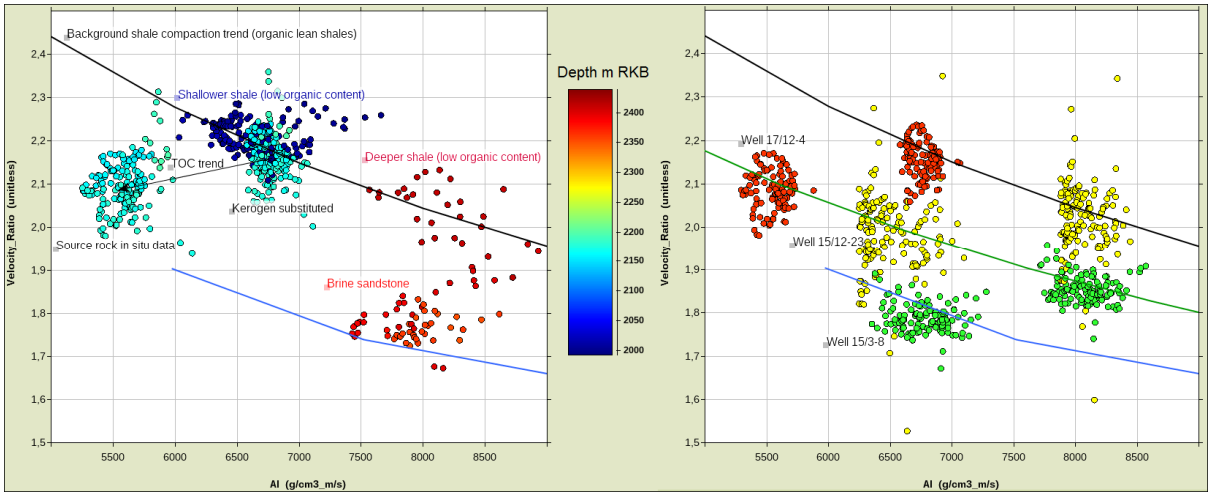

Figure 3 *(left) TOC trend in Vp/Vs-AI space shown with data from well 17/12-4.(right) In situ and kerogen substituted well log data (4<TOC<6 wt. %) for three wells. Green line shows shifted compaction trend for ~5 wt. % TOC, black line represents inorganic shale compaction and blue line shows the brine saturated sandstone trend.*

By taking into account the effects of (1) burial and compaction and (2) content of organic matter, we can identify an expected range of Vp/Vs and AI values for shales at a certain depth and TOC. Additionally, data from the known mature source rock encountered at ~3800 m (BSF) indicated to be in an area at peak oil window maturity (geochemical analysis data; NPD FactPages, 2017; Isaksen and Ledje, 2001) should be able to give us an indication about the effect of oil generation. By considering the deviation from a shifted compaction trend that appears to nicely capture data from shallower organic-rich intervals (4<TOC<6 wt. %; Fig. 3), we can assess the predicted fluid effect. Additionally lowered Vp/Vs and AI is observed in well 15/3-8 for data with 4<TOC<6 wt. % compared to the shifted TOC trend, i.e. TOC (kerogen substitution) alone does not explain the significantly low Vp/Vs and AI observed. Considering that even though shales in principle violate the assumptions of the Gassmann equation, it has been shown by e.g. Lucier et al. (2011) to provide satisfactory predictions of the acoustic response when substituting brine in the place of in situ gas. Good knowledge about the shale mineralogy and associated densities and moduli are required in order to expect reliable results. As argued in Lucier et al. (2011), however, and in our case, we can use this approach as an indicator tool for quick assessment. For well 15/3-8, we can substitute in situ oil saturation for brine, and observe that the predicted response for data with 4-6 wt. % TOC matches the trend representing ~5 wt. % TOC based on less mature wells (Fig. 4). Subsequently, kerogen substitution shifts the point towards the background shale trend. Although there are uncertainties associated with these observations, they appear consistent with our local reference trends.

Conclusions

The goal of this simple model exercise has been to investigate how we can expect our data to move as an effect of TOC and maturation to the point of hydrocarbon generation. These trends now provide us

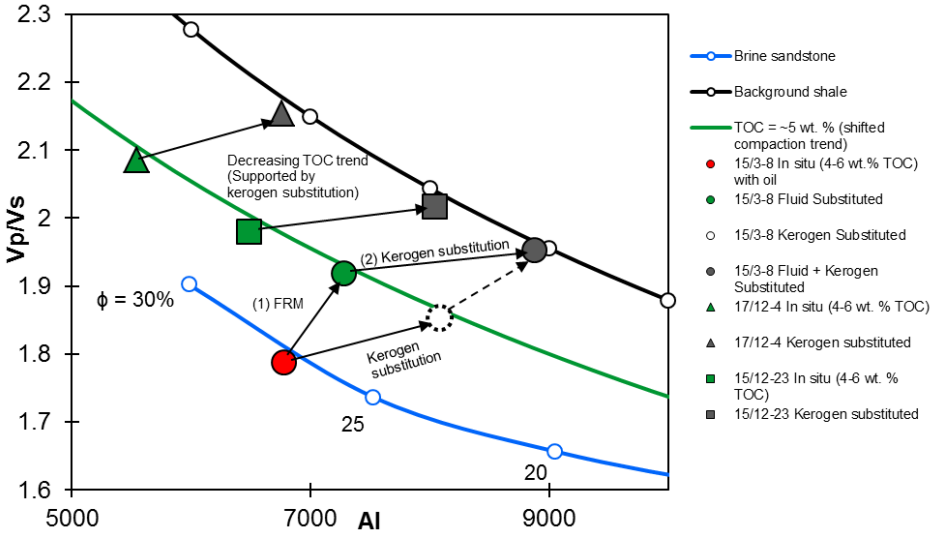

Figure 4 *Data from three wells represented by average values (TOC 4-6 wt. %). Modeled responses are indicated for kerogen substitution and fluid substitution (15/3-8 only).*

with some boundaries which might help us evaluate seismic inversion results or data from other wells where source rock maturity is in question.

Acknowledgements

We extend our sincere thanks to Eni Norge for funding and encouraging our work under the ReSource project (Quantitative analysis of **re**servoir, **source** and cap rocks of the Central North Sea) - an R&D collaboration between the University of Oslo and Eni Norge. All data is obtained from DISKOS.

References

Alfred, D. and Vernik, L. [2012] A new petrophysical model for organic shales. SPWLA 53rd Annual Logging Symposium, Cartagena, Colombia, June 16-20.

Carcione, J. M. and Avseth, P. [2015] Rock-physics templates for clay-rich source rocks. Geophysics, **80**(5), D481-D500.

Guo, Z., Li, X., Liu, C., Feng, X. and Shen, Y. [2013] A shale rock physics model for analysis of brittleness index, mineralogy and porosity in the Barnett shale. Journal of Geophysics and Engineering, **10**, 1-10.

Isaksen, G. H. and Ledje, K. H. I. [2001] Source rock quality and hydrocarbon migration pathways within the greater Utsira High area, Viking Graben, Norwegian North Sea. AAPG Bulletin, **85**(5), 861-883.

Lucier, A. M., Hofmann, R. and Bryndzia, L. T. [2011] Evaluation of variable gas saturation on acoustic log data from the Haynesville Shale gas play, NW Louisiana, USA. The Leading Edge, **30**(3) 300-311.

Løseth, H., Wensaas, L., Gading, M., Duffaut, K. and Springer, M. [2011] Can hydrocarbon source rocks be identified on seismic data?. Geology, **39**(12), 1167-1170.

NPD FactPages [2017] [Online]. Norwegian Petroleum Directorate. Available: http://factpages.npd.no/FactPages/

Vernik, L. and Landis, C. [1996] Elastic Anisotropy of Source Rocks: Implications forHydrocarbon Generation and Primary Migration. AAPG Bulletin, **80**(4), 531-544.

Vernik, L. [2016] Seismic petrophysics in Quantitative Interpretation. Society of Exploration Geophysicists, pp. 226.

Zhao, L., Qin, X., Han, D., Geng, J., Yang, Z. and Cao, H. [2016] Geophysics, **81**(5), D527-D541.

Ødegaard, E. and Avseth, P. [2004] Well log and seismic data analysis using rock physics templates. First Break, **22**(10), 37-43.

Extended abstract D

Cap Rock Evaluation of Central North Sea Shales, Through Log-Derived Poisson's Ratio and Young's Modulus

Jørgen André Hansen
James Ronald Johnson
Nazmul Haque Mondol

Sixth EAGE Shale Workshop
28 April–1 May 2019, Bordeaux, France

Mo P02

Cap Rock Evaluation of Central North Sea Shales, Through Log-Derived Poisson's Ratio and Young's Modulus

J.A. Hansen[1]*, J.R. Johnson[1], N.H. Mondol[1,2]

[1]University of Oslo; [2]Norwegian Geotechnical Institute (NGI)

Summary

We present an evaluation of shale dominated cap rocks relevant for Middle Jurassic sandstone reservoirs in the Central North Sea, based on well log data from the Norwegian Continental Shelf. Previously established indicators for brittleness and seal quality, E (Young's modulus) and ν (Poisson's ratio), are utilized in the analysis. Similar ductile to fairly ductile behaviour is found in different formations for five analysed wells, of which two are oil discoveries, one contains only oil shows, and two are dry. Cap rocks in the discovery wells are comparatively most brittle, compared to a published E–ν template. Uplift of ~500 m in one of the discovery wells is not found to have compromised the sealing capability. We also investigate how organic content influence an organic-rich shale interval in terms of cap rock properties by using kerogen substitution and comparing to the other more organic-lean shales, which does not support a direct correlation between TOC and ductility. Finally, we consider how observed properties of different shales relate to different mineralogical composition.

Introduction

Middle Jurassic sandstone-dominated formations are main target reservoirs for hydrocarbon in the Central North Sea on the Norwegian Continental Shelf. Potential cap rocks for these reservoirs are primarily the Egersund, Heather and Draupne shale-dominated formations, or in some cases shaly intervals within the Sandnes or Bryne sand-dominated Formations. Due to limited amounts of hydrocarbon generation in the area, related to source rock maturity status and upliftment, seal quality must be good enough to retain oil and gas accumulations that are likely not being replenished. This study therefore aims to evaluate proven and potential cap rocks from the aforementioned formations in wells from the Central North Sea area. The database is summarized in Table 1. Young's modulus (E) and Poisson's ratio (ν) are properties that have been used to indicate brittleness and serve as cap rock quality indicators in previous studies (e.g., Grieser and Bray 2007; Perez and Marfurt 2014; Mondol 2018). We consequently utilize crossplots of these properties to perform our analysis.

Table 1 *Summary of wells and cap rock shales in this study.*

Well (prospect)	Cap rock depth (maximum burial) m BSF	Cap rock formation	Content
17/12-4 (Vette)	2568-2573	L. Sandnes – U. Bryne silty shale	Oil
16/8-3 S (Lupin)	2687-2708	Draupne organic rich shale	Dry
17/6-1 (Svanegle)	2875-2888	Egersund silty shale	Shows
15/12-21 (Grevling)	2888-2903	Heather silty shale	Oil
9/2-11 (Aubrey)	2989-3001	Egersund shale	Dry

Theory and methods

Seal quality is highly influenced by brittleness and consequent fracture potential, which can be particularly important in uplifted regions like the Central North Sea. The brittleness of a rock is dependent on lithology, rock strength, texture, stress, temperature, fluid content, diagenesis (compaction) and organic content (Walles 2004; Perez and Marfurt 2014). Uplift magnitude and corrected maximum burial depth was predicted by comparing shale velocity-depth data to experimental compaction trends (Hansen et al. 2017). Increasing TOC (soft matter) is typically described to have an inverse influence on shale brittleness (Walles 2004). Conversely, depending on the distribution of kerogen in relation to matrix grains, Perez and Marfurt (2014) find that kerogen does not directly relate to higher ductility when the source rock quartz content is significant. In their findings from the Barnett Shale, grains around intergranular kerogen support the stress, meaning that the high-TOC source rock is brittle stratigraphically.

Wireline log recordings of V_p, V_s and bulk density can be used to calculate dynamic elastic parameters such as E, ν, $\lambda\rho$ and $\mu\rho$. We also calculate a TOC log from bulk density as (Vernik and Landis, 1996; Carcione, 2000):

$$\text{TOC (wt. \%)} = a\,[\rho_k(\rho_m - \rho_b)] / [\rho_b(\rho_m - \rho_k)] \quad (1)$$

Here, ρ_k is kerogen density which has a range of 1.1–1.6 g/cm^3, and is dependent on maturity (Vernik and Landis 1996; Dang et al. 2016). ρ_m is matrix density, which in reality varies according to mineralogy and diagenesis, i.e., clay mineral transformation (Carcione and Avseth 2015). ρ_b is the bulk density log measurement, and a is a constant related to the fraction of carbon in organic matter and can vary according to maturation level. Additionally, a method referred to as kerogen substitution proposed by Vernik (2016) has been applied to the Draupne Formation in the Lupin well (16/8-3 S), to predict elastic properties of the same rock at different organic content. Input parameters for this modelling are determined from core plug measurements of TOC, porosity, maturity, grain- and bulk density.

Examples

Figure 1 shows data from the five cap rock intervals in our database in crossplots of *E* versus *v*. Considering that these cap rocks have fairly similar maximum burial (max. difference ~450 m), oil reservoir cap rocks have comparatively lower *v* and lower *E* than the Svaneøgle cap rock which has signs of leaking (oil shows only). $\mu\rho$, another parameter that can be indicative of stiffness and brittleness, display slightly higher values in the Svaneøgle and Aubrey wells, but is overall similar to the Grevling oil discovery well (Table 1). The thin cap rock interval in the Vette well (oil) has slightly lower values of *E* and $\mu\rho$. An important difference is however that Aubrey, Svaneøgle and Vette locations all have experienced uplift in the order of ~500 m, whereas the area of Lupin and Grevling is predicted to have minor to no uplift history (Hansen et al. 2017). Uplift-induced stress release can lead to fracturing, which in turn would decrease compressional and shear stiffness of the rock (Bjørlykke 2015). Contrarily, if fractures are already present in situ, the velocity- and density log-derived elastic properties could lead to bias, giving the impression of a more ductile behaviour (i.e., *less* prone to fracturing). In either case, the uplift has apparently not affected the seal integrity in the Vette well which retains oil (intra Sandnes–Bryne Formation). There is also a thin coal layer within this particular shaly interval which could aid sealing capacity.

TOC is comparatively low in four of the seal intervals (predominantly < 3 wt. %), whereas the Draupne Formation (Lupin) contains fairly uniformly ~5–8 wt. % TOC (Figure 1). The Draupne Formation has both source- and cap rock potential in the North Sea. Lower *E*, $\mu\rho$ and higher *v* are observed for this organic-rich shale. Skurtveit et al. (2015) find that the Draupne Formation in the Lupin well has very good sealing properties based on core measurements, with vertical permeability around $1.2–1.4 \times 10^{-7}$ mD. The fact that the fluid in this particular reservoir is brine is most likely due to a lack of mature source rock to charge it rather than cap rock integrity.

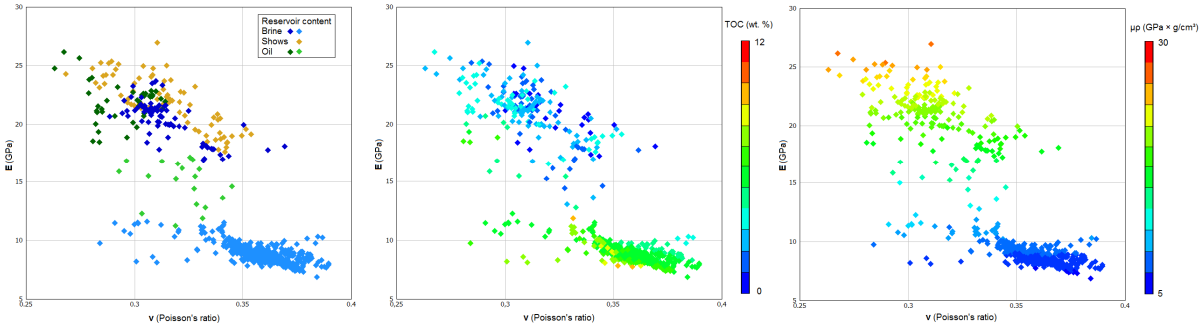

Figure 1 *E–v crossplot showing five shale dominated rocks serving as seals above reservoirs containing brine, oil shows, and oil. Color coded after well/reservoir content (left), cap rock TOC (middle), and μρ (right).*

E– *v* relationships between cap rocks that retain oil, leak (Svaneøgle), or cap brine reservoirs do not display any direct correlation with brittleness interpretations based on mineralogy proposed by Perez and Marfurt (2014). All are classified as ductile to fairly ductile, as the "brittle region" in this template is outside the left side of the plot axis (Figure 2). Predicted *E* and *v* after applying kerogen substitution indicate that variable organic content mainly relates to changing Young's modulus, and does in fact not lead to an interpretation of increased brittleness (Figure 2). Kerogen-substituted properties fall onto a fairly narrow trend of other cap rock data. If instead observing the trend of mineral properties (clay to quartz – ductile to brittle) in this domain, data in the upper left region of the plot is indicated as more brittle. This indicates relatively more favourable properties in Vette and Lupin wells, but the proven functional Grevling well cap rock also plot towards the upper left. The range of values observed in our data is nevertheless small compared to quartz mineral properties ($E = 95$, $v = 0.074$).

Some mineralogical data are available for the Egersund Formation, which is time equivalent to the Heather Formation, from other wells in the Egersund Basin (Kalani et al. 2015). Furthermore, five core samples are available from the Draupne Formation in the Lupin well (Ling Depression). The core

analysis is courtesy of the CO2SEAL project (financed by the RCN, Gassnova and Equinor). Based on averages, the Draupne Formation is richer in quartz and K-feldspar, whereas mixed-layer illite/smectite is more abundant in the Egersund Formation (Figure 3). Total clay is on average 46% and 66%, respectively. However, the Draupne Formation still displays the most ductile properties along the mineral property trend. Data from the Egersund and Heather Formations plot around theoretical mineral properties of clay (Mondol, 2018). Calcite and dolomite content is negligible in terms of determining the brittleness of both these formations. A thin section image under UV light indicates scattered organic matter rather than continuous accumulations (Figure 3).

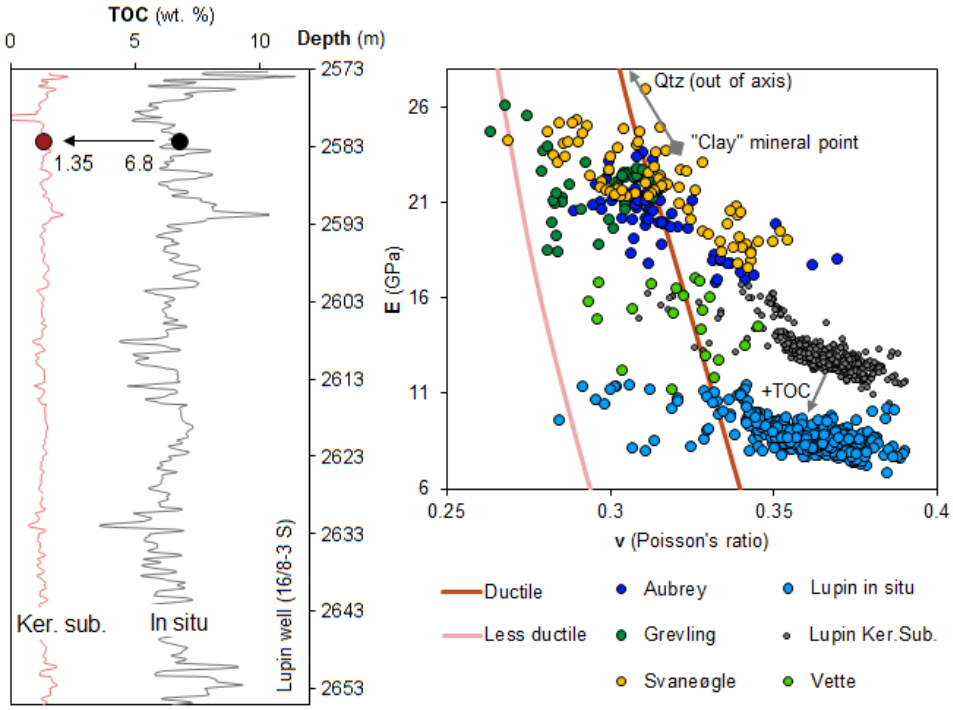

Figure 2 *TOC signature of the Draupne Formation in the Lupin well (left) with one calibration sample, before and after applying kerogen substitution to predict the v-E response (right) with reduced TOC influence. Ductile-less ductile cutoffs are adapted from Perez and Marfurt (2014).*

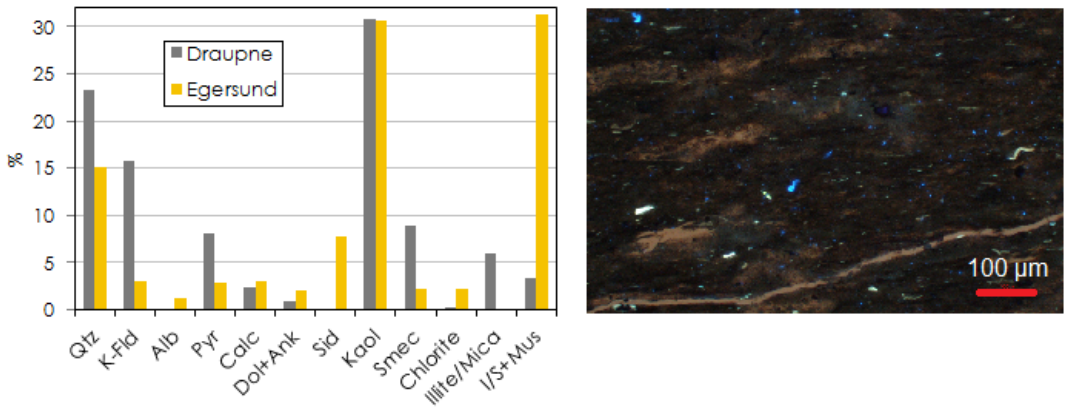

Figure 3 *Average mineralogy of Egersund and Draupne Formations (left), and thin section image from a Draupne Formation sample in Lupin well (right). Blue fluorescence indicates organic matter.*

Conclusions

According to the relationship between Young's modulus and Poisson's ratio, seal quality of the studied formations is not separated by differences in brittleness or ductility. All five wells are characterized as fairly ductile based on a proposed classification template, and if anything, the cap

rocks in oil discovery wells are shifted slightly towards the brittle side compared to wells encountering oil shows or brine. Relating brittleness to the trend of mineral-points in the *E*–*v* domain infers a higher brittleness towards increasing *E* and decreasing *v*. This type of classification still does not differentiate hydrocarbon-sealing and brine-sealing cap rocks. Uplift can potentially influence both the measured properties and the actual sealing capacity, but has not caused seal failure in an uplifted, thin, intra-reservoir shale interval (well 17/12-4, Vette discovery). Kerogen substitution predicts a minor increase in *v* (+0.05) and around ~3 GPa increase in *E* by decreasing TOC from 5–8 to 1–2 wt. %, fairly consistent with data from shales with lower organic content. Consequently, this modelling does not reflect a more brittle behaviour from increasing the amount of brittle minerals. This is counterintuitive in terms of individual mineral properties, but not necessarily erroneous on larger scales, as earlier studies display the importance of rock texture and kerogen distribution on brittle/ductile behaviour.

Acknowledgements

This study was carried out under the ReSource project, an R&D collaboration between the University of Oslo and Eni Norge. We extend our sincere thanks to Eni Norge for funding the project. Data used in this study was provided by DISKOS (Norwegian Petroleum Directorate). Academic software licences were provided by Lloyd's Register for Interactive Petrophysics and Ikon Science for RokDoc.

References

Bjørlykke K. [2015] Petroleum Geoscience: From Sedimentary Environments to Rock Physics – Second Edition. Springer-Verlag Berlin Heidelberg.

Carcione, J.M. [2000] A model for seismic velocity and attenuation in petroleum source rocks. GEOPHYSICS, **65**, 1080-1092.

Carcione, J.M. and Avseth, P. [2015] Rock-physics templates for clay-rich source rocks: GEOPHYSICS, **80**, D481-D500.

Dang, S. T., C. H. Sondergeld and C. S. Rai [2016] A New Approach to Measuring Organic Density. Petrophysics, **57**, 112-120.

Grieser, B. and Bray, J. [2007] Identification of production potential in unconventional reservoirs: SPE Production and Operations Symposium. SPE #106623.

Hansen, J.A., Yenwongfai, H.D., Fawad, M. and Mondol, N. H. [2017] Estimating exhumation using experimental compaction trends and rock physics relations, with continuation into analysis of source and reservoir rocks: Central North Sea, offshore Norway: SEG, Expanded Abstracts, 3971-3975.

Kalani, M., J. Jahren, N.H. Mondol and J. I. Faleide [2015] Petrophysical implications of source rock microfracturing. Internation Journal of Coal Geology, **143**, 43-67.

Mondol, N.H. [2018] Seal quality prediction using E-Poisson's ratio rock physics templet- A case study from the Norwegian Barents Sea. GeoConvention

Perez, R.A. and Marfurt, K.J. [2015] Identification of brittle/ductile areas in unconventional reservoirs using seismic and microseismic data: Application to the Barnett Shale. Interpretation, **2**, T255-T271.

Skurtveit, E., Grande, L., Ogebule, O.Y., Gabrielsen, R.H., Faleide, J.I., Mondol, N.H., Maurer, R. and Horsrud, P. [2015] Mechanical testing and sealing capacity of the Upper Jurassic Draupne Formation, North Sea. 49th US Rock Mechanics/Geomechanics Symposium, ARMA, Expanded Abstracts.

Vernik, L. [2016] Seismic petrophysics in Quantitative Interpretation. Society of Exploration Geophysicists.

Vernik, L. and Landis, C. [1996] Elastic anisotropy of source rocks-implications for hydrocarbon generation and primary migration. AAPG Bulletin, **80**, 531-544.

Walles, F. [2004] A new method to help identify unconventional targets for exploration and development through integrative analysis of clastic rock properties. Houston Geological Society Bulletin, **47**, 35–49.